

Investigation of Defluoridation of Groundwater for Drinking Using Nano-Alumina Modified Bone Char (NAMBC)



Betelihem Tadiyos Bogale

A Thesis Submitted to

The Department of Chemical Engineering

School of Mechanical, Chemical, and Materials Engineering

Presented in Partial Fulfillment of the Requirement for the Degree of Master's in
Chemical Engineering (Specialization in Process Engineering)

Office of Graduate Studies

Adama Science and Technology University

September, 2023

Adama, Ethiopia

Investigation of Defluoridation of Groundwater for Drinking Using
Nano-Alumina Modified Bone Char (NAMBC)

Betelihem Tadiyos Bogale

Advisor: Dr. Mulugeta Yilma

Co-Advisor: Dr. Alemu Gizaw

A Thesis Submitted to

The Department of Chemical Engineering

School of Mechanical, Chemical, and Material Engineering

Presented in Partial Fulfillment of the Requirement for the Degree of Master's in
Chemical Engineering (Specialization in Process Engineering)

Office of Graduate Studies

Adama Science and Technology University

September, 2023

Adama, Ethiopia

DECLARATION

I hereby declare that this thesis proposal entitled “**Investigation of Defluoridation of Groundwater for Drinking Using Nano-Alumina Modified Bone Char (NAMBC)**” is my original work and has not been submitted to any other university for similar purpose. The reference used in this proposal are duly recognized by proper citations.

Betelihem Tadiyos Bogale

Name of student

Date

Signature

ADVISOR’S RECOMMENDATION

I, the major advisor/supervisor of this research proposal, hereby certify that I have closely advised/supervised the student while developing this proposal and read the draft thesis/dissertation proposal entitled “**Investigation of Defluoridation of Groundwater for Drinking Using Nano-Alumina Modified Bone Char (NAMBC)**” prepared under my guidance by **Betelihem Tadiyos**. Therefore, I recommend the submission of the proposal to the department for further review and evaluation.

Dr. Mulugeta Yilma (Ph.D.)

Major Advisor

Signature

Date

Dr. Alemu Gizaw (Ph.D.)

Co-advisor

Signature

Date

APPROVAL PAGE

We hereby certify that the recommendation and suggestion given by the proposal review committee are appropriately incorporated into the final thesis proposal entitled **“Investigation of Defluoridation of Groundwater for Drinking Using Nano-Alumina Modified Bone Char (NAMBC)”** by **Betelihem Tadiyos**.

_____	_____	_____
Major Advisor	Signature	Date
_____	_____	_____
Co- Advisor	Signature	Date

Approval of Board of Reviewers

We, the undersigned, members of the Board of Reviewers of the proposal open defense by Betelihem Tadiyos have read and evaluated the thesis proposal entitled “**Investigation of Defluoridation of Groundwater for Drinking Using Nano-Alumina Modified Bone Char (NAMBC)**” and assessed the understanding of the candidate about the conducted research. This is, therefore, to certify that the thesis/dissertation is accepted and it meets the required standard.

_____	_____	_____
Chairperson	Signature	Date
<u>Dr. Wondalem Misganaw</u>		<u>19-10-2023</u>
Reviewer 1	Signature	Date
_____	_____	_____

Reviewer 2	Signature	Date
------------	-----------	------

Finally, approval and acceptance of the thesis is contingent upon the submission of its final copy to the Office of Postgraduate Studies (OPGS) through the Department Graduate Council (DGC) and School Graduate Committee (SGC).

_____	_____	_____
Department Head	Signature	Date
_____	_____	_____
School Dean	Signature	Date
_____	_____	_____
Office of Postgraduate Studies, Dean	Signature	Date

ACKNOWLEDGMENT

First of all, I would like to thank the Almighty GOD, for giving limitless blessings, wisdom, peace, protection and ability to do work. Next, I would like to express my deepest gratitude and heartfelt thanks to my advisor Dr. Mulugeta Yilma for his intellectual guidance, valuable advice and giving freedom of work while doing the experiments and accomplishing my thesis work. I would also like to express my deepest gratitude to my co-advisor Dr. Alemu Gizaw for taking time to advise and assist me throughout every stage of the thesis work.

My sincere gratitude goes to my family for the numerous times they spent to help and pray for me. When times were tough, my family's effort was countless, their encouragement, financial support, and constant prayer were much welcomed and acknowledged.

And also, I would like to express my deepest appreciation for Chemical Engineering department laboratory assistants for their support during the experimental work, and thanks to my classmates for their support whenever I need them in every aspect of my thesis work, it was a pleasure to share and enjoy every situation with them. Finally, I would like to thank all the people who take part a contribution and helped me while accomplishing my thesis work.

Table of Contents

ADVISOR’S RECOMMENDATION	iv
APPROVAL PAGE	v
LIST OF TABLE	xiii
LIST OF FIGURE.....	xv
LIST OF ABBREVIATIONS	xvi
ABSTRACT.....	xviii
CHAPTER ONE	1
1 .INTRODUCTION	1
1.1. Background	1
1.2. Statement of problem	2
1.3. Research question and choice of a system	3
1.4. Objectives of the research	4
1.4.1. General objective	4
1.4.2. Specific objectives	4
1.5. Significance of the Study	4
1.6. Scope of the Study.....	5
CHAPTER TWO	6
2. LITERATURE REVIEW	6
2.1. Fluoride and Human Health	6
2.2. Fluoride Occurrence	7
2.2.1. Fluoride Occurrence in the World	7
2.2.2. Fluoride containing water occurrence in Ethiopia	8
2.3. Removal of Fluoride from Water	9
2.3.1. Precipitation and Coagulation.....	12

2.3.2. Membrane Filtration (Reverse Osmosis and Electro dialysis)	12
2.3.3. Adsorption method	13
2.4. Adsorbents for Fluoride Removal	13
2.4.1. Defluoridation by Bone Char.....	13
2.4.2. Defluoridation by nano alumina	17
2.5. Modified Bone char.....	20
2.6. Factors Affecting Defluoridation Process	22
2.6.1. PH	23
2.6.2. Contact Time	24
2.6.3. Effect of Initial Fluoride Concentration	24
2.6.4. Effect of Adsorbent Dose	24
2.7. Adsorption Isotherm.....	24
2.8. Adsorption Kinetics Model.....	27
2.9. The regeneration potential of modified bone char	28
CHAPTER THREE	30
3. MATERIALS AND METHODES	30
3.1. Materials and Chemicals	30
3.1.1. Materials	30
3.1.2. Chemicals and reagents	30
3.2. Methodology	30
3.2.1. Preparation of Bone char	30
3.2.2. Synthesis of Alumina Nanoparticle (Al ₂ O ₃ -NPs) by sol-gel method.....	32
3.2.3. Preparation of Nano alumina modified Bone char (NAMBC)	33
3.3. Analysis of Physicochemical parameters of alumina and BC.....	34
3.3.1. Moisture Content	34

3.3.2. Volatile Matter	34
3.3.3. Ash content	35
3.3.4. Fixed Carbon Content	35
3.4. Characterization of alumina nanoparticle (Al_2O_3 -NPs).....	35
3.4.1. Crystallographic structural analysis.....	35
3.4.2. Functional group analysis	36
3.4.3. Particle size analysis by PSDA	36
3.4.4. Thermogravimetric analysis (TGA)/ differential thermal analysis (DTA).....	37
3.5. Characterization of Bone char (BC) and Nano alumina modified bone char (NAMBC) ...	37
3.5.1. pH at Potential of Zero Charge (pHpzc)	37
3.5.2. Crystallographic structural analysis.....	37
3.5.3. Functional group analysis	38
3.5.4. BET Analysis	38
3.5.5. Thermogravimetric analysis (TGA) /differential thermal analysis (DTA).....	38
3.6. Preparation of Adsorbent Solution.....	38
3.7. Determination of Adsorption Capacities	38
3.8. Effect of Parameters on Fluoride Removal Efficiency of NAMBC	39
3.8.1. Effect of pH	40
3.8.2. Effect of Contact time.....	40
3.8.3. Effect of adsorbent dose	40
3.8.4. Effect of initial fluoride concentration	40
3.9. Adsorption isotherms model	40
3.10. Adsorption kinetics model	41
3.11. NAMBC regeneration	42
3.12. Characterization of selected representative groundwater.....	43

CHAPTER FOUR.....	45
4. RESUT AND DISCUSSION.....	45
4.1. Effect of pyrolysis temperature and time on removal efficiency of BC	45
4.2. NAMBC for fluoride removal.....	47
4.3. Physicochemical analysis of BC and alumina.....	48
4.4. Characterization of Al ₂ O ₃ -NPs.....	50
4.4.1. Crystallographic structural analysis of Al ₂ O ₃ -NPs.....	50
4.4.2. Functional group analysis of Al ₂ O ₃ -NPs.....	54
4.4.3. Particle size analysis for Al ₂ O ₃ -NPs.....	55
4.4.4. Thermogravimetric analysis for Al ₂ O ₃ -NPs.....	56
4.5. Characterization of BC and NAMBC	57
4.5.1. pH at Potential of Zero Charge (pHpzc) determinations for NAMBC	57
4.5.2. Crystallographic structural analysis of BC and NAMBC.....	58
4.5.3. Functional group analysis of BC and NAMBC	63
4.5.4. BET analysis of BC and NAMBC.....	65
4.5.5. TGA/DTA analysis	65
4.6. Parameter effects on fluoride removal	66
4.6.1. Effect of pH	66
4.6.2. Effect of contact time.....	68
4.6.3. Effect of adsorbent dose	69
4.6.4. Effect of initial fluoride concentration	70
4.7. Experimental Result on Adsorption Isotherm.....	72
4.8. Adsorption kinetics model	74
4.9. Comparison with other adsorbents	77
4.10. Regeneration of the NAMBC	78

4.11. Application on real water sample	80
CHAPTER FIVE	81
5. CONCLUSION AND RECOMMENDATION	81
5.1. Conclusion.....	81
5.2. Recommendation.....	82
REFERENCE.....	83
Appendix.....	92
Appendix A: Colors of treated fluoride water	92
Appendix B: Proximate Analysis of bone char and alumina	93
Appendix C: Particle size analysis (PSA), particle size distribution of Al ₂ O ₃ -NPs	95
Appendix D: characterization of real water	97
Appendix E: Thermal analysis of alumina and bone	98
Appendix F: BET analysis of BC and NAMBC	99

LIST OF TABLE

Table 2. 1: Fluoride concentration (mg/L) in 10 Rift Valley and 2 highland lakes	9
Table 2. 2: Advantage and disadvantage of various defluoridation technique.	10
Table 2. 3: Fluoride removal capacity of different defluoridation techniques	12
Table 2. 4: The effect of charring temperature and residence time on the bone char fluoride uptake	15
Table 2. 5: Methods for synthesis nano alumina for defluoridation	18
Table 2. 6: Removal capacity and experimental conditions for fluoride removal on modified bone char.....	21
Table 2. 7: Adsorption capacities and other parameters for the removal of fluoride by raw bone char and modified bone char.	23
Table 2. 8: Reported isotherm models relevant to BC adsorbents.....	25
Table4. 1: Effect of Charring Temperature and Time of Bone char on its Fluoride Removal Efficiency.....	45
Table4. 2: The different ratio of bone char (M) and Al ₂ O ₃ -NP (N) and their percentage removal of fluoride.....	47
Table4. 3: The proximate analysis of BC and alumina.....	48
Table4. 4: Crystalline size and d-spacing of alumina nanoparticle	52
Table4. 5: Particle size analysis of Al ₂ O ₃ analyzed by PSDA	55
Table4. 6: Experimental data for determination of zero point charge	57
Table4. 7: Crystalline size and d-spacing of BC and NAMBC	60
Table4. 8: Effect of pH on fluoride removal efficiency.....	67
Table4. 9: The effect of contact time on % fluoride removal	68
Table4. 10 : The effect of adsorbent dose on fluoride removal efficiency	69
Table4. 11 : The effect of initial fluoride concentration on fluoride removal efficiency	71
Table4. 12: Langmuir's (C _e Vs C _e /q _e) and Freundlich's (logC _e Vs logq _e) adsorption isotherm data	72
Table4. 13: Langmuir and Freundlich isotherm model parameters describing the NAMBC fluoride adsorption at a constant adsorbent dose of 2 g and contact time of 6 hr.	73

Table4. 14: Kinetic data obtained by varying the contact time using a constant adsorbent dose of 2 g NAMBC, and 10 mg/L of fluoride concentration	74
Table4. 15: Adsorption kinetic parameters for pseudo-first-order kinetics and pseudo-second-order kinetics.....	77
Table4. 16: Comparison of uptake capacity of NAMBC with other adsorbents	78
Table4. 17: number of cycle of regenerated NAMBC	79

LIST OF FIGURE

Figure 3. 1: Experimental set up for the synthesis of bone char	31
Figure 3. 2: Experimental setup for the synthesis of alumina nanoparticle	32
Figure 3. 3: experimental set up for nano alumina modified bone char	33
Figure 3. 4: experimental setup to determine residual concentration of fluoride	39
Figure 3. 5: experimental setup for NAMBC regeneration	43
Figure 4. 1: Fluoride removal percentage of bone char after different charring condition	46
Figure 4. 2: Fluoride removal efficiencies at various bone char to alumina ratio	48
Figure 4. 3: XRD pattern of alumina (a) at 800 °C and (b) at 900 °C.....	50
Figure 4. 4: XRD pattern of alumina (a) at 1000 °C and (b) at 1200 °C.....	51
Figure 4. 5: FTIR spectrum of γ -Al ₂ O ₃ nanoparticle	54
Figure 4. 6: TGA/DTA curve for nitrate – citrate precursor gel.....	57
Figure 4. 7: Point zero charge of NAMBC composite.....	58
Figure 4. 8: XRD pattern of (a) BC and (b) NAMBC	59
Figure 4. 9: XRD pattern of BC (a) before adsorption and (b) after adsorption.....	61
Figure 4. 10: XRD pattern of NAMBC (a) before adsorption and (b) after adsorption	62
Figure 4. 11: FTIR pattern of BC and NAMBC	63
Figure 4. 12: FTIR pattern of NAMBC before and after adsorption	64
Figure 4. 13: TGA/DTA curve for raw bone	66
Figure 4. 14: pH effect on fluoride adsorption efficiency	67
Figure 4. 15: The effect of contact time on the percentage removal of fluoride	69
Figure 4. 16: The effect of adsorbent dose on the percentage removal of fluoride	70
Figure 4. 17: The effect of initial fluoride ion concentration on the percentage removal of fluoride using 2 g NAMBC and 2hr contact time	71
Figure 4. 18: Adsorption isotherms of NAMBC a) Langmuir Isotherm b) Freundlich Isotherm	73
Figure 4. 19: Adsorption kinetic models for NAMBC a) Pseudo-first-order kinetics b) Pseudo-second-order kinetics	76
Figure 4. 20: NAMBC regeneration experiment	79

LIST OF ABBREVIATIONS

Al ₂ O ₃ NP	Alumina Nano Particle
AC	Ash Content
ASTM	America Society for Testing and Materials
BC	Bone Char
BET	Brunauer-Emmett-Teller
DD	Donnan Dialysis
DTG	Derivative thermo gravimetric
ED	Electro Dialysis
FCC	Fixed Carbon Content
FTIR	Fourier-Transform Infrared Spectroscopy
MER	Main Ethiopian Riftvally
MC	Moisture Content
MNP	Magnetic Nano particle
NAMBC	Nano Alumina Modified Bone Char
NF	Nano Filtration
pH	potential of Hydrogen
PSA	Particle Size Analysis
RO	Reverse Osmosis
rpm	Revolution Per Minute
TGA	Thermogravimetric analysis
UF	Ultra Filtration
VM	Volatility Matter

WHO World Health Organization

XRD X- Ray Diffraction

ABSTRACT

Fluoride contamination in drinking water is a widespread problem affecting millions globally. Bone char (BC) is an inexpensive, natural material that has shown promise as an adsorbent for defluoridation. However, BC has limited adsorption property toward fluoride. The utilization of nano alumina effect was not well investigated. The main objective of this research was to enhance the fluoride removal capacity of bone char by modification with nano alumina. Cattle bone char synthesized by controlled pyrolysis and modified bone char with gamma alumina nanoparticle developed by sol-gel method were characterized by FTIR, XRD, TGA and BET analysis. Nano alumina used to produce a composite with bone char at ratios of 1:0, 1:1, 2:1, and 0:1. Moreover, bone char and modified bone char physicochemical properties were tested. The spent adsorbent could be regenerated using NaOH. The bone char was shown the highest fluoride removal of 84.2 % from a 10 mg/L fluoride solution. The 2:1 composite displayed the best performance with 97.3 % fluoride removal and the maximum adsorption capacity was 3.47mg/g. Characterization confirmed that fluoride adsorption occurred due to hydroxyapatite ion exchange in bone char and hydroxyl groups provided from nano alumina. Fluoride adsorption isotherm was well fitted by Langmuir isotherm model and the adsorption kinetic followed the pseudo-second-order model. Application of NAMBC was carried out on the real water containing 7.95 mg/L of fluoride. Despite the presence of co-existence ion and additional parameter in real water sample, fluoride concentration could be reduced to 1.3 mg/L (83.6 % removal), which was lower than World Health Organization (WHO) standard (1.5 mg/L). This research demonstrated the promise of bone char-nano alumina composites as low-cost and effective adsorbent for defluoridation from water.

Keywords: *Adsorption; Bone char; Fluoride removal; Groundwater; Nano alumina; Nano alumina modified bone char.*

CHAPTER ONE

1 .INTRODUCTION

1.1. Background

Water is the source of life and economic development. The quality of water resources has been declining and deteriorating in recent years. Fluoride (F^-) contamination in groundwater has been recognized as one of the most serious problems worldwide. Fluoride in nature mostly exists as combined state mainly including fluorite (CaF_2), fluoroapatite ($Ca_5(PO_4)_3F$), cryolite (Na_3AlF_6) and these were in contact with groundwater what provokes its dissolution under several chemical conditions. Fluoride-containing wastewater from electroplating, metal processing, electronic manufacturing sector and other industries could cause water pollution (He et al., 2020).

An estimated 200 million people who were exposed to groundwater containing fluoride concentrations above the World Health Organization (WHO) guideline value of 1.5 mg/L (World Health Organization, 2011). Elevated fluoride concentrations in water was widely available in areas of India, China, and the Rift Valley of Africa which includes the Main Ethiopian Rift Valley (MER). Human consumption of elevated fluoride concentrations is problematic due to the dental and skeletal fluorosis that often result from high fluoride intake (Brunson & Sabatini, 2014). Fluoride removal from drinking water could be achieved by chemical precipitation, adsorption, membrane and ion exchange (Nie et al., 2012).

Compared to the other technologies mentioned above, adsorption has been demonstrated as a practical method for removing excessive fluoride from water because of its cost effectiveness, ease of operation, high removal capacity, and ability to reuse the adsorbent. These characteristics encouraged researchers to continue to explore adsorbents for additional potential. This process has been used extensively by many researchers and has shown remarkable results (He et al., 2020). There is a wide choice of cost-effective adsorbents. Among many different types of adsorbent materials including activated carbon, cellulosic materials, zeolites, aluminum nanomaterials, biochars and bone char were commonly used (S. S. A. Alkurdi et al., 2019).

Bone char was considered to be one of the most recommended adsorbents in defluoridation since World Health Organization regarded bone char as the high-performance adsorbent of fluorine ion

in undeveloped regions (H. Li et al., 2014). The fluoride adsorption properties of bone char could be improved by the incorporation of metallic species on its surface. The modification of bone char with multivalent cations could change its surface chemistry enhanced its affinity for fluoride ions. This surface modification strategy has been extensively applied for the modification of other adsorbents used in water defluoridation such as activated carbon (Rojas-Mayorga et al., 2015). The aluminum can impregnate onto the surface of bone charcoal, improving the effect of the defluoridation (H. Li et al., 2014). Inspired by this reason, nano alumina modified bone char was developed to effectively defluoridation by adsorption.

This study aimed to synthesis nano-alumina modified bone char (NAMBC) to improve fluoride removal efficiency and defluoridation studies were carried out under various conditions (adsorbent dose, solution pH, contact time and initial fluoride concentration).

1.2. Statement of problem

About 25 countries around the world have been affected by fluorosis, while the number of fluorosis is alarming. Fluoride contamination in drinking water is a serious issue affecting many parts of the world. Excess fluoride consumption could lead to dental and skeletal fluorosis (He et al., 2020). In Ethiopia alone more than 8 million people, primarily in rural areas of the Main Ethiopian Rift, were at high risk due to regular exposure to fluoride-contaminated groundwater, the largest source of water for public consumption (Sani et al., 2016). Bone char, made from animal bones, has been investigated as an inexpensive adsorbent for removing contaminants from water. However, there were several limitations related to the use of bone char as an adsorbent.

Many researchers have reported successfully fluoride remediation using different adsorbents (He et al., 2020; Wajima et al., 2009). However, most of the commercially available adsorbents were derived from synthetic chemicals, which were non-biocompatible, expensive, and toxic. Besides, most of the adsorbents had lower fluoride removal efficiency (de Melo et al., 2018; Delgadillo-Velasco et al., 2017; Mondal et al., 2012; Shahid et al., 2020). This problem should be solved by utilization of non-toxic, and renewable adsorbents. Fluoride removal such as bone char (S. S. A. Alkurdi et al., 2020) and aluminum ion (García-Sánchez et al., 2013), have been studied previously. However, the efficiency of those adsorbents is lower due to the limited surface area and pore volume. Thus, the fluoride adsorption properties of bone char can be improved by the incorporation of metallic species on its surface. Reported research incorporated regenerating spent

bone char and recycling the material was very limited (Roba et al., 2023; Shahid et al., 2019). Most studies used bone char in batch tests without regenerating it. More work on bone char regeneration would make it more practical and cost-effective was required.

The fluoride adsorption properties of bone char could be improved by the incorporation of nano alumina on its surface. The doping of bone char with multivalent cations could change its surface chemistry enhancing its affinity for fluoride ions. Based on this reason, this work was aimed to investigate the defluoridation effect of modified bone char and finding out the mechanism of adsorption.

1.3. Research question and choice of a system

Research question: This proposal was designed to answer the following question:

- How does alumina modification affect the adsorption capacity and selectivity of bone char for contaminant removal from water?
- What is the optimal ratio of alumina to bone char to maximize adsorption capacity and selectivity?
- How does alumina modification influence the sorption kinetics and isotherms of bone char?
- What are the mechanisms by which alumina modification alters the surface chemistry of bone char to enhance its fluoride adsorption properties?
- How does the performance of alumina-modified bone char compare to other adsorbents?

Choice of a System: Based on the above research questions the choice of the system, methodology and characterization procedures were framed as follows:

- Bone char has shown promised as an adsorbent for removing excessive fluoride from drinking water. Its hydroxyapatite structure provides active sites for fluoride adsorption.
- Adding nano alumina could potentially enhance the adsorption capacity and selectivity of bone char for fluoride ions. The surface charge and OH functional group of alumina nanoparticles has main contribution to adsorption.

1.4. Objectives of the research

1.4.1. General objective

The main objective of this study was to investigate the removal of fluoride from water using nano alumina modified bone char.

1.4.2. Specific objectives

- Synthesis and characterization of bone-char using BET, XRD, FTIR and TGA
- Synthesis (using sol-gel method) and characterization of nano-alumina using XRD, FTIR, PSA and TGA
- Synthesis and characterization of surface modified bone-char (NAMBC) using BET, XRD and FTIR
- Conduct batch adsorption experiments to investigate the effect of operating parameters on the fluoride removal by NAMBC
- Investigate the adsorption isotherm and kinetics of the adsorption process of NAMBC
- Evaluate the regeneration potential of NAMBC

1.5. Significance of the Study

The significance of this study is comprised of both economy and environment. Since the adsorbent is going to be produced from bone, this study can be considered as one way of transforming a solid waste into useful material. Additionally this study demonstrated effective regeneration protocols to restore the adsorption capacity of bone char after use in water remediation. This shows studying regeneration and re-use provides crucial data on operational feasibility, economics, and environmental impacts of utilizing modified bone char for water remediation.

To our knowledge, the dispersion of gamma alumina nanoparticle into bone char has never been investigated. Therefore, this research demonstrating a new method to alter the surface chemistry and textural properties of bone char for defluoridation. Providing insight into how the addition of nano alumina affected critical performance factors like surface area, pore size distribution, and adsorption capacity for different adsorbate species. This expanded knowledge on tuning bone char properties. Generally, the significance of the research is devising a new approach for engineering bone char adsorbents using nano scale surface modification, and generating valuable knowledge to inform further optimization and applications of modified bone char materials.

1.6. Scope of the Study

The scope of the thesis work within the given time and resources include:

- Synthesis of alumina nanoparticle and conducting analysis such as TGA, FTIR, PSA (particle size analysis), and XRD analysis.
- Synthesis of BC and conducting analysis such as BET, FTIR, TGA and XRD analysis.
- Synthesis of NAMBC and conducting analysis such as BET, FTIR, and XRD analysis.
- Evaluating adsorption capacity and parameters (pH, adsorbent dose, contact time and initial fluoride concentration) for fluoride contaminants of interest under batch conditions.
- Elucidating the roles of surface area, surface complexation, in the adsorption behaviour of the modified sorbent.
- Using adsorption models to describe the experimental data. Deriving isotherms and rate equations.
- Developing effective regeneration procedures and assessing performance over multiple cycles.
- Using the modified bone char in real contaminated water sources to demonstrate proof-of-concept.

CHAPTER TWO

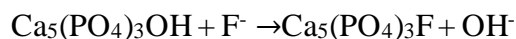
2. LITERATURE REVIEW

2.1. Fluoride and Human Health

Major fluoride exposure comes from drinking water and minor amounts from food stuffs and water based beverages contribute a significant fluoride concentration for total dietary intake (H. Liu et al., 2014). Depending on the level, fluoride can affect human health either positively or negatively. The strengthening of bones and prevention of tooth decay are two important fluoride benefits for humans (Gill et al., 2014). Fluoride has a crucial role in the mineralization of teeth and bone, fertility maintenance, activation of enzyme, and the production of blood cells. A small amount of F^- in diets reduced acid formation by preventing the bacterial breakdown of carbohydrates. The general health impact of F^- on humans include affected or damaged soft tissues, muscles, erythrocytes, gastrointestinal mucosa, ligaments, spermatozoa and thyroid glands; brittle bones; inferior growth; Alzheimer disease; pain; or impeded movement due to bony and dental lesions (Kabir et al., 2020). An Excessive amounts of fluoride in drinking water may cause irreversible demineralization of bone and tooth tissues, a condition called fluorosis, and long-term damage to the brain, liver, thyroid, and kidney (Yadav et al., 2018). Apatite, which is a mixture of more hydroxyapatite (HAP), $Ca_{10}(PO_4)_6(OH)_2$ and less fluoroapatite (FAP), $Ca_{10}(PO_4)_6F_2$ makes up the majority of the structural inorganic material in bones and teeth. F_2 and OH_2 are interchangeable in this structure. The parts of the apatite molecules which are FAP determine the properties of this hard tissue. At extremely low FAP ratios, teeth are easily soluble under acidic conditions, increasing the risk of dental carries. At higher FAP ratios, the solubility is reduced. However, too high a ratio causes dental fluorosis (Kaseva, 2006a).

Long-term intake of water with fluoride levels between 1.5 and 4.0 mg/L results in dental fluorosis. The teeth will turn dark and have a mottled appearance. Long-term consumption of water with fluoride levels between 4.0 and 10 mg/L produces skeletal fluorosis, and when water with fluoride levels over 10.0 mg/L is consumed, debilitating fluorosis may result. The science underlying the effects of fluoride on the skeletal structure both good and bad is based on potential ion exchange interactions between hydroxide and fluoride ions in calcium hydroxyphosphate, the primary

component of the skeleton. Fluoroapatite, a more acid-resistant structure, is produced when hydroxide ions are swapped out for fluoride ions (Thole, 2013).



The tooth enamel is shielded from acids from meals by fluorapatite, which is more resistant to acid damage than hydroxyapatite. It stops dental caries. However, excessive fluoride consumption could speed up the reaction and cause it to surpass hydroxide replacement,



This indicates that phosphate and fluoride ions engage in ion exchange. Calcium decafluoride, the resulting product, is an extremely hard and brittle substance that is inappropriate for the functions of the skeletal skeleton (Kaseva, 2006a; Thole, 2013).

Calcium intake through diet reduces the retention of fluoride in teeth and bones and has a detrimental impact on the interaction between calcium and fluoride. The percentage of calcium in vegetables, cereals and fruits are rich in calcium, while milk is known to be the richest source of calcium, therefore these food items considerably decrease the effect of fluorosis (Ofori et al., 2020).

2.2. Fluoride Occurrence

2.2.1. Fluoride Occurrence in the World

There are three belts with a high incidence of F^- . The first is dispersed along East Africa's Great Rift Valley from Eritrea to Malawi. The distribution of the second product comes from Turkey and goes through Iraq, Iran, Afghanistan, India, Thailand, and China, while the third product goes through America and Japan (Kabir et al., 2020).

Fluoride is frequently found in geological settings where there is volcanic activity and the presence of thermal waters. Low quantities of calcium and magnesium, high levels of sodium and bicarbonate ions, and high pH are all proxy markers of high fluoride levels in groundwater. Fluoride beds, which cover sections of Iraq, Iran, Syria, Turkey, Algeria, and Morocco, as well as the East African rift system, which stretches from the Jordan Valley down to Sudan, Ethiopia, Uganda, Kenya, and Tanzania, are places with high concentrations of fluoride in groundwater. There are high fluoride areas in other parts of the world (Thole, 2013). Throughout 200 million

people rely on water sources with excessive fluoride, which has detrimental effects on their health. Fluoride is present in water supplies in more than 25 nations throughout the world (Kimambo et al., 2019).

Fluorine, which is naturally present as CaF_2 , is extremely reactive. In crystals like topaz ($\text{Al}_2\text{SiO}_4(\text{F},\text{OH})_2$), fluorite (CaF_2), fluoroapatite ($\text{Ca}_5(\text{PO}_4)_3\text{F}$), cryolite (Na_3AlF_6), and phosphorite ($\text{Ca}_5(\text{PO}_4)_3\text{OH}$), it is a necessary component. The land, water, and environment all contain fluoride. Through the weathering of rocks, precipitation, or waste runoff, it gets into the soil. Unless surface waters are contaminated by outside sources, they typically don't have fluoride concentrations beyond 0.3 mg/L. Though drinking water is the major contributor (75–90% of daily intake), other sources of fluoride poisoning are food, industrial exposure, drugs, cosmetics, etc. (Maheshwari, 2006).

2.2.2. Fluoride containing water occurrence in Ethiopia

The great African Rift Valley extends from Syria and Jordan in the Middle East to Mozambique. It is connected to elevated groundwater fluoride levels. Deep wells are the primary drinking sources of fluoride in the semiarid Rift Valley regions. The fluoride levels of the deep wells in the Rift Valley, even within the same region, vary significantly. This is most likely related to the varied regions of the Rift Valley's climatic circumstances, geophysical, and geochemical properties. Consumption of waters from deep wells in the Rift Valley has led to endemic fluorosis in several Northeast and East African countries, notably Ethiopia, Sudan, Tanzania, Kenya and Uganda (Tekle-Haimanot et al., 2006).

According to studies, up to 8 million of the 10 million residents of the Main Ethiopian Rift, or MER, in the Ethiopian Rift Valley are at danger due to regular exposure to high quantities of naturally occurring fluoride (Bianchini et al., 2020; Kimambo et al., 2019). As shown in Table 2.1 (Tekle-Haimanot et al., 2006) list occurrence of fluoride in water around different area of Ethiopia countries.

F is typically found in groundwater that has been exposed to volcanic rocks, which are common in high-temperature geothermal settings (Bianchini et al., 2020). The rifting processes in the MER have created a variety of volcano-tectonic depressions, which has favored the growth of closed lacustrine basins in the rift floor. Clastic particles from rock weathering were also transported and redeposited in fluvio-lacustrine sedimentary facies (Bianchini et al., 2020). The MER lakes are

separated into three groups: the northern Koka, Beseka, Gemeri, and Abe lakes; the centre Ziway, Langano, Abijata, and Shala lakes; and the southern Awasa, Abaya, and Chamo lakes. High-temperature thermal springs frequently surround the MER lakes; their prevalence is caused by the geothermal circulation of hot fluids, most likely as a result of the persistence of magmatic systems at shallow depths(Bianchini et al., 2020).

Table 2. 1: Fluoride concentration (mg/L) in 10 Rift Valley and 2 highland lakes

Lakes	Fluoride (mg/l)
Shala	264
Abijata	202.4
Beseka	32.2
Langano	12.89
Chamo	8.4
Awasa	8.1
Abaya	7.2
Afrera chew	3.9
Ziway	1.7
Gamari	2.8
Alemaya(highland near harer)	1.1
Tana(highland)	1.0

2.3. Removal of Fluoride from Water

Fluoride removal is an important topic in water research because of the rising exposure to it and the health risks it brings with it. The construction and use of safe water sources, the reduction/control of anthropogenic F- producing sources, and the application of appropriate defluoridation procedures are the alternate methods for reducing F- concentrations in water. Defluoridation is the most effective method for F-remediation when substitute sources are unavailable (Dhillon et al., 2017).

When no alternative source is available, defluoridation of drinking water is the only workable solution to the issue of excessive fluoride in drinking water. Extensive study has been done on various strategies for removing fluoride from water and wastewater in the years after it was known that fluoride was the cause of fluorosis. These procedures are based on the principal of adsorption, ion-exchange, electrolytic defluoridation, electro dialysis, precipitation–coagulation, membrane separation process, etc.(Maheshwari, 2006). Although various conventional methods, are used for defluoridation, most have drawbacks in efficiency, cost-effectiveness, or other limitations, such as the generation of secondary pollutants and the requirement of sludge handling. The different techniques for F⁻ removal are discussed in the following sections, and the points of interest and restrictions regarding those techniques are summarized in Table 2.2.

Table 2. 2: Advantage and disadvantage of various defluoridation technique.

Technology	Advantages	Disadvantages	Ref
Coagulation/precipitation: calcium hydroxide; aluminum hydroxide	High-performance, readily available chemical	Costly, efficiency depends on pH and the presence of co-ions in the water, pH adjustments and readjustments are necessary, the residual aluminum concentration is elevated, sludge is formed with a high concentration of toxic aluminum fluoride complex and a high concentration of retained water (sludge dewatering is necessary before disposal)	(Kalaitzidou et al., 2020)
Membrane filtration: reverse osmosis; nanofiltration	High efficiency; remove eliminate	High initial costs, high ongoing costs, and the production of toxic	(Alhassan et al., 2021)

	additional contaminates		
Electrochemical treatments: dialysis; electro-dialysis; electro- coagulation	High efficiency and selectivity	High upfront costs for installation and upkeep	(Zhu et al., 2007)
Ion-exchange: Strong basic anion-exchange resin with quaternary ammonium functional groups	High efficiency	Costly, prone to interference by ions (sulphate, phosphate, chloride, bicarbonate, etc.), replacement of media after numerous regenerations, used media present toxic solid waste, regeneration creates toxic liquid waste, efficiency highly pH- dependent	(Thole, 2013)
Adsorptive materials: activated alumina; activated carbons; other natural and synthetic adsorbents	Greater accessibility, affordability, ease of use, and the availability of a wide of adsorbents	High efficiency frequently necessitates pH adjustments and readjustments, and several common water ions can prevent fluoride from being absorbed.	(Yadav et al., 2018)

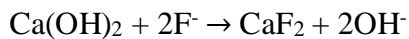
As shown on Table 2.3 these technologies have shown certain degrees of success in fluoride removal; however, they have their own capacity in treating fluoride contaminated groundwater.

Table 2. 3: Fluoride removal capacity of different defluoridation techniques

Defluoridation techniques	Materials	Defluoridation capacity (%)	Ref.
Membrane filtration	gold nanoparticles (AuNPs)	94.8	(He et al., 2014)
Electro chemical	aluminum anode and cathode	90	(Pulkka et al., 2014)
coagulation	inorganic polymeric coagulant(alum)	56.7	(Solanki et al., 2021)
Adsorption	Bone char	97	(Chatterjee, Mukherjee, et al., 2018)

2.3.1. Precipitation and Coagulation

The Nalgonda technique is a widely known precipitation-coagulation defluoridation method. Coagulant is added as part of the precipitation process to help the sparingly soluble fluoride salts crystallize into fluoroapatite. The procedure involves rapidly mixing the raw water with the specified amounts of lime, alum, and bleaching powder, followed by flocculation, sedimentation, filtration, and disinfection (Zhu et al., 2007). The two most often used coagulants are lime and alum. Water that contains fluoride ions reacts with newly added coagulants to generate complex precipitates ($\text{Al}(\text{OH})_3 \cdot x\text{F}_x$, CaF_2), which are then removed by precipitation/filtration (Kabir et al., 2020). Fluoride is precipitated as insoluble calcium fluoride when lime is added. Following this reaction, fluoride precipitate is produced:



2.3.2. Membrane Filtration (Reverse Osmosis and Electro dialysis)

Membrane is a substance that performs selective separation. Membrane separation, which includes reverse osmosis, nanofiltration, dialysis, and electro-dialysis, is the process of selectively separating membranes to separate, purify, and concentrate various feed liquid components

(He et al., 2020). Reverse osmosis (RO), Nano filtration (NF), ultrafiltration (UF), electro dialysis (ED), and Donna dialysis (DD) are some of the membrane technologies that have been industrially established over time in a variety of fields, including medicine and the chemical industries. However, their application for removing inorganic anions like fluorides and nitrates from drinking water has not been fully explored(Kabir et al., 2020).

With the help of a potential gradient and a semipermeable membrane, ions are separated electrochemically during electro dialysis. The fluoride ions can pass through the membranes made of ion exchange polymers due to the electrical charges on them. The electro dialysis membranes used for fluoride treatment have the ability to only transport negatively charged fluoride ions while rejecting other ions Maheshwari, (2006).

Pressure is applied to the feed water during the reverse osmosis process in order to push the fluoride-contaminated salts through a semipermeable membrane and out the other side. The amount of pressure exerted on the membrane depends on how big the contaminants are that are left behind(Kabir et al., 2020).

2.3.3. Adsorption method

The raw water used in the adsorption process is run through a bed of defluoridation material. Fluoride is retained in the substance through ion exchange, chemical, or physical processes. After some time of use, the adsorbent becomes saturated and needs to be regenerated (Hu et al., 2017).

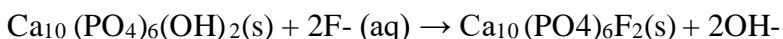
The various adsorbents used to remove fluoride include activated alumina, carbon, bone charcoal, activated alumina coated silica gel, calcite, activated saw dust, magnesia, serpentine, tricalcium phosphate, activated soil sorbents, carbion and other synthetic ion exchange resins(Hu et al., 2017).

2.4. Adsorbents for Fluoride Removal

2.4.1. Defluoridation by Bone Char

Bone char is charcoal made by heating animal bones under controlled conditions of temperature, time, and oxygen content. Since the 1940s, bone char has been employed as a defluoridation technique. Bone char's application in water treatment facilities in industrialized nations is no longer necessary because it is outdated. Bone char's ability to remove fluoride is thought to be due to the presence of hydroxyapatite in its composition. Fluoroapatite and hydroxyl ions are created when hydroxyapatite and fluoride ions combine (Thole, 2013). Because OH⁻ and F⁻ in HAP are

interchangeable, hydroxyapatite from the structure of bone char is thought to play a significant role in the fluoride adsorption process (Kaseva, 2006a).



The main component of bones and enamel is hydroxyapatite, and when fluorides are present, the hydroxides are switched out for fluoride, creating a more insoluble fluoroapatite. In addition to being readily available, bone char is a natural adsorbent with strong fluoride adsorptive ability even at neutral pH. The structural inorganic component of bones and teeth has an interchangeable unit of F_2 and $(\text{OH})_2$ (Kaseva, 2006a).

2.4.1.1. Synthesis of bone char

By calcination bones in a low-oxygen atmosphere (also known as partial calcination) or by pyrolysis bones in an oxygen-free environment, bone char can be created. To create bone char for water defluoridation, thermal procedures with restricted air present at 500–600 °C are frequently utilized (Albertus et al., 2000; Moreno-Piraján et al., 2010). The bone charcoal (BC) residue is the result of a pyrolysis process according to the following process (Giraldo, 2011):

Animal bones $\xrightarrow{\text{pyrolysis}}$ bone chars residue + oil + steam + liquor ammonia

The investigations on bone char synthesis are shown in Table 2.3. These studies seldom address the type and origin of bone residues and pyrolysis condition (temperature, residence duration, gas environment, and heating rate), which might vary the physiochemical properties of bone char. Regarding the impact of the synthesis conditions on the adsorption characteristics of bone char for fluoride removal from water, several research that are currently available in the literature have found differences and various outcomes. For example, Eli Dah(Dahi, 2015) established how well the white, grey, and black bovine bone chars—obtained through thermal treatments at 350°C (black), 450°C (grey), and 600°C (white)—removed fluoride. According to this investigation, black bone char had the best adsorption abilities. In order to pyrolyze the raw material into a porous substance, carbonization of crushed animal bones involves heating a carbonaceous precursor to temperatures mostly above 500 °C and below 700 °C in a low oxygen environment (S. S. A. Alkurdi et al., 2019). In such a process, the volatile matter will partially evolve from the carbonaceous precursor. The physical characteristics of the bone char will change if the pyrolysis temperature is raised further beyond 700 °C. (Rojas-Mayorga et al., 2015) revealed that a gradual

color change of the bone to white was observed after increasing the temperature from 650 °C up to 1000 °C, indicating the full removal of the organic materials in the bone char structure. Therefore, the functional groups degrade at that high pyrolysis temperature, decreasing the effectiveness of water defluoridation.

Pyrolysis temperature is a critical operating parameter for the synthesis of bone char for fluoride removal from water. Specifically, this temperature has a major effect on the fluoride adsorption properties of bone char due to the dehydroxylation process of the hydroxyapatite contained in this adsorbent.

As can be shown in Table 2.4, bone char produced under the N₂ environment has a higher fluoride adsorption rate than bone char produced under air environment. When bone char is being created, N₂ creates an inert environment that helps prevent oxidation and corresponding changes in the crystallinity of hydroxyapatite. Low adsorption in the case of an air environment may be attributed to the bone char's crystallinity, which is brought on by the dehydroxylation of hydroxyapatite and the loss of elemental carbon (Shahid et al., 2020).

Fluoride adsorption capacities of the bone char samples obtained at different pyrolysis conditions of the experimental design are reported in Table 2.4.

Table 2. 4: The effect of charring temperature and residence time on the bone char fluoride uptake

Bone char	Pyrolysis condition				Bone char performance	Reference
	Temperature(°C)	Time(hr.)	Heating rate, °C/min	under N ₂ environment or air environment		
	650	2	10	N ₂ environment	6.51	
		4			6.63	

Cow bone char	700	2 4	10	N ₂ environment	7.32 7.16	(Rojas-Mayorga et al., 2013)
	800	2 4	10	N ₂ environment	6.71 6.57	
	900	2 4	10	N ₂ environment	3.03 3.01	
	1000	2 4	10	N ₂ environment	1.24 1.25	
Chemical treated bone char	300	1	60	Air environment	1.2	(Chatterjee, Jha, et al., 2018)
	400	1	60	Air environment	4.3	
	550	1	60	Air environment	8.3	
	700	1	60	Air environment	3.2	
	800	1	60	Air environment	3	
	550	2	60	Air environment	5	
	550	4	60	Air environment	12.5	
	550	6	60	Air environment	8.3	
Cattle bone char	450	3	12	Air environment	1.4	(Roba et al., 2023)
Cattle bone	350		15	Air environment	3.63	

	400		15	Air environment	3.02	(Shahid et al., 2019)
	500		15	Air environment	2.94	
	600		15	Air environment	2.08	
	700		15	Air environment	0.16	
Sheep leg bones	500	1	10	N ₂ environment	2.5	(S. S. A. Alkurdi et al., 2020)
		2			1.7	
	650	1	10	N ₂ environment	2.33	
		2			1.5	
800	1	10	N ₂ environment	1.25		
	2			1.2		
900	1	10	N ₂ environment	1.1		
	2			1.1		

2.4.2. Defluoridation by nano alumina

Metal oxides, particularly those made of iron and aluminum, have been found to be excellent sorbents for the removal of anions from aqueous solutions because, in general, they have positive surface charges, which attract negatively charged anions by electrostatic attraction (Kumar et al., 2011).

Water treatment using nanomaterials is quickly increasing in relevance. Nano-materials are a desirable alternative for water filtration because of characteristics including increased reactivity, increased surface area, and self-assembly. Many nanoscale materials, including alumina, magnesium oxide, hydroxyapatite, and composites, have been investigated for water defluoridation. Despite the commercial availability of nanomaterials, synthesized adsorbents can be better adapted for a particular need (Shivaprasad et al., 2018).

As shown, on Table 2.5 alumina was widely utilized to remove fluoride from water. Aluminum ions were thought to be potential acid ions. Conventionally, the defluoridation of water has been

accomplished using a variety of micron-sized alumina-based compounds. Additionally, several adsorbents based on aluminum elements, such as carbon nanotubes supported by amorphous alumina, (Y.-H. Li et al., 2001), nano aluminum oxide hydroxide(Wang et al., 2009), nano Magnesium aluminum mixed Oxide (Shukla et al., 2010) have also been prepared and used for defluoridation of water by many researchers.

In this perspective, it was thought desirable to test the potential of nano-alumina for fluoride removal as containing compounds have a high affinity toward fluoride.

2.4.2.1. Synthesis of nano alumina

Physical or chemical methods can be used in conventional Al₂O₃ NP synthesis. Chemical procedures include hydrothermal, vapor phase reaction, co-precipitation, combustion, sol gel processes, and kaolin leaching; some physical methods include mechanical milling, laser ablation, and flame spray. However, sol-gel method is preferred for obtaining a highly pure nano alumina particles (Dubey et al., 2017; Singh et al., 2016; Suhasinee Behera et al., 2017). Researchers use different method to produce alumina successfully in their nano sized range for defluoridation purposes (Table 2.5).

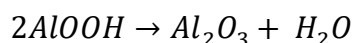
Table 2. 5: Methods for synthesis nano alumina for defluoridation

S.N	Preparation materials	Method	Result(q _e (mg/g))	Ref.
1	aluminum nitrate (precursors), urea (fuel), CTAB (surfactant)	Surfactant-assisted solution combustion method	32	(Chinnakoti et al., 2017)
2	Aluminum nitrate and ammonia solution(precursors), Starch solution(surfactant)	Modified sol-gel method	0.72	(Belekar & Dhoble, 2018)

3	Al(NO ₃) ₃ ·9H ₂ O(precursor), ammonium carbonate(fuel), SDBS(surfactant)	Sol-gel	2.55 and 5.66 for pure and modified nano alumina respectively.	(Shivaprasad et al., 2018)
4	aluminum isopropoxide	Sol-gel	14	(Singh et al., 2016)

The method known as "sol-gel" entails creating an amorphous gel from a precursor solution. Metal alkoxides are frequently used as the starting material in this molecular precursor-based approach. Better uniformity and purity from the raw materials, lower preparation temperatures that conserve energy, and the capacity to create novel compositions are some benefits of the sol-gel process (Mirjalili et al., 2010).

Aluminum alkoxide is hydrolyzed in water to generate boehmite (AlOOH) as gel, which is then calcined at 400–800°C to form γ -Al₂O₃ after releasing one molecule of water according to the following reaction:



Alkoxide is typically hydrolyzed in a non-aqueous (alcohol) or aqueous (water) solvent. It is inexpensive to use water as a solvent, and open systems can be used to carry out hydrolysis reactions (Singh et al., 2016).

This intriguing ceramic material can be divided into two main groups based on the arrangement of oxygen anions: face-centered cubic (fcc) and hexagonal close-packed (hcp). In contrast, the Al₂O₃ structures based on hcp packing are α (trigonal), κ (orthorhombic), and χ (hexagonal). The Al₂O₃ structures based on the fcc lattice include γ , η (cubic), θ (monoclinic), and δ (either tetragonal or orthorhombic). The other phases, known as transition phases, are thermally unstable at room temperature with the exception of α and γ -alumina (Santos et al., 2000). Among them, γ and α alumina have been the center of attention. Because of its high surface area, good adsorption

potential, and superior mass transfer capacity, gamma alumina (γ - Al_2O_3) is of particular importance (Dubey et al., 2017; Tabesh et al., 2018). For this phase transition metal precursor to chelating agent molar ratio and sintering temperature has important role. (J. Li et al., 2006; Suhasinee Behera et al., 2017) Investigations were made into the molar ratio of citric acid to metal nitrate (C/N) in the sol-gel process, which was crucial in influencing the morphology and phase transition of alumina. According to their findings, the phase transition from γ - to α - Al_2O_3 was found to be more favorable with increasing molar ratios of C/N, but the precursor with C/N = 1 produced an ultrafine γ - Al_2O_3 powder that was comparatively well dispersed. The C/N ratio is typically kept at one in the traditional citrate sol-gel method. When C/N 1, combustion takes place, and ash instead of gel is produced. Higher values (C/N > 1.5) were cited as contributing to the degrading powder characteristics. (Farahmandjou, 2015; Rajaeiyan & Bagheri-Mohagheghi, 2013b; Tabesh et al., 2017) examined the sol gel process's sintering temperature, which was crucial in phase transition. The findings demonstrated that the γ phase forms around 600 °C and the phase changes $\gamma \rightarrow \alpha$ Al_2O_3 during calcination at temperatures more than 1000 °C. Among all the metastable polymorphic forms of alumina that exist, the highly stable phase is α -alumina and the less stable form is γ -alumina. Controlling the shape and size of the material is the major goal of all preparation techniques. Adjusting experimental conditions, adding cationic, anionic, and nonionic surfactants, as well as various structure-directing agents, are used to accomplish these results (Avinash Chunduri et al., 2014).

2.5. Modified Bone char

By increasing the pore volume, surface area, or variety of pore sizes available to the adsorbent, or by changing the surface functional groups in a way that makes the adsorbent more selective towards particular contaminants, appropriate activation methods can increase the adsorption capacity of carbonaceous materials. Examinations of bone char following various modification techniques, however, show that there have been no appreciable increases in the surface area (Delgadillo-Velasco et al., 2017). Thus, considerations regarding improvement in adsorption capacity of bone chars are mostly related to altering the functional groups on the surface. Table 2.6 summarizes the effect of different modification methods and experimental conditions on the removal capacity of F^- on modified bone char samples.

Bone char alteration can enhance the char absorptivity of F, however the degree of enhancement varies depending on the element. Due to their small size and high electronegativity, fluoride ions in solution was strongly attracted to multivalent metal ions (such as aluminum, iron, zinc, etc.) (Tchomgui-Kamga et al., 2010). Thus, the difference in the electronegativity of the used multivalent metal ions are the main reason behind their higher removal capacity of some metal ions. For instance, the higher difference in electronegativity between fluoride and Al (III) that resulted in higher removal capacity of fluoride ions from solution with Al(III) coated bone char.

Table 2. 6: Removal capacity and experimental conditions for fluoride removal on modified bone char

Modified bone char	Fluoride removal(mg/g)	Initial concentration(mg/l)	Surface area(m ² /g)	Pore volume (cm ³ /g)	Ref.
HCl washed cow BC	6.2	10	138.8	0.308	(Nigri et al., 2017)
carbonized natural bone meal (CBM)	14	–	–	–	(Chatterjee, Jha, et al., 2018)
Carbonized bone meal treated with aluminum sulfate and calcium oxide	150	–	–	–	(Chatterjee, Mukherjee, et al., 2018)
Aluminum sulfate modified cattle BC	31	10-100	110	0.233	(Rojas-Mayorga et al., 2015)

Cattle BC modified with Ce ⁺⁴	13.6	50-300	–	–	(Zúñiga-Muro et al., 2017)
Ag doped thermally treated BC	1.28	20	59	0.109	(Delgadillo-Velasco et al., 2017)

The relative quantities and qualities of a composite material's constituent parts determine its properties. Chemical bonding, Van der Waals forces, and mechanical interlocking hold the composite materials together. Via the interface, a high level of mechanical characteristics are provided by good bonding (adhesion) between the matrix and dispersed phase. Additionally, interfaces are critical in redox reactions, heterogeneous catalysis, adsorption, and many other processes involving electron transfers. Composites typically serve as adsorbents, electrochemically active substances, catalysts, and photo catalysts in this application area (Fouda et al., 2016).

With all this in mind, it stands to reason to investigate a new composite material fabricated from; bone char and nano alumina for defluoridation.

2.6. Factors Affecting Defluoridation Process

Apart from the mineral and chemical composition of the adsorbent affecting adsorption properties, the solution parameters play a major role in determining the performance of the adsorbent in an adsorptive system. The effect of pH, contact time, adsorbent dose and adsorbate concentration on uptake of fluoride ion from aqueous media was investigated on different adsorbents. As shown on Table 2.7 many researchers study effect of adsorption parameters.

Table 2. 7: Adsorption capacities and other parameters for the removal of fluoride by raw bone char and modified bone char.

Bone char	Factors				Effect	Reference
	PH	Dose of adsorbent(g/l)	Fluoride initial concentration(mg/l)	Contact time(hr.)	Fluoride up take(%)	
Chemical treated bone char	6.1	5	10	1	15%	(Chatterjee, Mukherjee, et al., 2018)
Cuttlefish bone char	7.2	15	5	1	80%	(Ben Nasr et al., 2011)
Al doped bone char	-	10	1	1	97%	(Zhu et al., 2007)
cow bone	7.6	100	1-6	10	80%	(Smittakorn et al., 2010)
Cattle bone	8.9	2	11.72	2	91.2%	(Roba et al., 2023)
		2		1:30	89.4%	
		1.5		2	85.3%	

2.6.1. PH

The pH value of the solution plays an important role in the whole adsorption process and particularly on adsorption capacity. It would affect both aqueous chemistry and surface binding sites of adsorbents. The pH intern depends on the charge on the adsorbent surface. If the adsorbent surface is negatively charged, at lower pH, hydrogen ion (H^+) neutralizes the negatively charged adsorbent surface, thereby reducing hindrance to the diffusion, and better adsorption. If the surface charge of the adsorbent is positively charged, the H^+ compete effectively with the cations of the solution causing a decrease in the amount of metal ion adsorbed (Ushakumary 2013). The solution

of pH changes as fluoride adsorption progressed, necessitating HNO₃ or NaOH addition of solutions to keep the pH constant. During defluoridation of drinking water using bone char the solution pH always increases during the adsorption at pH ≤ 7, but always diminishes slightly at pH ≥ 8. This observation indicates that H⁺ ions were adsorbed on the bone char at pH ≤ 7 causing an increase in the pH while the H⁺ ions were released at pH ≥ 8 causing a decrease in the pH of solution. This behavior is due to the amphoteric character of the bone char since it has acidic and basic sites (Medellin-Castillo et al., 2007).

2.6.2. Contact Time

The amount adsorbed on to the adsorbent is in a state of dynamic equilibrium with the amount desorbed from the adsorbent. The time required to attain this state of equilibrium is termed as equilibrium time. Contact time is the time for which fluoride is in contact with the adsorbent. In adsorption fluoride gets adsorbed in the vacant spaces in the adsorbent, so when the spaces are filled and no more fluoride can go inside, the adsorption stops and it is possible also that desorption may take place (Mall et al., 2005).

2.6.3. Effect of Initial Fluoride Concentration

Concentration is the abundance of constituent or solute in a known volume of a mixture (Plush & Hayball, 2017). Fluoride removal efficiency decreases with an increase in fluoride concentration. This is due to free sites on the adsorbent surface in lower initial fluoride concentrations (Dehghani et al., 2017).

2.6.4. Effect of Adsorbent Dose

Adsorbent dose is the mass of adsorbent prepared for adsorption for a specific amount of adsorbate. It has the greatest regression coefficient and the greatest effect on fluoride removal. An increase in the adsorption with an increase adsorbent dosage can be attributed to a greater surface area and more available adsorption sites at higher adsorbent dosage (Dehghani et al., 2017).

2.7. Adsorption Isotherm

An equilibrium model that is used to characterize equilibrium behavior by describing the amount of adsorbate adsorbed as a function of gases or liquids at a constant temperature is called an isotherm (G. Liu et al., 2015). Adsorption mechanisms include chemical adsorption which involves the formation of chemical bonds between the contaminant and adsorbent, physical adsorption due

to van der Waals attraction, and ion exchange. The adsorption data can be described by isotherm models, which are critical for designing an adsorption system. Furthermore, models of adsorption isotherms help predict the mechanisms of adsorption and estimate the maximum adsorption capacity, which is important in evaluating adsorbent performance (Hart et al., 2023). Table 2.8 summarizes some isotherm models applicable to BC and alumina adsorbents for the removal of contaminants from wastewater. Whereas, Langmuir and Freundlich adsorption isotherm is the most customary used models (Al-ghouti & Da, 2020).

Table 2. 8: Reported isotherm models relevant to BC adsorbents.

Adsorption isotherm model	Remarks	Ref.
Freundlich isotherm(linear form) $\log q_e = \log K_f + \frac{1}{n} \log C_e$	<ul style="list-style-type: none"> ✓ Adsorbents' surface are heterogeneous, and the distribution of active sites and their energies is exponential. ✓ The Freundlich equation does not predict an adsorption maximum, which is one of its major limitations. Second, the equation has no theoretical basis, purely empirical one. ✓ The Freundlich isotherm model is used to describe the adsorption of molecules arranged in multilayers with interaction between them 	(Sawangjang et al., 2021; Workeneh et al., 2019)

<p>Langmuir isotherm(linear form)</p> $\frac{c_e}{q_e} = \frac{1}{bq_{max}} + \frac{C_e}{q_{max}}$	<ul style="list-style-type: none"> ✓ The Langmuir isotherm model assumes that adsorption occurs at homogeneous sites within an adsorbent (i.e. all sites are equal, resulting in equal adsorption energies). ✓ Adsorption proportional to the fraction of adsorbent surface which is expose, while desorption occurs as a function of the fraction of adsorbent surface which is covered by pollutants. ✓ Pollutants adhere to a specific site on the surface of the adsorbent, forming a single-layer/monolayer. ✓ Adsorption occurs at constant energy, and pollutant molecules do not migrate or interact on the surface. 	<p>(Sawangiang et al., 2021; Workeneh et al., 2019)</p>
<p>Redlich-Peterson (R-P) isotherm (linear form)</p> $\ln \left(k_R \frac{c_e}{q_e} - 1 \right) = \ln(a_R) + \beta \ln(c_e)$	<ul style="list-style-type: none"> ✓ It includes both the features of Langmuir and Freundlich isotherms to form an empirical adsorption isotherm of three parameters. ✓ Its versatility allows it to be used in either homogeneous or heterogeneous systems. ✓ Unlike ideal monolayer adsorption, the adsorption mechanism is mixed 	<p>(Musah et al., 2022; Wu et al., 2010)</p>
<p>Temkin isotherm(liner form)</p> $q_e = \frac{RT}{b} \ln k_T + \frac{RT}{b} \ln C_e$	<ul style="list-style-type: none"> ✓ According to the Temkin isotherm model, adsorption heat decreases linearly with increasing adsorbent coverage ✓ Upon adsorption, binding energies are uniformly distributed up to a maximum. ✓ Multilayer adsorption ignores extremely small and extremely large concentration values, but considers interactions between the adsorbent and the contaminant. 	<p>(Musah et al., 2022)</p>

where q_e (mg/g) is the adsorption capacity at equilibrium time, q_m (mg/g) is the maximum adsorption capacity achieved by the adsorbent, K_L (L/mg) is the Langmuir adsorption constant, C_e (mg/L) is the equilibrium concentration, K_F is the Freundlich constant [(mg/g)(L/g)^{1/n}] which represents binding energy of the adsorbents, and n is the adsorption intensity, b denotes Temkin constant relating to the heat of adsorption (J/mol), R gas constant, T temperature, and K_T is Temkin isotherm constant (L/g), K_R denotes R-P constant (L/g), a_R the R-P constant (L/mg) and β the exponent which is the slope of the plot, value between 0 and 1.

2.8. Adsorption Kinetics Model

To accurately evaluate contaminants' adsorption rates, kinetic models are essential. Adsorption processes are commonly analyzed using experimental kinetic data to determine the effect of the external film boundary layer, internal diffusion resistance and adsorbent surface sorption.

The amount of contaminant adsorbed per unit mass of the adsorbent, q_e (mg/g) and percentage removal (%R) and of the contaminants by the adsorbent can be calculated using Eq (2.1) and Eq (2.2) respectively.

$$qt = \frac{C_0 - C_t}{W} * v \quad (2.1)$$

$$\%R = \frac{C_0 - C_t}{C_0} * 100\% \quad (2.2)$$

Where C_0 and C_t are the liquid-phase concentrations at an initial and predetermined time (mg/L), respectively, v is the volume of solution (L) and w is the dry weight of the added adsorbent (g) (Priyantha, 2011). Intra-particle diffusion model, Elovich model, Ritchie mode, Pseudo-first and pseudo-second-order are kinetics models applicable to BC and alumina adsorbents for the removal of contaminants from wastewater. Among them Pseudo-first and pseudo-second-order reactions were observed, as the most common cause for adsorption modeling(Qiu et al., 2009).

Pseudo-first-order Kinetic Model:

A reaction which is not first- order reaction naturally but made first order by increasing or decreasing the concentration of one or more reactants. It is based on the assumption that the rate of sorption is proportional to the number of free active sites on the sorbent surface (Priyantha, 2011).The rate constant of adsorption can be determined from the pseudo-first-order Eq (2.3).

$$\log(q_e - q_t) = \log q_e - \frac{k_1 t}{2.303} \quad (2.3)$$

Where q_e and q_t are the amounts of solute adsorbed at equilibrium and at time (mg/l), respectively, t is contact time (min) and K_1 is the adsorption rate constant (min^{-1}), larger adsorption rate constant k_1 usually represents a quicker adsorption rate.

Pseudo-Second-Order Kinetic Model:

It is based on the assumption that the rate controlling step is the adsorption on the surface that involves chemisorption, where the removal from a solution is owing to physiochemical interaction between the two phases (Ho, 2004). The pseudo-second-order equation based on the equilibrium adsorption is expressed as:

$$\frac{t}{q_t} = \frac{1}{q_e^2 K_2} + \frac{t}{q_e} \quad (2.4)$$

where, K_2 (g/mg. min) is the rate constant of second-order adsorption, the larger K_2 value the slower the rate of adsorption.

2.9. The regeneration potential of modified bone char

Regeneration capacity is of utmost importance to evaluate the reusability of bone char efficiency in the removal of contaminants from water. Regeneration of bone char could provide recovery of pollutants, reusability of adsorbents, reducing the process cost and reducing wastes to be processed.

The reuse of adsorbent is required to make the process economic and environmental friendly. Various regeneration techniques like thermal, electrochemical, ultrasonic, chemical methods are reported for regeneration. In many investigations successful recovery of solute was also reported. The need of recovery and regeneration depends on cost of solute and adsorbent and cost of recovery and also on the effect of the solute on the environment and weather it is to be disposal off in water reservoir or atmosphere (Kulkarni & Kaware, 2014).

(Kaseva, 2006b) examined the effect of thermal regeneration in the temperature range of 100–800 °C, with regeneration time of (30–240 min) on the bone char efficiency for fluoride removal from water. (Kaseva, 2006b) proposed the release of hydrogen fluoride (HF) gas from saturated bone char upon exposure to thermal treatment as a regeneration mechanism. Technically, this can

probably happen when there is a source of hydrogen to react with fluoride. The result showed that the F⁻ adsorption capacity of the regenerated bone char increased from 0.2 to 0.75 mg/g after raising the regeneration temperature from 100 to 500 °C for 120 min residence time. However, further increases in the regeneration temperature resulted in decreasing the uptake capacity of F⁻ on bone char.

The optimum conditions for the regeneration in the study by (Nigri et al., 2017) were different from the results reported by Kaseva (2006b) as the experimental conditions were different. The optimum temperature for the regeneration process of the bone char was 400 °C resulting in 2.25 mg/g F⁻ uptake capacity.

(Ben Nasr et al., 2011) examined the effect of chemical regeneration. Removal of fluoride ions using cuttlefish bones. The regeneration of the cuttlefish bone was performed with a NaOH solution (10 g of cuttlefish bone/1000 mL NaOH 3 M). After 1 h of agitation, 95% of fluorides were desorbed. Following regeneration, the adsorbent can be used for further removal of fluoride.

CHAPTER THREE

3. MATERIALS AND METHODES

3.1. Materials and Chemicals

3.1.1. Materials

Equipment required for the completion of this study were muffle furnace (SX-2.5-12), shaker (model: HY-5C), air drying oven (model: NE9-56S), sieve (model: CEN-MKII-00-A), mechanical size reduction (mortar and pestle), analytical balance (JA203H), beakers, vacuum pump, magnetic stirrer (XMTD-231), pH meter (SL-145), different size conical and Erlenmeyer flasks, measuring cylinders, ultra-sonic (LeelaSonic-50), dry ball mill (BST/BM-1) and ion selective electrode (model number: S-613F).

3.1.2. Chemicals and reagents

Different chemicals and reagents (analytical grade) were used for the synthesis of alumina nanoparticle, and for conducting pH adjustment. The chemicals and reagents include; Aluminum nitrate nonahydrate $\text{Al}(\text{NO}_3)_3 \cdot 9\text{H}_2\text{O}$ (Alpha chemika from India), citric acid monohydrate ($\text{C}_6\text{H}_8\text{O}_7 \cdot \text{H}_2\text{O}$) (ranchem analytical reagent), deionized water, sodium chloride (99%) (Blulux analytical reagent), sodium hydroxide (99.8%) (AR source from Turkey) and nitric acid (69%) (Blulux analytical reagent).

3.2. Methodology

3.2.1. Preparation of Bone char

Bone char was prepared based on previous works (S. S. A. Alkurdi et al., 2020; Chatterjee, Jha, et al., 2018; Roba et al., 2023; Shahid et al., 2019, 2020). The bone residue were obtained from the food markets of Adama town. The bones were cut into small size and thoroughly cleaned to remove any remaining meat and fat. The bones were cleaned thoroughly with boiled water for several times to remove the traces of protein and fats. The cleaned bones were then oven-dried at 105 °C for 24 hours. The cleaned and dried bone was crushed to a manageable size and transferred to a rectangular muffle furnace (model: SX-2.5-12) for pyrolysis. The pyrolysis process used a temperature ramp-up rate of 12 °C per min to six different temperature set points of 450°C, 500°C, 550°C, 600°C, 700°C and 800°C. Pyrolysis was carried out under air environment. Two holding

times were examined for each of the temperature set points: 1 and 2hr. The obtained BC was grounded by a mortar and a pestle, and sieved to achieve a particles size between 250 and 500 μ m then stored in air tight plastic bag. The optimal BC adsorbent with better fluoride ion removal performance was chosen after a batch adsorption test and it was then processed for further modification. The flow diagram signifying methodology is shown in Figure 3.1.

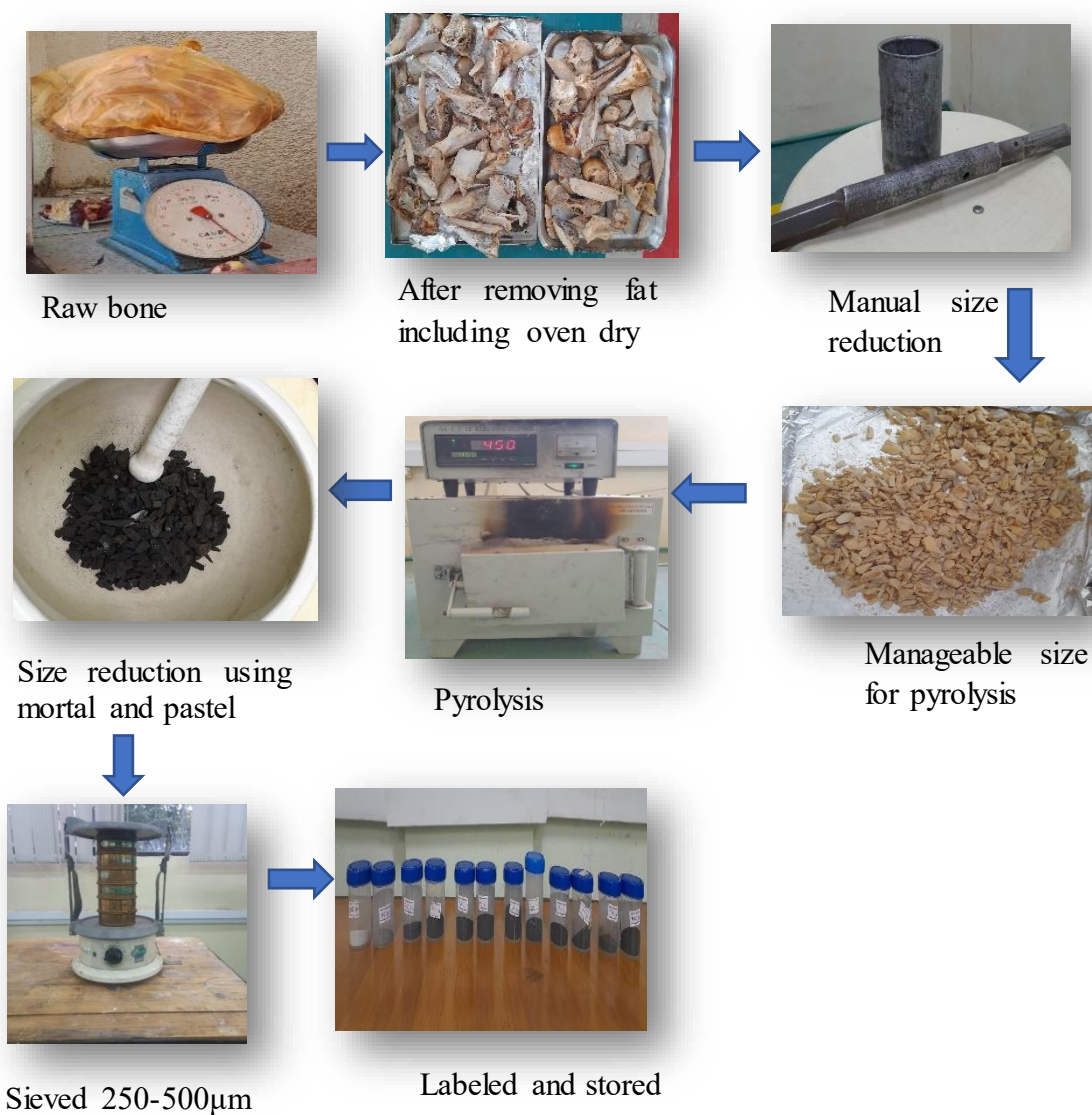


Figure 3. 1: Experimental set up for the synthesis of bone char

3.2.2. Synthesis of Alumina Nanoparticle (Al₂O₃-NPs) by sol-gel method

Alumina nanoparticle was synthesized via sol-gel method using aluminum nitrate nonahydrate (Al(NO₃)₃·9H₂O) as a precursor and citric acid monohydrate (C₆H₈O₇·H₂O) as a metal complex forming agent. Figure 3.2 described experimental setup for the synthesis of alumina nanoparticles.

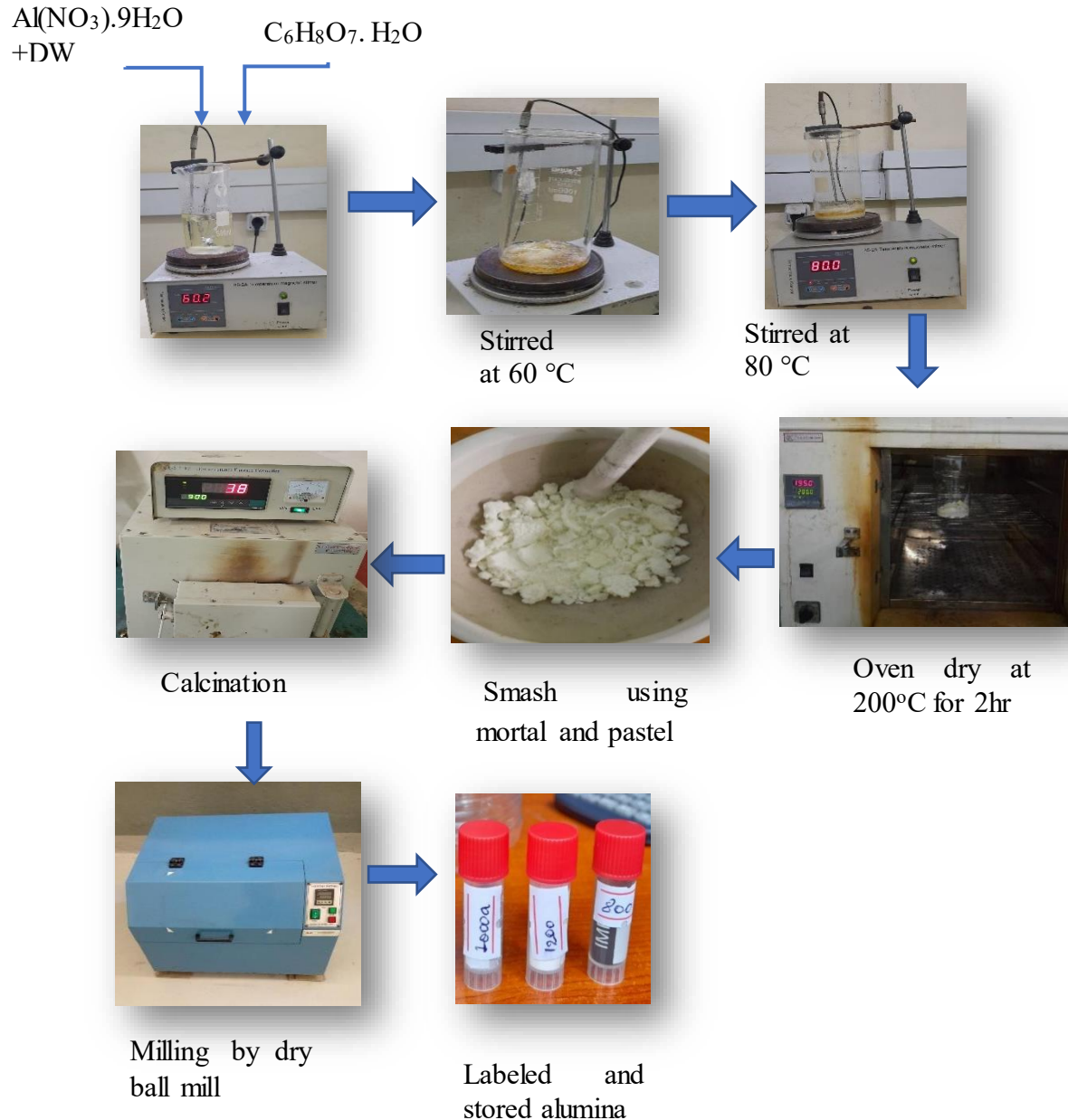


Figure 3. 2: Experimental setup for the synthesis of alumina nanoparticle

The synthesis of alumina nanoparticles was conducted by following the previous study by (J. Li et al., 2006; Mohamad et al., 2019; Suhasinee Behera et al., 2017). Citric acid and aluminum nitrate were dissolved in deionized water to create the starting solution. Aluminum nitrate was present at a concentration of 0.5 M. The citrate/nitrate molar ratio (C/N) used was 1. The mixture was continuously stirred while being kept at a temperature of around 60°C until a yellowish sol was produced. After that, the mixture was continuously stirred at a temperature of 80°C until the formation of transparent and highly viscous gel. The gel was dried at 200°C in the oven for 2 hr which turns into a fluffy mass. This fluffy mass was reduced to powder and calcined at 800,900, 1000, and 1200 °C for two hours in a muffle furnace. Finally, size reduction using dry ball mill was carried out for the alumina.

3.2.3. Preparation of Nano alumina modified Bone char (NAMBC)

Modified bone char using nano alumina was prepared according to (S. Alkurdi et al., 2022; Niu et al., 2021). The bone char was modified with alumina nanoparticles in the proportion of 1:0, 1:1, 2:1 and 0:1 (M bone char: N nano alumina). Bone char and the alumina nanoparticles were uniformly mixed at 250rpm speed for 4h and ultrasonically dispersed for 2 h. The composite was separated using filtration (vacuum filter) and then placed in drying oven at 110°C for 12 h. Finally, smash using ceramic mortar and pastel and store for later use. Figure 3.3 described experimental setup for the preparation of NAMBC.

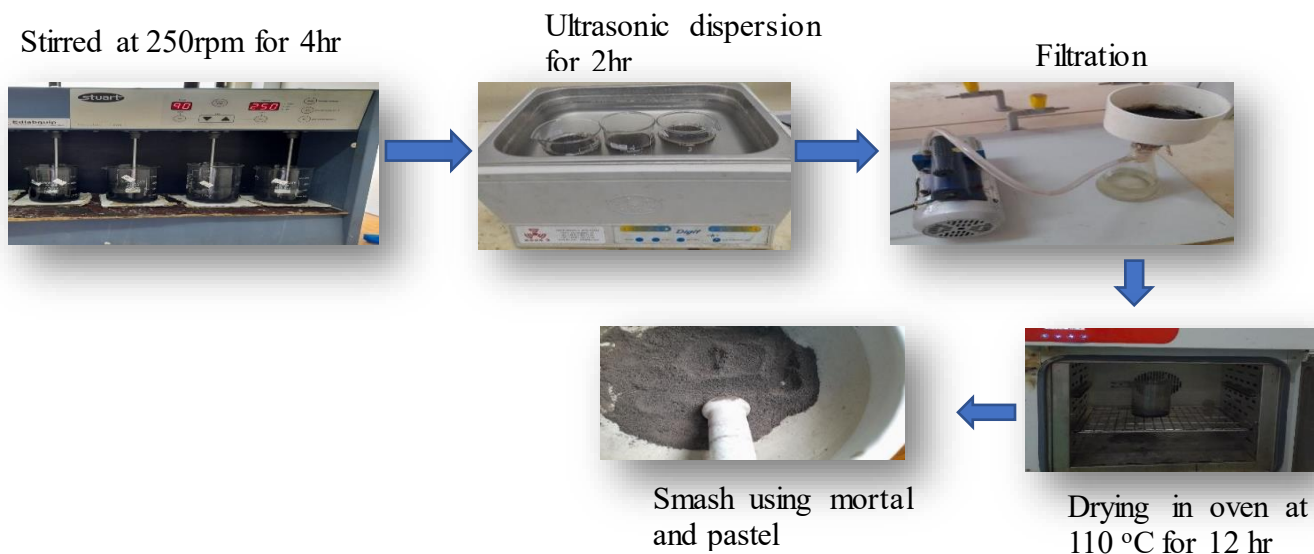


Figure 3. 3: experimental set up for nano alumina modified bone char

3.3. Analysis of Physicochemical parameters of alumina and BC

The proximate analysis of BC and alumina was done based on ASTM standard. Hence, as defined by ASTM, proximate analysis is the determination of moisture, volatile matter, fixed carbon, and ash content by prescribed methods.

3.3.1. Moisture Content

The moisture content calculated from Eq (3.1) as loss in mass on drying divided by initial weight of the sample multiplied by 100 (Of et al., 2012):

$$\%Moisture\ content(MC) = \frac{W_1 - W_2}{W_1 - W_3} * 100 \quad (3.1)$$

where, W_1 =weight of sample and crucible before drying, W_2 =weight of sample and crucible after drying, W_3 =Mass of empty crucible .

The percentage of moisture content of the BC and alumina samples were determined according to ASTM D2867. 2g of each samples were weighed and dried in oven continuously for a 2 h at 110 °C and weight. The crucible and its content was retrieved and cooled in desiccators. The difference in mass was recorded and calculate moisture content using Eq (3.1).

3.3.2. Volatile Matter

The volatile matter content was determined by following formula:

$$\%Volatile\ Matter(VM) = \frac{W_1 - W_2}{W_1 - W_3} * 100 \quad (3.2)$$

where, W_1 =weight of sample and crucible before drying, W_2 =weight of sample and crucible after drying, W_3 =Mass of empty crucible

The percentage of volatile matter of the BC sample was determined by the standard method (ASTM D5832). 2 grams of BC sample were measured on the balance and placed in a crucible. And then, both the sample and the crucible weighed (W_1). It was then heated up to 950°C for exactly 7 minutes in a furnace. After heating, the sample was removed, cooled in desiccators and then weighed (W_2) (Nyanguru & Mosima Osano, 2020) and calculate volatile matter using Eq (3.2).

The percentage of volatile matter of the alumina samples was determined by the standard method (ASTMC25). 2 grams of alumina sample were measured on the balance and placed in a crucible.

And then, both the sample and the crucible weighed (W_1). It was then heated up to 900°C for 1hr in a furnace. After heating, the sample was removed, cooled in desiccators and then weighed (W_2) (Srivastav & Srivastava, 2009) and calculated volatile matter using Eq (3.2).

3.3.3. Ash content

The ash content was determined by following the formula:

$$\%Ash\ Content(AC) = \frac{W_2 - W_3}{W_1 - W_3} * 100 \quad (3.3)$$

where, W_1 =weight of sample and crucible before drying, W_2 =weight of sample and crucible after drying, W_3 =Mass of empty crucible

The ash content of BC sample was determined by the standard method (ASTM D2866). Its determination was done by taking 2 g of BC sample with the crucible and weighed them on the balance (W_1). It was kept for 4 hr in the furnace at 550 °C. After heating, the sample was removed, cooled in desiccators and then weighed to obtained weight (W_2) (Nyanguru & Mosima Osano, 2020) and AC was determined by Eq. (3.3).

The ash content of alumina sample was determined by the standard method (ASTM D7348). Its determination was done by taking 2 g of alumina sample with the crucible and weighed them on the balance (W_1). It was kept for 5 hr in the furnace at 550 °C until constant weight achieved. After heating, the sample was removed, cooled in desiccators and then weighed to obtained weight (W_2)(Srivastav & Srivastava, 2009) and ash content was determined by Eq. (3.3),

3.3.4. Fixed Carbon Content

Fixed carbon was a calculated value and it is obtained by subtracting of summation of percentage of moisture content, ash content, and volatile matter content from 100 (Nyanguru & Mosima Osano, 2020). The BC and alumina fixed carbon content was determined according to Eq. (3.4).

$$\text{Fixed carbon content (\%)} = 100 - (\text{moisture, \%} + \text{ash, \%} + \text{volatile matter, \%}) \quad (3.4)$$

3.4. Characterization of alumina nanoparticle (Al_2O_3 -NPs)

3.4.1. Crystallographic structural analysis

The XRD analysis of the as prepared Al_2O_3 -NPs was conducted using (XRD-700 XRAY diffractometer, shimadzu Corporation, Japan) with continuous scanning at a speed of 3°/min within

(10° - 80°) diffraction angles. During the XRD analysis, the sample was placed into the center of the instrument and illuminated with a beam of X-rays, and the XRD patterns from the sample was recorded via measurements of the diffraction angles of X-ray beams altered by the interference of atomic structure of the sample.

Scherrer equation (Eq 3.5):

$$D = \frac{K\lambda}{\beta \cos\theta} \quad (3.5)$$

where; 'D' is Crystallite size, 'K' is shape factor (Scherrer constant = 0.9), 'λ' is wave length of X-ray (λ = 0.15406 nm), 'β' is Full width half maxima (FWHM), 'θ' is diffraction angle.

Bragg's equation (Eq 3.6):

$$d = \frac{n\lambda}{2\sin\theta} \quad (3.6)$$

Where; 'd' is d-spacing, 'n' is order of diffraction (n = 1), 'θ' is diffraction angle, and 'λ' is wave length of incident X-ray (λ = 0.15406 nm).

3.4.2. Functional group analysis

FTIR analysis of Al₂O₃-NPs was performed to understand its macromolecular structure so as to confirm the existence of expected function groups within the nanoparticle. The FTIR spectrum of prepared Al₂O₃-NPs was measured using FTIR spectrometer with a model number (FT/IR-6600 type A). The sample was first diluted at 1:20 with KBr before the analysis, and a background of pure KBr was acquired before scanning the sample.

3.4.3. Particle size analysis by PSDA

The analysis of particle size for the Al₂O₃-NPs was performed using Particle Size Analyzer (PSA)/Zetasizer-Nano, model number ZEN 3600 (Malvern Instrument Ltd. Worcestershire, UK). The size measurement of PSA was based on dynamic light scattering (DLS), which measures the particle size with a measurement range of (0.3 nm to 10 μm). Particle size distribution analyzer (PSDA) was determined from the distribution of the scattered light energy using the rigorous Mie light scattering theory.

Before the analysis, the sample was dispersed using two types of dispersants (sodium hydroxide and ethanol) for 50 minute. The sample dispersed in both dispersant solvents was analyzed to

understand the effect of dispersant on the particle size of the nanoparticle. The result of PSA was reported by percent intensity to determine the average particle size of the nanoparticle.

3.4.4. Thermogravimetric analysis (TGA)/ differential thermal analysis (DTA)

The thermal behavior of dried gel has been investigated by using thermal gravimetric analysis (TGA) and differential thermal analysis (DTA). In the typical thermal analysis procedure, 8.157mg sample has been located in alumina ceramic sample holder and data have been recorded upon heating up to 1200 °C at a heating rate of 15 °C.min⁻¹ at nitrogen atmosphere at a flow rate of 50ml/min.

3.5. Characterization of Bone char (BC) and Nano alumina modified bone char (NAMBC)

3.5.1. pH at Potential of Zero Charge (pHpzc)

The isoelectric point or point of Zero charge (PHzpc) of the carbon samples were measured by using the method described by (Ben Nasr et al., 2011; Nyanguru & Mosima Osano, 2020). 0.1 M of 10ml NaCl solutions having the initial pH values ranging from 2 to 11 with 1 increment were prepared in duplicate using 0.1 M HCl and 0.1 M NaOH. While in one each duplicate 0.5 g of NAMBC was added and mixed for 24 hr. Then the solutions were filtered off and the adsorbent was separated. The final pH values of the ten solutions were measured and thereby calculation of ΔpH was made by subtracting the initial pH values from final pH values. The graph was drawn by plotting the final pH values against ΔpH . From the graphs plotted, the pHpzc (point of zero charge) of the adsorbent was determined.

3.5.2. Crystallographic structural analysis

The XRD analysis was conducted on BC and NAMBC adsorbents to reveal information about the crystallographic structure. Crystalline size and d-spacing of BC and NAMBC is calculated using Eq (3.5) and Eq (3.6) respectively. A Crystalline phase of BC and NAMBC before and after the uptake of fluoride was identified by XRD (XRD-700 X-RAY diffractometer, shimadzu Corporation, Japan) with continuous scanning at a speed of 3°/min within (10° - 80°) diffraction angles.

3.5.3. Functional group analysis

The FTIR study was conducted on BC and NAMBC adsorbents sample to determine the various organic and inorganic groups on the surface of adsorbent. This FTIR gave important information about the groups of substances involved in ion exchange reactions during adsorption.

Detection of the surface functional groups for the BC and NAMBC before and after the uptake of fluoride was carried out in Bahirdar university using Fourier Transform Infrared (FT-IR, JASCO-FT/IR 6600) technique (Smith, 2011), The scanning range was 400–4000 cm^{-1} .

3.5.4. BET Analysis

The specific surface area (SSA) of the adsorbents used for comparison was determined using Brunauer, Emmett, and Teller (BET) analyzer. Load an accurately weighed quantity of each BC and NAMBC samples (0.08 g) into the analysis tube and connect to the NOVA version 0.00 model instrument using nitrogen as adsorbent under 77.3 K temperature.

3.5.5. Thermogravimetric analysis (TGA) /differential thermal analysis (DTA)

The thermal behavior of raw bone has been investigated by using thermal gravimetric analysis (TGA) and differential thermal analysis (DTA). In the typical thermal analysis procedure, a 7.090mg sample has been located in calcium phosphate ceramic sample holder and data have been recorded upon heating up to 1000 °C at a heating rate of 15 °C.min⁻¹ in a stream of nitrogen (50ml/min) to study the hydroxyapatite thermal stability.

3.6. Preparation of Adsorbent Solution

Anhydrous sodium fluoride (2.210 g) was weighed and transferred into 1000 mL volumetric flask. It was dissolved in deionized water and then diluted to 1 L. The resultant solution containing 1000 mg/L of fluoride was considered as stock fluoride solution (Mondal et al., 2015). Standard solutions were prepared from the stock solution (1000mg/L) in the different range of by serial dilution (dilution law, $C_1V_1 = C_2V_2$). Where, C_1 and V_1 were concentration and volume of stock fluoride solution, respectively and C_2 and V_2 were concentration and volume of standard solutions that were prepared, respectively.

3.7. Determination of Adsorption Capacities

As shown in Figure 3.4 the batch adsorption experiments were performed in a 250 mL Erlenmeyer flasks holding 100 mL of the synthetic water carried out at the same fluoride concentration (10

mg/L F⁻), contact time(2hr) and amount of adsorbent (2 g) to estimate the adsorbent capacity of removing fluoride ion. The Erlenmeyer flasks were shaken at 200 rpm for 2 h in an orbital shaker at ambient temperature (23 ± 3 °C) and filtered through a filter paper (Whatman No.1 filter paper) before fluoride analysis. All the adsorption studies were performed in triplicate, and average values were used to plot the graphs. The residual fluoride concentration in the samples were determined using ion-selective electrode (model number: S-613F)(S. S. A. Alkurdi et al., 2020; Hu et al., 2017). The potential readings (mV) of the sample were converted into concentration of fluoride (mg/L) using Microsoft excel program. The fluoride removed per unit quantity of adsorbent material at a measured time “t” (qt, mg/g) was calculated by Eq (3.7). The efficiency of the adsorption process (% R) was calculated by Eq (3.8) (Hart et al., 2023):

$$qt = \frac{C_0 - C_t}{W} * v \quad (3.7)$$

$$\%R = \frac{C_0 - C_t}{C_0} * 100\% \quad (3.8)$$

where, Co and Ct are the concentration of fluoride in the sample (mg/L) at time zero and at a measured time (t), respectively, m is the adsorbent mass (g) and V is the solution volume (L).

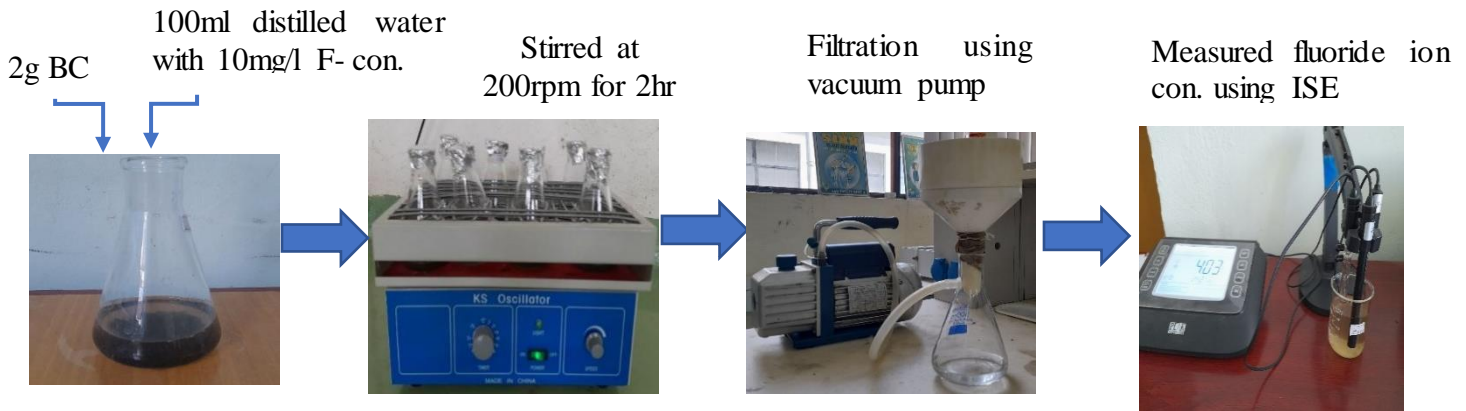


Figure 3. 4: experimental setup to determine residual concentration of fluoride

3.8. Effect of Parameters on Fluoride Removal Efficiency of NAMBC

Different factors affect the defluoridation efficiency of an adsorbent including adsorbent dose, pH level of the solution, initial fluoride concentration and contact time are main factors that should be deal during defluoridation. Optimization is carried out to make this parameters function at their best by varying one parameter while keeping other parameters constant.

3.8.1. Effect of pH

To study the effect of solution pH on fluoride removal, the test solutions containing 10 mg/L of fluoride and pH of 6.57 was adjusted to pH values of 3, 5, 7, 9, and 11 using 1M HCl and 1M NaOH at room temperature (Asra & Kebede, 2016; Getachew et al., 2015). Then 2 g of NAMBC was added to 100 mL of the test solutions separately and stirred for 2 hr. Residual fluoride ion concentration was analyzed in each experiment after 2 hr contact time. Finally pH versus percentage removal was plotted to describe the adsorption behavior of the adsorbent at each pH.

3.8.2. Effect of Contact time

Residual F⁻ concentrations were measured for different contact time of adsorption (0.5, 2, 4, 6, 8 and 12 hr) with 2 g of the selected adsorbent mixture in 100 mL of fluoride solution in order to investigate the effect of contact time. Other parameters, pH(6.57), concentration of the solution(10 mg/L) remain constant (Ben Nasr et al., 2011; Smittakorn et al., 2010).

3.8.3. Effect of adsorbent dose

Experimental investigations were carried at different dosages of adsorbent 2,3, 6 and 9 g/100 mL of fluoride solution with 10 mg/L initial fluoride concentration at 2h contact times and pH=6.57 (Getachew et al., 2015).

3.8.4. Effect of initial fluoride concentration

To investigate the effect of initial fluoride concentration, experiments were conducted at various fluoride concentrations (5, 10, 15, and 20 mg/L) keeping pH = 6.57 and temperature constant with fixed 2 g of adsorbent and 2 h contact time (Getachew et al., 2015).

3.9. Adsorption isotherms model

Adsorption isotherms were determined using treated adsorbents at room temperature. The experiments for adsorption isotherm were performed for initial fluoride concentrations varied (5, 10, 15 and 20mg/l) with constant adsorbent dose (2g). The mixture was agitated for 6 h to ensure the equilibrium, and residual fluoride was determined after filtration. Based on the data generated, adsorption isotherms were plotted. The Langmuir and Freundlich isotherm models were fitted with the adsorption data to predict the mechanism of adsorption on the produced NAMBC adsorbents (Hart et al., 2023).

The Langmuir isotherm is given by linear Equation (3.9):

$$\frac{C_e}{q_e} = \frac{1}{K_L q_{max}} + \frac{C_e}{q_{max}} \quad (3.9)$$

where q_e is the equilibrium amount of fluoride ion adsorbed per unit mass of adsorbent, mg/g; C_e is the equilibrium adsorbate concentration in solution, mg/L and q_{max} and K_L are Langmuir constants representing maximum adsorption capacity and binding strength, respectively. where C_e/q_e is plotted against C_e , a straight line with slope $1/q_{max}$ is obtained which shows that the adsorption follows the Langmuir isotherm. The Langmuir constants q_{max} and k_L are calculated from the slope and intercept with Y-axis. The essential characteristics of a Langmuir isotherm can be expressed in terms of dimensionless separation factor, and describe the type of isotherm defined by (Eq 3.10):

$$R_L = \frac{1}{1 + C_o K_L} \quad (3.10)$$

where C_o is the initial concentration of fluoride (mg/L) and k_L is the Langmuir constant (in g/L). The value of separation factor R_L , indicates the isotherms shape and the nature of the adsorption process as unfavorable ($R_L > 1$), linear ($R_L = 1$), favorable ($0 < R_L < 1$) and irreversible ($R_L = 0$) (Mittal et al., 2007).

The linearized Freundlich adsorption isotherm is given in Eq (3.11):

$$\log q_e = \log K_f + \frac{1}{n} \log C_e \quad (3.11)$$

where, q_e is the equilibrium amount of F- ions adsorbed per unit weight of adsorbents (mg/g), C_e is the equilibrium concentration in solution (mg/L) K_f and $1/n$ are the Freundlich constants. K_f and n are the indicators of the adsorption capacity and adsorption intensity, respectively. If $1/n < 1$, bond energies increases with surface density, if $1/n > 1$, bond energy decreases with surface density and if $1/n = 1$, all surface sites are equivalent. C_e (mg/L) is the equilibrium concentration. Linear plots of $\log q_e$ vs $\log C_e$ at different adsorbent doses are applied to confirm the applicability of Freundlich models (Mittal et al., 2007).

3.10. Adsorption kinetics model

Adsorption kinetics was determined using constant surface loading of 2g of adsorbent to corresponding the initial fluoride concentration of 15 mg/L. Residual fluoride concentrations were

measured at different contact time intervals of 0.5, 2, 4, 6, 8 and 12 hr. Finally the calibration graphs were plotted based on Eq (3.12) and Eq (3.13) to explain the adsorption kinetics of the adsorbents. The adsorption kinetics was analyzed by the pseudo first order and pseudo second order models (Hart et al., 2023).

The pseudo first order is given in the following equation:

$$\log(q_e - q_t) = \log q_e - \frac{k_1 t}{2.303} \quad (3.12)$$

Where, q_e and q_t refer to the amount of fluoride ion adsorbed per unit mass of the adsorbate at equilibrium time and any time (mg/g), respectively. K_1 is the rate constant of pseudo-first-order adsorption. The rate constant K_1 and equilibrium adsorption capacity q_e can be predicted from the slope and intercept, respectively, of the linear plots of $\log (q_e - q_t)$ versus t .

The Pseudo-Second-Order Kinetic Model is given in the following equation:

$$\frac{t}{q_t} = \frac{1}{q_e^2 K_2} + \frac{t}{q_e} \quad (3.13)$$

Where, K_2 is the rate constant of the pseudo-second-order equation (g/mg.min.) and q_e is the equilibrium adsorption capacity (mg/g). The values of q_t and K_2 can be determined experimentally from the slope and intercept, respectively, of the plots of t/q_t versus t .

3.11. NAMBC regeneration

The same set up employed for both adsorption modeling Figure 3.5 was applied for regeneration experiments. Bone char was loaded with 10mg/l F^- until its reached saturated concentration for 6hr. The time to get to this condition was from previous tests and this value was considered in the subsequent adsorption experiment associated with the regeneration step.

To understanding the onsite application of NAMBC, a single cycle of adsorption-desorption was tested according to (Ben Nasr et al., 2011; Hu et al., 2017) method. Desorption of fluorides from modified bone was carried out with a NaOH solution. The same solution was used several times to realize the adsorbent regeneration. The method used for desorption consisted of NAMBC in the basic solution (10 g of NAMBC/500 mL of NaOH 0.5 M) for 1 hr at a stirring speed of 200 rpm. The concentration of fluorides was then measured in this solution following filtration. The NAMBC was removed and rinsed with distilled water until neutral pH was attained. It was then

dried in an air oven at 100°C for 12 hr and grounded using mortar and pastel. Then reused for a new adsorption. After the regeneration, the ability of NAMBC adsorbent to remove fluoride from solution was again tested in an adsorption experiment using a similar procedure.

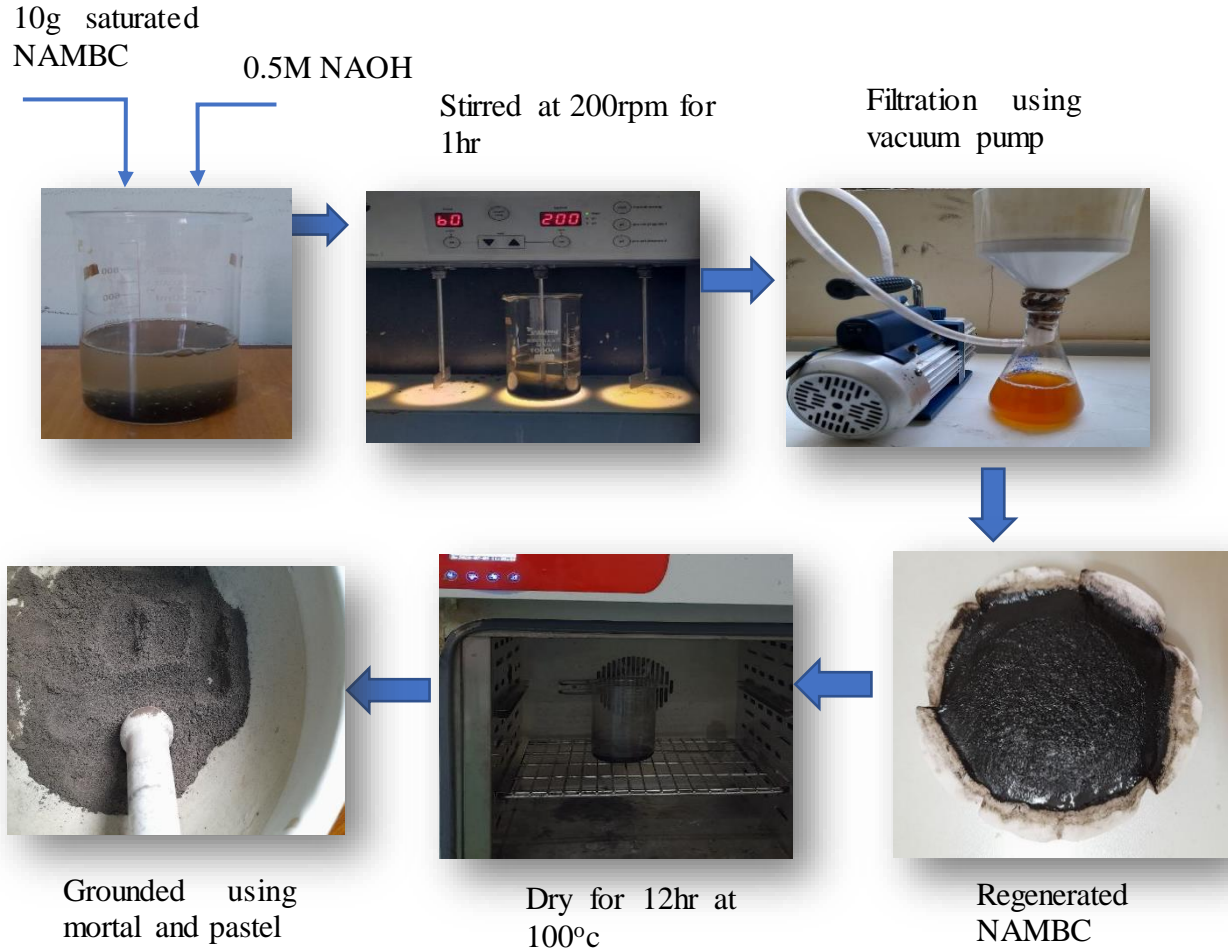


Figure 3. 5: experimental setup for NAMBC regeneration

3.12. Characterization of selected representative groundwater

As an approximation of the results of the present work for application to a real problem, fluoride containing water collected from East Shoa zone which is around Methara town, Ethiopia. The water samples is called Beseka water which is found in Fentale Woreda.

The field groundwater batch tests were run in same manner from the synthetic water tests (Figure 3.4.). In these tests, 100 mL of the field groundwater sample, was placed in 250mL flask with 2 g of NAMBC. The bottles were shaken in orbital shaker at room temperature for 6hr to ensure the equilibrium, and residual fluoride was determined after filtration.

In this thesis work, three ions which co-exist with fluoride ions were investigated. Those coexisting ions are Sulphate (mg/l SO_3^-), Calcium (mg/l Ca^{2+}) and Magnesium (mg/l Mg^{2+}) were analyzed. Additionally, Physical parameters such as pH, total hardness (TH), total dissolved solvent (TDS), chemical oxygen demand (COD), biological oxygen demand (BOD), total suspended solid (TSS), turbidity and color were measured.

CHAPTER FOUR

4. RESUT AND DISCUSSION

4.1. Effect of pyrolysis temperature and time on removal efficiency of BC

Charring temperature and time are the two most significant factors that affect the ability of bone char to remove Fluoride from aqueous media. In this study, cattle bones were used to remove F⁻ from synthetic and ground water to optimize the pyrolysis conditions. Table 4.1 was shown the results achieved for the removal of 10 mg/L F⁻ from synthetic water using 2 g bone char for 100 mL solution. As indicated in Figure 4.1, the lower the pyrolysis temperature, the greater the F⁻ uptake. Thus, the highest removal capacity of F⁻ was 0.421 mg/g using bone char samples prepared at 450 °C for 3 hr of thermal treatment, which was similar to reference data (Roba et al., 2023). Samples made at 700 °C and 800 °C showed a very low uptake of F⁻ from solution. This could be explained by the lower OH groups which resulted in the reduction of surface functional groups and lower ion exchange capability, which was the main removal mechanism (Medellin-Castillo et al., 2014). Additionally, the increase in the negative surface charge of the char as pyrolysis temperature increased may negatively affect the electrostatic interaction between F⁻ and bone char. Electrostatic interaction was found to have an important role in F⁻ removal using bone char (S. S. A. Alkurdi et al., 2019).

Table 4. 1: Effect of charring temperature and time of bone char on its Fluoride removal efficiency

Pyrolysis condition		Residual fluoride con. mg/l			Avg final con., (mg/l)	Bone char performance	
Temperature ,°C	Residence time, h	Trial-1	Trial-2	Trial-3		%R	qe(mg/g)
450	2	1.93	1.94	1.94	1.94	80.6	0.403
	3	1.59	1.57	1.57	1.58	84.2	0.421
500	2	1.77	1.77	1.77	1.77	82.3	0.4115

	3	2.35	2.34	2.34	2.34	76.6	0.383
550	2	3.44	3.47	3.47	3.46	65.4	0.327
	3	3.81	3.76	3.78	3.79	62.1	0.3105
600	2	4.89	4.9	4.86	4.88	51.2	0.256
	3	4.14	4.17	4.15	4.16	58.4	0.292
700	2	5.23	5.23	5.22	5.23	47.7	0.2385
	3	5.63	5.62	5.60	5.61	43.9	0.2195
800	2	7.91	7.92	7.92	7.92	20.8	0.104
	3	7.39	7.39	7.39	7.39	26.1	0.1305

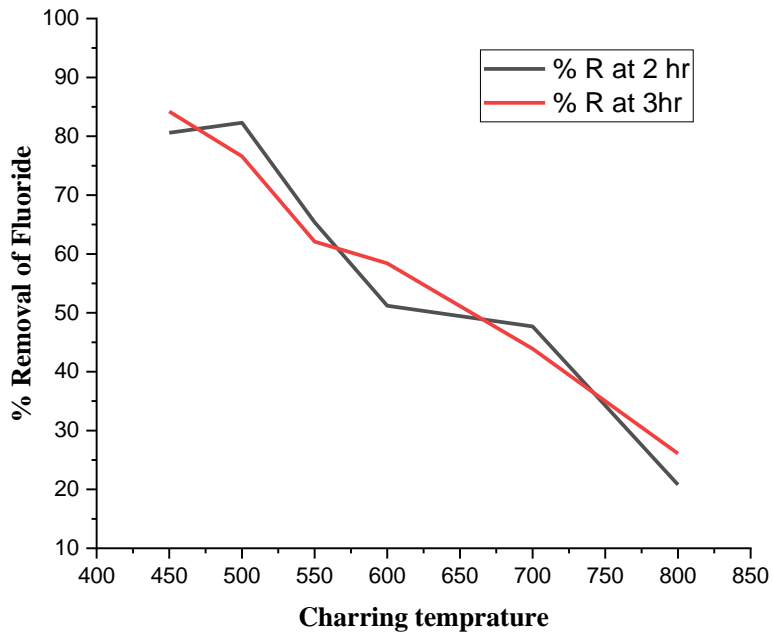


Figure 4. 1: Fluoride removal percentage of bone char after different charring condition

4.2. NAMBC for fluoride removal

The defluoridation efficiency of bone char, Al₂O₃-NPs and composites were examined in the experiment. It has reported in literature that fluoride removal by bone char is associated with the two main mechanisms of ion exchange and chemical precipitation as calcium fluoride

(Rojas-Mayorga et al., 2013) while fluoride-alumina interaction was expected due to fluoride being the most electronegative element, exhibits a high affinity for alumina (Shivaprasad et al., 2018).

Table4. 2: The different ratio of bone char (M) and Al₂O₃-NP (N) and their percentage removal of fluoride

Sample No.	M:N	Residual fluoride Con. (mg/L)			Final con. (mg/L)	NAMBC performance	
		t-1	t-2	t-3		F ⁻ Removal (%)	F ⁻ removal(mg/g)
1	1:0	1.58	1.58	1.59	1.58	84.2	0.421
2	1:1	0.46	0.43	0.44	0.45	95.5	0.4775
3	2:1	0.27	0.27	0.26	0.27	97.3	0.4865
4	0:1	1.84	1.84	1.89	1.86	81.4	0.407

Fluoride adsorption by the composite materials has been proposed to occur via ion exchange with lattice OH⁻, chemical precipitation as CaF₂ and interaction with cationic centers. Table 4.2 was shown the results of experiments testing different ratios of bone char to nano alumina for fluoride removal from water. When only bone char was used (1:0 ratio), it removed 84.2% of fluoride while a 1:1 ratio of bone char to nano alumina, the removal increased to 88%, slightly better than using bone char alone. The 2:1 ratio of bone char to nano alumina had the highest removal at 91.5%. Using only nano alumina (0:1 ratio) had the lowest removal at 78.7%. The adsorbent prepared by bone char modified using nano alumina with ratio of 2:1 was found to have better performance in defluoridation of water and used for other parameter optimization.

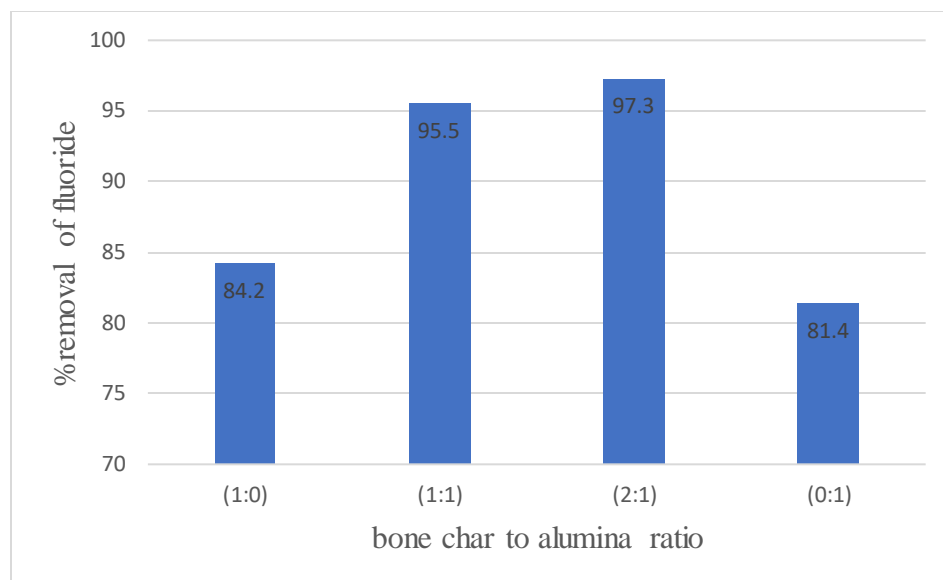


Figure 4. 2: Fluoride removal efficiencies at various bone char to alumina ratio

The observed results shown that combining bone char and nano alumina improved fluoride removal compared to using just one adsorbent alone. The higher the proportion of bone char relative to nano alumina, the greater the fluoride removal. The bone char likely provides most of the adsorption capacity, while the nano alumina might help improve the bone char's performance by modifying surface chemistry (Tchomgui-Kamga et al., 2010). As shown in Figure 4.2, the synergy between the two materials produces the best result at a 2:1 ratio of bone char to nano alumina.

4.3. Physicochemical analysis of BC and alumina

Proximate analysis provides key information on bone char and alumina composition that reveals its adsorptive properties and quality. It served as a valuable characterization tool for bone char and alumina production and practical use. The result of the analysis is presented in Table 4.3. The detailed calculation part is also included under appendix B.

Table 4. 3: The proximate analysis of BC and alumina

Samples	%MC	%VM	%AC	%FCC
BC	4	22.54	52	21.46
Alumina	2.5	0.5	97	0

Bone char (BC):

As shown in Table 4.3, moisture content result observed was a typical moisture level for bone char, indicating a moderately dry sample. The low moisture content is beneficial for adsorption applications. Similar moisture content values were recorded by (Nyanguru & Mosima Osano, 2020). The presence of high moisture content (heterogeneous oxygen groups) on the adsorbent surface is known to reduce the adsorption capacity due to adsorption of water onto these groups using hydrogen bonding. The increased in number of oxygen-containing surface functional groups increased the polarity of carbon surfaces. Hence, the selectivity of carbon surface for water increased, and thus adsorbed water clusters may block active site of the carbon (Mwakabona et al., 2014). Volatile Matter (22.54%) value was in the higher end for bone char. It indicated a significant portion of organic matter/carbon was driven off during heating. The result was nearly similar to Nyanguru & Mosima Osano (2020). Ash Content (52 %) result was moderately high for bone char. This result was higher compare to Nyanguru & Mosima Osano (2020). This implied there was a good mineral content remaining from the bone after carbonization. Higher ash can contribute to adsorption capacity. Calcination process was followed by activation, which increased the adsorption capacity by removing contaminants from the surface of the adsorbent (Gabelman, . Fixed Carbon Content (21.46 %) level was typical for bone char. The relatively high fixed carbon provided adsorption sites and capacity. Overall, the bone char has a balanced composition (Nyanguru & Mosima Osano, 2020).

Alumina:

As shown in Table 4.3, the moisture content of alumina was hygroscopic meaning it absorbs moisture from the air. However, high purity alumina powder was usually dried to have very low moisture content before being used industrially. The alumina sample has absorbed a small amount of ambient moisture. But the moisture level was still low. Volatile matter was negligible, this indicated high purity inorganic alumina with no significant volatile (Srivastav & Srivastava, 2009). Alumina was an inorganic compound and does not contain organic matter that could volatilize or burn off. Ash content value was very high, this confirmed the alumina sample was predominantly the intrinsic aluminum oxide composition, with minimal impurities.

(Srivastav & Srivastava, (2009). The fixed carbon result was expected verified the alumina has no fixed carbon, consistent with its inorganic nature.

In general, the data indicated typical bone char properties and high purity alumina. The bone char was shown good potential to be used as an adsorbent due to its carbon content. The alumina was primarily the oxide with minimal volatile content.

4.4. Characterization of Al₂O₃-NPs

4.4.1. Crystallographic structural analysis of Al₂O₃-NPs

XRD analysis was used to identify the crystalline structure of Al₂O₃-NPs as well as the crystalline phase of the nanoparticle. The XRD pattern of the prepared Al₂O₃-NPs was shown in Figure 4.3 and Figure 4.4, in which different peaks were observed with respect to angle of diffraction. Comparative XRD patterns of Al₂O₃-NPs produced at various temperatures are shown in Figures 4.3 and Figure 4.4. It was known that the temperature of the calcination substantially influenced the phase change.

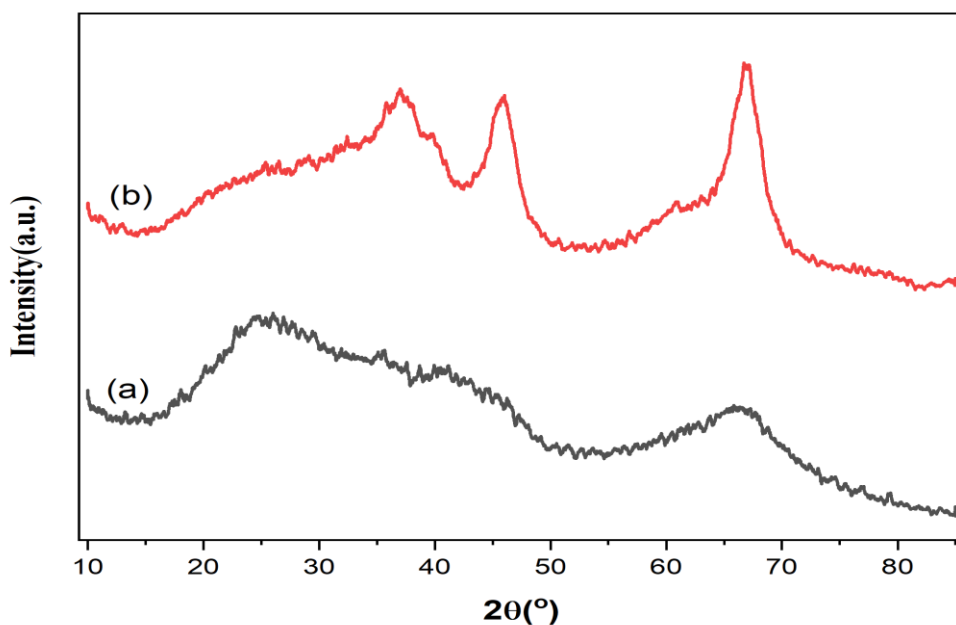


Figure 4. 3: XRD pattern of alumina (a) at 800 °C and (b) at 900 °C

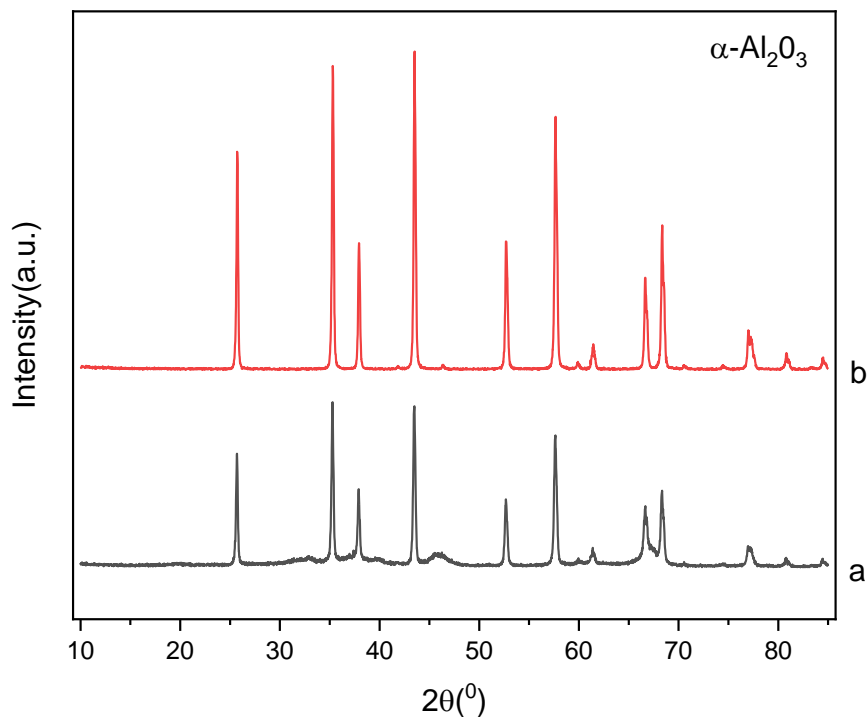


Figure 4. 4: XRD pattern of alumina (a) at 1000 °C and (b) at 1200 °C

The XRD pattern at 800 °C revealed broad peaks that were signs of the creation of crystallite structures and nano-sized dimensions (Banerjee & Sujatha Devi, 2007). Broad peaks indexed for $\gamma\text{-Al}_2\text{O}_3$ in Figure 4.3(a) shown the development of imperfectly crystallized alumina. Aqueous amorphous Al_2O_3 did exist at this temperature, as could be observed in (Potdar et al., 2007), which is introduced as a precursor of gamma alumina. A low crystallization rate was indicated by the broadness of the peaks (Ma et al., 2008). When the sintering temperature was increased to 900°C, peaks were appearing at diffraction angle (2θ) values, 37.2°, 39.72°, 45.8° and 66.94°, which reflects to the γ -alumina peaks that indicated the transition of amorphous structure into γ -alumina phase. Raising the temperature to 900 °C increased the diffraction pattern of the gamma phase, which fitted to card [JCPDS No. 10-0425]. The X-ray diffraction pattern was compared with standard data, the 100% intensity occurred at 2θ value of 66.90°, which was nearly similar to reference data (Belekar & Dhoble, 2018). As temperature increased from 900 °C to 1200 °C gamma phase completely replaced with alpha phase and all reflections fitted with $\alpha\text{-Al}_2\text{O}_3$ structure (JCPDS Card No: 46-1212, Figure 4.4 (b)). Figure 4.4(b) shown, the diffraction peaks

have been appeared at 2θ values, 25.73° , 35.31° , 37.94° , 43.52° , 52.73° , 57.68° , 61.44° and 66.7° which reflects to the typical hexagonal and rhombohedral structure of the α - Al_2O_3 -NPs (Rajaeiyan & Bagheri-Mohagheghi, 2013b; Suhasinee Behera et al., 2017). In Figure 4.4 (b), another small peak was observed at a diffraction angle of 45.86° , which indicated the cubic structure γ -alumina nanoparticle (Kanwal et al., 2015).

The crystallite size and d-spacing of the prepared Al_2O_3 powder estimated from X-ray peak broadening using Eq. (3.5) and Eq. (3.6), respectively. At sintering temperature 800°C , since the structure was amorphous, no crystallite size could be determined. As shown in Table 4.4, sintered at 900°C , the average crystallite size was 2.4 nm. The obvious crystallite growth could be seen when the sintering temperature was raised to 1000°C and 1200°C where the average crystallite size were 23.95 nm and 30.84 nm, respectively. Rapid crystallite formation as a result of α -alumina particle coarsening at higher temperatures (Mohamad et al., 2019). It could be concluded that changing the calcination temperature has a remarkable effect on both the particle size and the phase of the synthesized nano-alumina.

Table4. 4: Crystalline size and d-spacing of alumina nanoparticle

Temperature($^\circ\text{c}$)	Peak position(2θ)	FWHM	Crystal size, D(nm)	D-average(nm)	d-spacing(nm)	Average d-spacing(nm)
900	37.22	4.474	1.873	2.401	0.077	0.077
	39.72	8.722	0.968		0.077	
	45.80	2.791	3.090		0.077	
	66.93	2.594	3.672		0.077	
1000	25.69	0.222	36.747		0.346	
	35.27	0.255	32.727		0.254	
	37.90	0.305	27.561		0.237	
	43.48	0.272	31.493		0.208	
	45.85	1.889	4.566		0.198	

	52.69	0.302	29.390	23.946	0.174	0.193
	57.64	0.326	27.776		0.160	
	61.39	0.462	19.996		0.151	
	66.74	0.826	11.516		0.140	
	68.35	0.410	23.405		0.137	
	77.13	0.557	18.232		0.124	
1200	25.72	0.203	40.215	30.843	0.346	0.193
	35.31	0.221	37.603		0.254	
	37.94	0.222	37.829		0.237	
	43.52	0.246	34.700		0.208	
	52.72	0.281	31.475		0.173	
	57.67	0.306	29.637		0.160	
	61.43	0.362	25.510		0.151	
	66.70	0.348	27.339		0.140	
	68.39	0.351	27.360		0.137	
	77.17	0.606	16.766		0.123	

The application of nanoparticles, such as adsorption, was greatly influenced by their crystalline size. The physical characteristics of a nanoparticle, such as its surface area and surface energy, was determined by its crystal size. The nanoparticle's small crystallite size allowed for a large surface area (Rajaeiyan & Bagheri-Mohagheghi, 2013b), which further could enhance its adsorption performance. In this study, a small crystal size of Al₂O₃-NPs (2.40 nm) was obtained, which was in good agreement with previous report by Abdellah et al. (2018). The value of the d-spacing obtained for 900°C derived γ -Al₂O₃ was 0.077nm compared to 0.193nm d-spacing value

respectively occurred for 1200°C derived α - Al_2O_3 samples. An essential characteristic that determines the distance between the layers in a crystal structure was the value of the d-spacing. The size of the nanoparticles' crystals was anticipated to rise as the interlayer distance increased (Dubey et al., 2017).

4.4.2. Functional group analysis of Al_2O_3 -NPs

The FTIR analysis for the as prepared Al_2O_3 -NPs is described in Figure 4.5, which describes the transmittance peaks attributed to stretching and bending vibration of the associated functional groups existing in the Al_2O_3 -NPs. The FTIR spectrum of the Al_2O_3 -NPs was analyzed and compared with its standard spectra. A characteristic peak was observed at 3486 cm^{-1} that indicated the O-H stretching of the adsorbed water, similar result was obtained previously (Kumar et al., 2011; Rajaeiyan & Bagheri-Mohagheghi, 2013a; Tabesh et al., 2018). Transmittance peaks were observed at 432 cm^{-1} , 445 cm^{-1} , 471 cm^{-1} , 568 cm^{-1} and 665 cm^{-1} , which were attributed to the stretching vibration of the (O-Al-O) groups. Those peaks were assigned to aluminum ions in octahedral and tetrahedral environment and indicated the presence of γ -phase (Belekar & Dhoble, 2018; Yu et al., 2023).

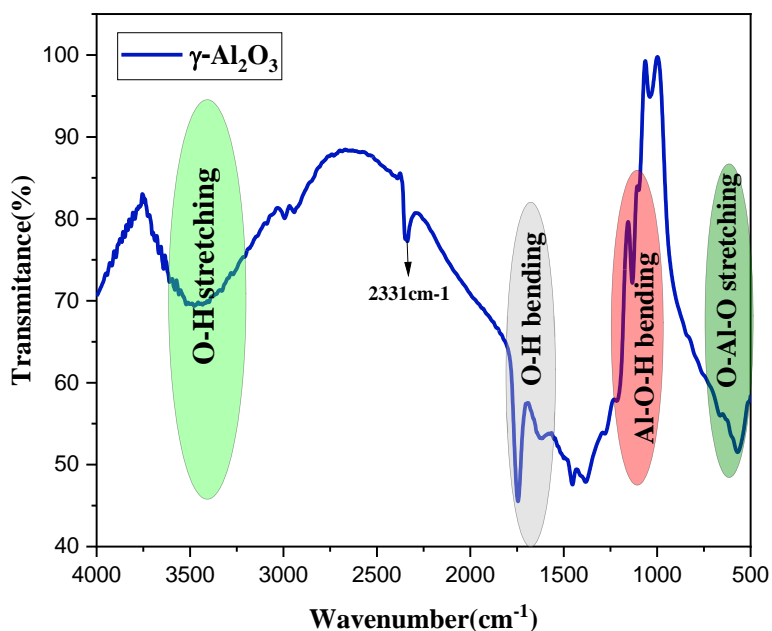


Figure 4. 5: FTIR spectrum of γ - Al_2O_3 nanoparticle

The one at 2331 cm^{-1} is related to CO_2 absorption from the surrounding environment by metal cations that did not remove even with increased temperature (Rajaeiyan & Bagheri-Mohagheghi, 2013b). The other transmittance peak was detected around 1076 cm^{-1} , which was attributed to the (Al–O–H) symmetric bending (Kumar et al., 2011; Tabesh et al., 2018), whereas the peak around 1625 cm^{-1} denoted the OH bending vibration (Rajaeiyan & Bagheri-Mohagheghi, 2013a; Tabesh et al., 2018). Thus, the characteristics transmittance peaks detected in the FTIR spectrum were evidence for the synthesis of $\gamma\text{-Al}_2\text{O}_3\text{-NPs}$.

4.4.3. Particle size analysis for $\text{Al}_2\text{O}_3\text{-NPs}$

The particle size of the as prepared $\text{Al}_2\text{O}_3\text{-NPs}$ was determined using particle size analyzer (PSA), which measures the size distribution of the nanoparticle based on intensity. The synthesis and analytical processes have an impact on the size of metal particles. The analysis was performed with two different dispersants at similar dispersion time to investigate the effect of dispersant on the size distribution of the nanoparticle. As shown in Table 4.5, the particle size of $\text{Al}_2\text{O}_3\text{-NPs}$ was obtained within the nano-size level (i.e. below 100 nm). The raw data of particle size analysis is shown in Appendix C.

Table4. 5: Particle size analysis of Al_2O_3 analyzed by PSDA

Dispersant	Dispersion time(min)	%intensity	Size(nm)	Phase
Ethanol	50	100	923.7	monophase
NaHO	50	57.4	79.82	polyphase
		42.6	15.23	

To prevent particle agglomeration, $\text{Al}_2\text{O}_3\text{-NPs}$ dissolved in ethanol and subjected to a 50-minute sonication process in the first run. However, the results of this run revealed that the highest particle sizes were 923.7 nm of the particles were in the monophase region. According to the aforementioned findings, it was crucial to alter the solvent.

The second test employed NaOH as the solvent and similar dispersion time. The obtained results demonstrated that a polydispersity of two peaks, peak-1 having 79.82nm particle size with 57.4

% intensity, and peak-2 being recorded with a very smaller particle size of 15.23 nm with 42.6 % intensity. The results was shown that the solvent had a considerable impact on the agglomerated particles. These outcomes provided a strong cue that the composites and manufactured particles were in the nano-size range. Finally, 50 minutes and NaOH were found to be the ideal sonication time.

4.4.4. Thermogravimetric analysis for Al₂O₃-NPs

Figure 4.6 demonstrate that the TGA-DTA curve for the aluminum oxide gel prepared by the sol-gel method before the calcination process (Appendix E1). A weight loss of about 19% was observed in the range of 45-178 °C. The result was nearly similar to (J. Li et al., 2007). This decrease was due to the elimination of residual water content absorbed on the surface of nanocrystalline boehmite(dry gel) particles (Fatemeh M, Hasmaliza M, 2011). Then, rapid slope weight loss at 180-535 °C associated with the rapid auto ignition was due to the quick evolution of the gases (CO₂, NO₂ ...). An exothermic peak in this region show typical behavior for the combustion of organic compounds (Tabesh et al., 2018). Thus, the calcination temperature was selected from 535 °C to 1200 °C to obtain alumina nanoparticles. Temperature at 894°C correspond to the amorphous/ γ -Al₂O₃ transformation, γ -/ α -Al₂O₃ transition at 1100°C .The exothermic peaks in the higher temperature range >1000 °C were due to the phase transformation of γ - Al₂O₃ to α - Al₂O₃ and crystal growth of α - Al₂O₃ (Suhasinee Behera et al., 2017). The total weight loss was around 51.98% (4.240mg).

The small difference in the crystallization temperature of phase transformation as observed in DTA and XRD could be because of the difference in heating schedule for the two samples. While XRD (Figure 4.3 and Figure 4.4) pattern was recorded on samples, which were held for 2 h at 1000 °C, the DTA was done without any isothermal hold (Chandradass & Kim, 2009).

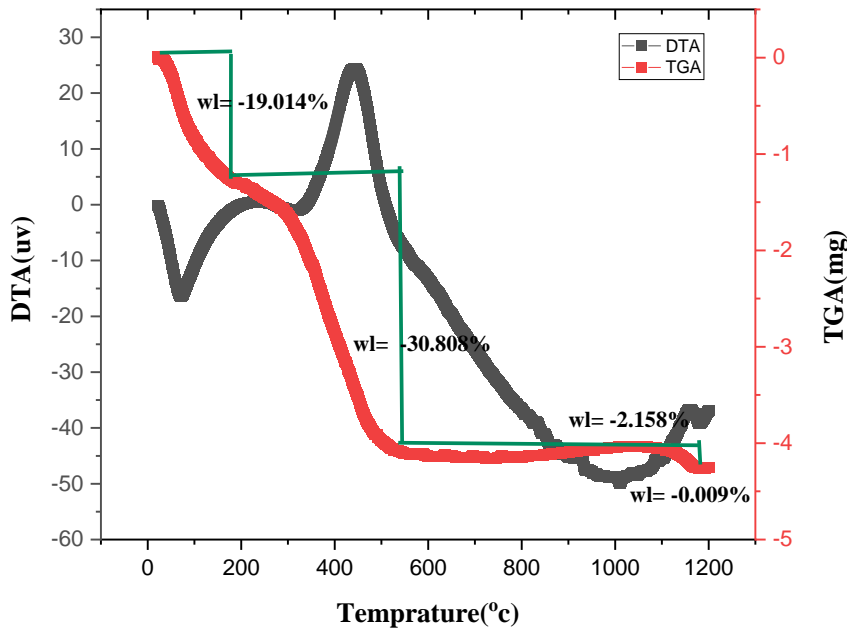


Figure 4. 6: TGA/DTA curve for nitrate – citrate precursor gel

4.5. Characterization of BC and NAMBC

4.5.1. pH at Potential of Zero Charge (pH_{pzc}) determinations for NAMBC

The point where ΔpH crosses zero, i.e. where initial pH equals final pH, indicated the pzc. Based on the Table 4.6 and Figure 4.6 data, this occurs between pH \sim 7.6. This indicated that it has an adsorption affinity for many negatively charged particles including fluoride ions (Brunson & Sabatini, 2014; Nie et al., 2012; Tchomgui-Kamga et al., 2010). For bone char, the pzc was typically around 7 (Chatterjee, Mukherjee, et al., 2018). For alumina, it was typically between 8-9 (Dubey et al., 2017). The pzc of the composite material appeared to be intermediate between the individual components, as expected.

Table4. 6: Experimental data for determination of zero point charge

pH _{initial}	2	3	4	5	6	7	8	9	10	11
pH _{final}	2.98	3.62	4.54	5.41	6.32	7.23	7.82	8.29	8.89	9.39
ΔpH (pH _f - pH _i)	0.98	0.62	0.54	0.41	0.32	0.23	-0.18	-0.71	-1.11	-1.61

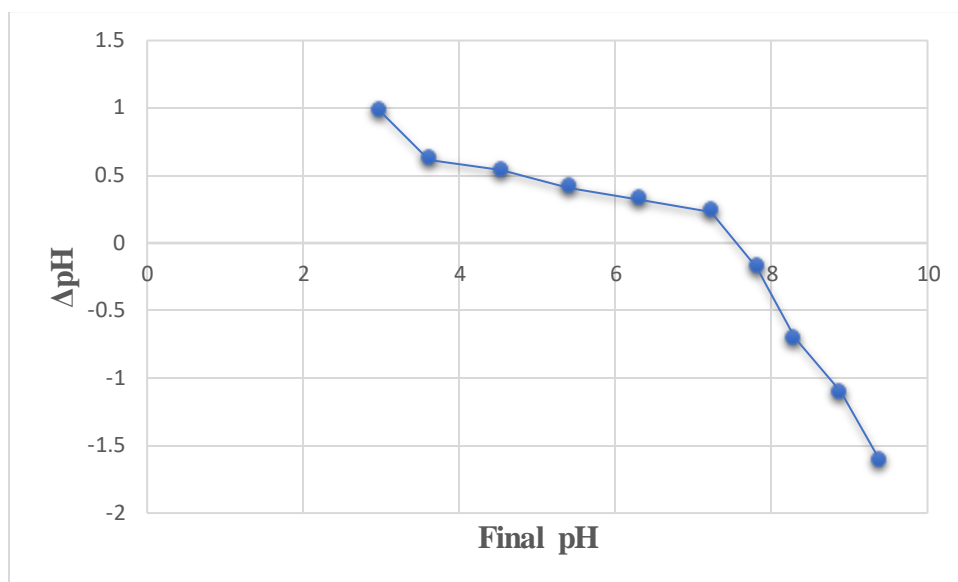


Figure 4. 7: Point zero charge of NAMBC composite

Fluoride removal was strictly associated to the NAMBC's surface charge, which was influenced by adsorbent's point of zero charge (pHpzc) and solution pH value. The pH values of the adsorbents generally fall in the slightly basic region and values of pHpzc >7 show dominancy of basic groups over acidic groups. The presence of basic functional group such as hydroxyl on the surface of thermally activated BC might cause the basic property of activated carbon. The NAMBC adsorbent becomes protonated and positively charged when the pH value falls below its PZC and the deprotonated and negatively charged when pH was above PZC. This was used to fix the optimum pH value used for the adsorption studies.

4.5.2. Crystallographic structural analysis of BC and NAMBC

The BC and NAMBC could be verified in the diffractogram shown in Figure 4.8. The peaks observed at 25.9, 32.3, 39.9, 46.8 and 50° 2θ were characteristic of hydroxyapatite. The peaks at 29.2 and 64.0° 2θ were relative to calcium carbonate (de Melo et al., 2018; Delgadillo-Velasco et al., 2017; Hart et al., 2023). The crystalline structure of Al₂O₃-NPs was identified by using powder X-ray diffraction (XRD) in Figure 4.3. The remarkable diffraction pattern occurred at 2θ 37.2°, 39.7°, 45.8° and 66.9°.

The presence of these four characteristic peaks (37.2°, 39.7°, 45.8°, 66.9°) in the NAMBC (25% Al₂O₃ NPs- 75% BC) composite samples, confirming that Al₂O₃NPs was effectively incorporated

in the BC matrix. Furthermore, no other peaks were visible in the diffraction pattern, confirmed that no other structural form was formed. From Figure 4.8(b) the peaks that represented the presence of Al_2O_3 NPs along with the crystalline structure of BC shown the formation of NAMBC. The characteristics diffraction peaks of Al_2O_3 NPs at 37.1° , 39.85° , 46° , and 66.9° , shown the presence of Al_2O_3 NPs. It could be concluded that the XRD patterns shown the formation of BC/ Al_2O_3 NP composite.

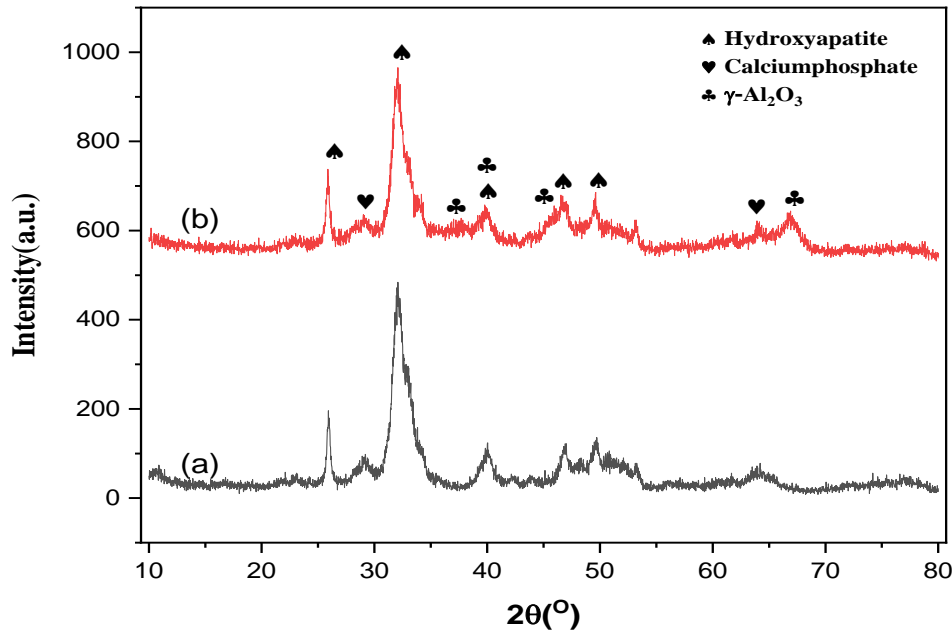


Figure 4. 8: XRD pattern of (a) BC and (b) NAMBC

The formation of NAMBC composite was studied from the XRD patterns and the fundamentals of detecting the formation of composite particles were comparing the crystallite size and the space between the planes of the pure (single) sample and the composites. The values for each Peak position were obtained using Scherrer and Bragg's equation given in Eq (3.5) and Eq (3.6) Using these equations the calculated values for crystallite size and the space between the planes were obtained. In Table 4.7 the values of crystallite size and the space between the planes for each peak position of 100% BC and 25% Al_2O_3 NPs- 75% BC composite were listed and the values for 100% BC were taken as a reference to saw the effect of Al_2O_3 NPs on crystalline size and D-spacing of NAMBC composite. The values of crystalline size (D) for BC and NAMBC were 7.31nm and

5.54nm respectively. These result compared to (Medellin-Castillo et al., 2016) small crystalline size due to lower calcination temperature, leading to a better adsorption capacity(Hart et al., 2023).

Table4. 7: Crystalline size and d-spacing of BC and NAMBC

Adsorbent	Peak position	FWMH	Crystalline size(D)(nm)	D-average(nm)	d-spacing	Average d(nm)
BC	25.93775	0.4674	17.44166717	7.311808	0.343238	0.239125
	29.04178	1.52404	5.384657191		0.307219	
	32.31065	1.9112	4.32759477		0.276845	
	39.96947	1.25516	6.734851622		0.225386	
	46.83572	0.81948	10.56449403		0.193818	
	50.02228	4.61089	1.901226886		0.182193	
	64.09093	1.94119	4.828164276		0.145177	
NAMBC	25.87054	0.46869	17.39131545	5.541115197	0.344114	0.229173937
	28.85508	1.24198	6.604761957		0.309164	
	32.18193	1.50158	5.506342576		0.277923	
	37.11893	5.50369	1.522634137		0.242013	
	39.85888	1.11783	7.559606098		0.225985	
	46.24762	2.23988	3.856592499		0.196145	
	49.91383	4.9445	1.772167656		0.182563	
	64.17449	5.23206	1.792155817		0.145009	
	66.95348	2.46458	3.864460579		0.139649	

In the 25% Al₂O₃ NPs- 75% BC composition, the concentration of Al₂O₃ NPs was much smaller than that of BC yet its effect in lowering the crystalline size and the D-spacing values. There was the formation of a new peak (66.9°) with high value of crystalline size, these phenomena confirmed the formation of NAMBC composite.

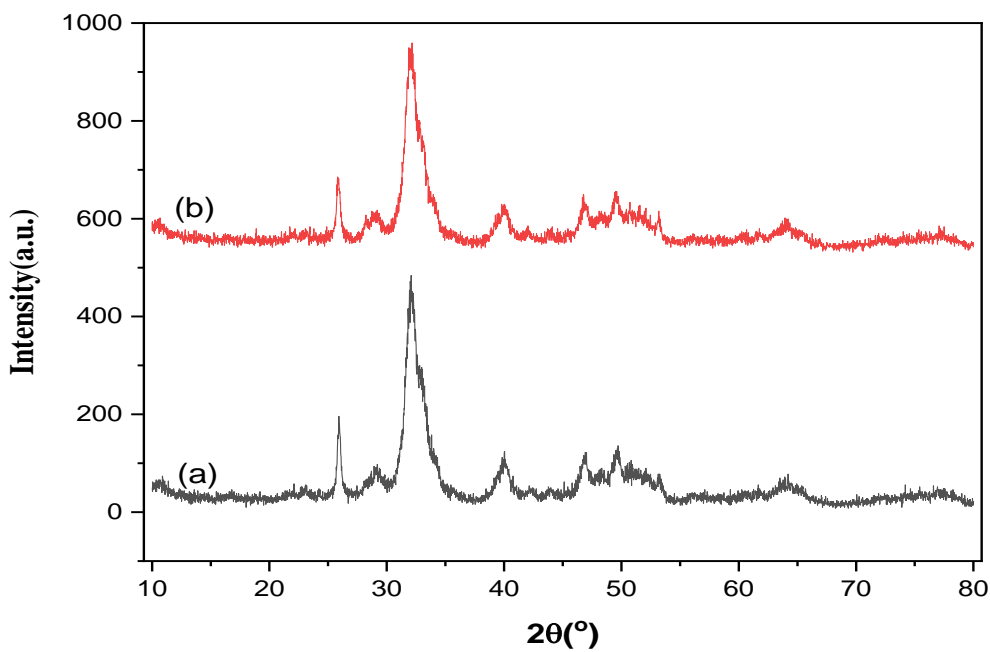


Figure 4. 9: XRD pattern of BC (a) before adsorption and (b) after adsorption

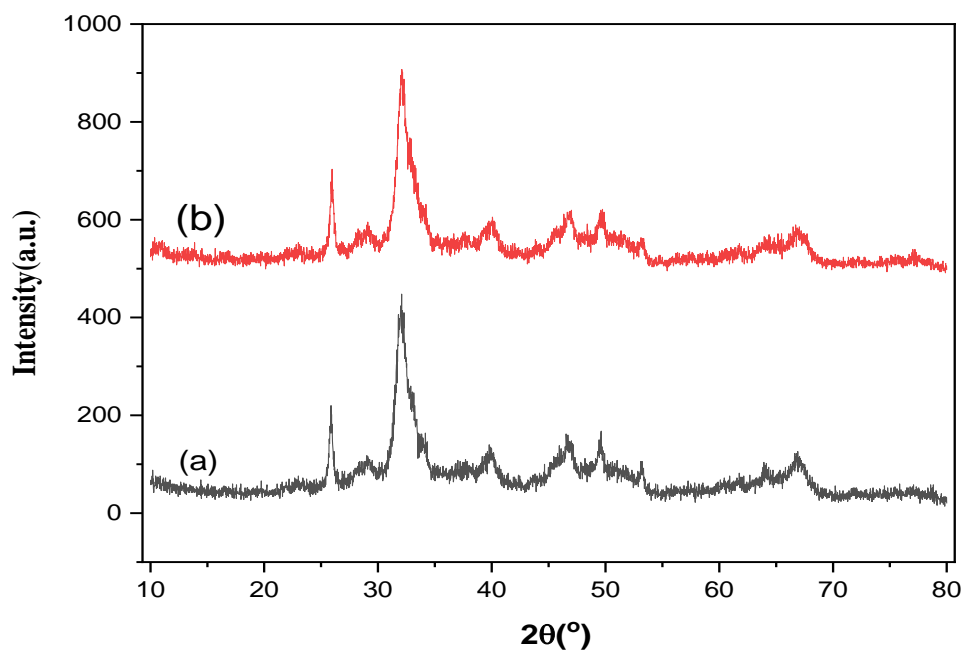


Figure 4. 10: XRD pattern of NAMBC (a) before adsorption and (b) after adsorption

The XRD of BC without fluorides had four main peaks located at 2θ of 25.9°, 29°, 32.3°, 39.97°, 46.8°, 50° and 64°. As shown, on Figure 4.9 there is no marked change in the XRD pattern of BC after adsorption. Only F^- ions have been replaced with hydroxyl functional groups of bone char. This finding was similar to the report of Poinern et al. (2011). On the fluoride adsorption onto hydroxyapatite. The bone char was primarily made up of hydroxyapatite ($Ca_{10}(PO_4)_6(OH)_2$), which has a very crystalline structure. The adsorption of fluorine ions mainly occurs on the surface of the hydroxyapatite crystals, so the bulk crystal structure is not altered (Hu et al., 2017). Fluorine has a similar ionic radius and charge as the hydroxyl group it was replacing on the hydroxyapatite crystal surface. This substitution of F^- for OH^- does not cause major distortions in the overall crystal structure (Aoba, 1997).

As shown in Figure 4.10(b), the diffraction characteristic peaks at 37.2°, 39.7°, 45.8° and 66.9° indicated that the $\gamma-Al_2O_3$ crystal phase of the sample remain unchanged after the adsorption of fluoride ions. However, peaks intensities become slightly lower after fluoride adsorption. This is due to the fact that the $\gamma-Al_2O_3$ is protonated to form Al-OH bonds in aqueous solution, and the generated -OH bonds was easily replaced by F^- (Yu et al., 2023).

4.5.3. Functional group analysis of BC and NAMBC

The adsorption mechanism of fluoride on BC and NAMBC was elucidated by performing the FTIR analyses of BC and NAMBC before and after adsorption of fluoride, and the spectra were shown in Figure 4.11 and Figure 4.12. In FT-IR spectrum diagram of the BC and NAMBC, there was P-O stretching vibration at 566 cm^{-1} and 1025 cm^{-1} indicated the existence of PO_4^{3-} (Delgadillo-Velasco et al., 2017; Niu et al., 2021). The characteristic peaks at 1410 cm^{-1} and 1627 cm^{-1} represented the vibration peaks of the alkoxy C-O stretching vibration, indicated the presence of CaCO_3 in the product (Hart et al., 2023). Peak at 2919 cm^{-1} is related to the stretching vibration of C-H of methyl groups and peaks at 3380 cm^{-1} could be assigned to the stretching vibration of O-H of hydroxyl groups (Delgadillo-Velasco et al., 2017; Rojas-Mayorga et al., 2015). The identification of these bands corroborated the presence of hydroxyapatite and other calcium phosphate minerals in the samples.

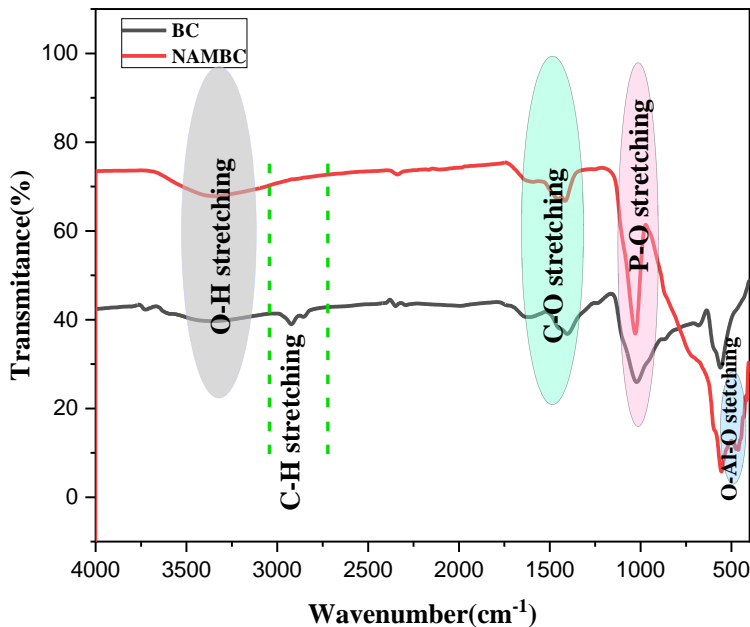


Figure 4. 11: FTIR pattern of BC and NAMBC

Note that FTIR spectra of the NAMBC was shown almost the same intensity for the absorption bands shown that the modification did not affect the structure of the hydroxyapatite (Figure 4.10). However after modification, in the stretching vibration area of hydrogen bond held together with

-OH, intensity of the typical absorption band of hydroxyapatite (3400 cm^{-1} nearby) has risen obviously. Similar findings have been reported in previous studies (H. Li et al., 2014). NAMBC shown a loss in the intensity for the absorption bands(C-H stretching). These results further confirmed the partial dissolution of the hydroxyapatite in the metallic solution used during the surface modification of bone chars (Rojas-Mayorga et al., 2015). In contrast, other peaks had tiny significant change. And also, new peaks were observed at $734, 597, 556, 474$ and 462 cm^{-1} for the NAMBC compared to the BC. These peaks were correspond to Al-O vibration, which indicated, successful incorporation of $\text{Al}_2\text{O}_3\text{NPs}$. This could be because of the ion exchange of the $\text{Al}(\text{OH})_4^-$ on the bone structure (H. Li et al., 2014). The appearance of aluminum on the NAMBC from the XRD (Figure 4.8(b)) and the FT-IR result supported the formation of the NAMBC composite.

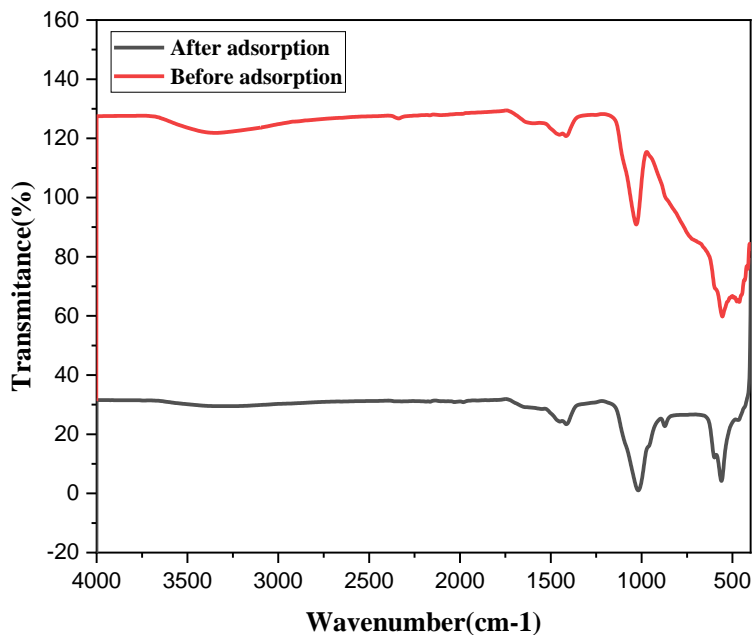


Figure 4. 12: FTIR pattern of NAMBC before and after adsorption

The FT-IR spectra of the NAMBC before and after fluoride ion adsorption, respectively were analyzed (Figure 4.12). The absorption band intensity at 3400 cm^{-1} decreased after adsorption indicated the adsorption through hydroxyl interchange with fluoride ion (Rojas-Mayorga et al., 2015). It was also evident that the $\text{Al}_2\text{O}_3\text{NPs}$ was directly participated in the adsorption process because of the strong peaks at 734 and 461 cm^{-1} on the NAMBC adsorbent vanished after the

interaction with fluoride ion during adsorption. The additional Al-O binding sites in modified bone char resulted in higher fluoride adsorption capacity compared to raw bone char. The spectrum of NAMBC saturated with fluoride presented the same bands as before adsorption and did not exhibit dramatic variations in the intensity or width of the bands due to fluoride adsorbed. This fact confirms that fluoride adsorption on thermally treated BC was mainly due to electrostatic interactions between the positively charged sites and fluoride ions, but chemisorption might not be disregarded (Hu et al., 2017; Medellin-Castillo et al., 2016).

Overall, the unique hydroxyl groups, high surface area, and reactive nature of nano alumina particles change the bone char surface chemistry significantly by adding new functional groups, altering inorganic content, and increasing reactivity. This can enhance adsorption capacity of bone char toward fluoride.

4.5.4. BET analysis of BC and NAMBC

The BET analysis was shown (Appendix F1 and F2) that the NAMBC reduced the SSA from 479.8 to 464.3 m²/g. The SSA of the BC was better when compared to the NAMBC adsorbent and the values presented by different researches done on BC (Roba et al., 2023). The reduction was expected because of the impregnation of the nano alumina in the pore spaces of the BC during the formation of the composite.

4.5.5. TGA/DTA analysis

The TGA/DTA results of cattle bone were shown in Figure 4.13. Shown three endothermic peaks. 50-180 °C, incorporated water is lost and this was supported by the DTA analysis. The result was nearly similar to (Hart et al., 2023). A continuous weight loss was observed between 200 °C and about 610 °C, which can be associated to the removal of organic portion such as collagen and proteins (Ooi et al., 2007). The weight loss in the temperature range of 721 °C to 929 °C was very small, which was attributed to the formation of gaseous elements eventually led to the formation of inorganic residue consist of hydroxyapatite. Moreover, in this temperature range the escape of carbon dioxide from calcium carbonate also took place (Farooq & Ramli, 2015). The curves further shown that weight loss above 930 °C was almost constant, thus confirmed the completion of decomposition process.

The average amount of water and organic phases removed during heat treatment was calculated as shown on Figure 4.13. The results indicated that approximately 28.237% of water was lost when

the bone sample was heated from room temperature to about 368°C. A further approximately 13.68% of organics was removed between 368°C and 613°C. Therefore, it could be inferred that about 42% of total weight loss was due to removal of water and organic substances from the cattle bone when annealed up to about 613°C.

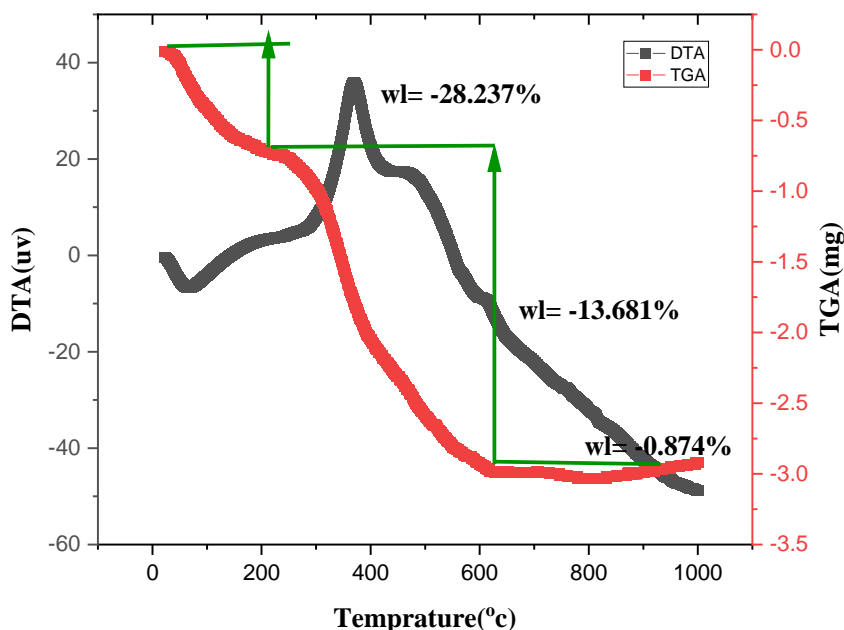


Figure 4. 13: TGA/DTA curve for raw bone

4.6. Parameter effects on fluoride removal

4.6.1. Effect of pH

The effect of solution pH on the capacity of NAMBC sample for adsorbing fluoride was studied by vary solution pH values and constant 2hr contact time, 2 g NAMBC and initial concentration of adsorbate was 10 mg/L, and results are graphed in Figure 4.14. As shown in Table 4.8, the fluoride adsorption capacity of NAMBC sample was significantly dependent on the solution pH since the capacity was raised by reducing the solution pH. At fluoride concentration of 10 mg/L, the percentage of fluoride removal was 98.8, 98.1, 97.3, 97 and 93.9 % at pH values of 3.0, 5.0, 6.57, 7.0 and 9.0, respectively. Hence, the adsorption capacity was decreased when the solution pH increased. Similar behavior has been reported for the adsorption of fluoride on BC and Al₂O₃ (Dubey et al., 2017; Medellin-Castillo et al., 2007, 2014).

Table4. 8: Effect of pH on fluoride removal efficiency

pH	Residual fluoride con. (Px)			Average final con. (mg/l)	NAMBC performance	
	Ct1	Ct2	Ct3		%F ⁻ Removal	Q(mg/g)
3	0.12	0.12	0.11	0.12	98.8	0.494
5	0.2	0.19	0.19	0.19	98.1	0.4905
6.57	0.27	0.28	0.27	0.27	97.3	0.4865
7	0.3	0.3	0.3	0.3	97	0.485
9	0.62	0.6	0.63	0.61	93.9	0.4695

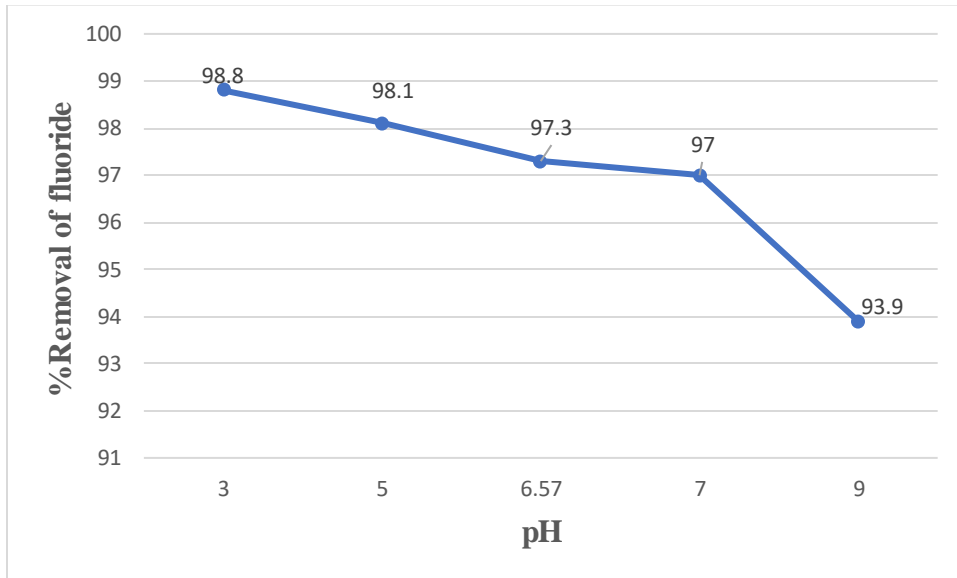


Figure 4. 14: pH effect on fluoride adsorption efficiency

The data revealed that the maximum adsorption capacity occurred at pH=3 so that should be the optimal pH. However, this value was in highly acidic range of pH, it was not advisable to treated drinking water. Therefore as the pH_{pzc} of the selected adsorbent was around 7.6, it was better to work at the pH of 6.57 which is the pH without adjusted and normal pH of the sodium fluoride solution. This is because at this pH, the WHO guide line value (<1.5mg/L) was well achieved since 97.3 % removal capacity gives 0.27mg/L residual fluoride concentration for this batch experiment.

The effect of pH on the adsorption capacity could be explained by considering the electrostatic interactions between the surface charge of NAMBC and the fluoride anion in solution. The pH_{PZC} of the NAMBC was ~ 7.6 (Figure 4.7). At pH values lower than pH_{PZC} , fluoride adsorption was favored because of the electrostatic attraction between the negative ions of fluoride in the solution and the positively charged surface of NAMBC. On the other hand, at pH values higher than pH_{PZC} , the surface was mainly charged negatively so that the electrostatic repulsion disfavored the adsorption of fluoride (Nie et al., 2012).

4.6.2. Effect of contact time

The effect of the length of contact time between fluoride water and the composite on percentage removal of fluoride could be observed at Figure 4.15 and table 4.9; as the adsorption time increased more fluoride ions from the solution would have more probability to stick to the available active site of the adsorbent until equilibrium reached. After equilibrium no more fluoride ion would be absorbed. This trend was also reported by other studies on defluoridation processes (Chatterjee, Mukherjee, et al., 2018; Dubey et al., 2017).

Table4. 9: The effect of contact time on % fluoride removal

Contact time(hr)	Residual fluoride con. (mg/L)			Average final con. (mg/L)	NAMBC performance	
	Ct1	Ct2	Ct3		%F ⁻ Removal	qt(mg/g)
0	10	10	10	10	0	0
0.5	0.59	0.61	0.62	0.6	94	0.47
2	0.48	0.48	0.47	0.48	95.2	0.476
4	0.34	0.32	0.35	0.33	96.7	0.4835
6	0.26	0.27	0.27	0.27	97.3	0.4865
8	0.27	0.26	0.27	0.27	97.3	0.4865
12	0.27	0.27	0.27	0.27	97.3	0.4865

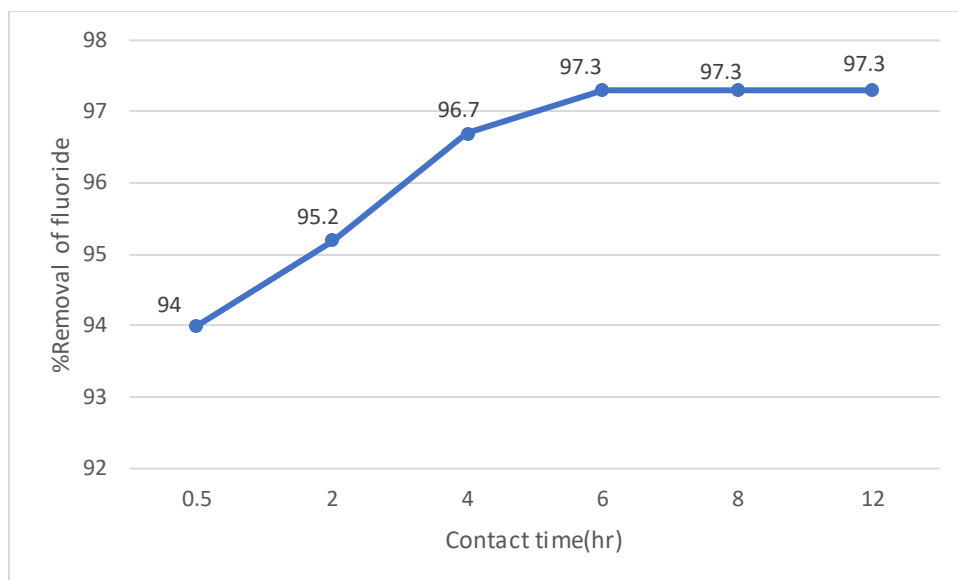


Figure 4. 15: The effect of contact time on the percentage removal of fluoride

The percent fluoride removal increased over time, from 94 % at 0.5 hr to 97.3 % at 6 hrs. This shown that the adsorbent became more effective at removing fluoride with increased contact time. The adsorption capacity (q_t) increased over time, leveling off after about 6 hrs at 0.4865 mg/g. This suggests that the adsorbent was reached saturation. Overall, the data was shown that the NAMBC adsorbent was effective at removal of fluoride from water over time.

4.6.3. Effect of adsorbent dose

Variation on percentage removal of fluoride ion from water on NAMBC composite adsorbent at 2 hr contact time and 10 mg/L initial fluoride concentration with varied adsorbent dosage was shown in Table 4.10. It was observed that the Percentage of defluoridation increases from 97.3 to 98.9 as the adsorbent dose was increased from 2 g to 9 g. This was due to increased adsorption of fluoride, which was facilitated by availability of more adsorption active sites. However, percentage of defluoridation remains roughly the same after this, due to overlap of active sites at higher adsorbent concentration.

Table4. 10 : The effect of adsorbent dose on fluoride removal efficiency

Dose	Residual fluoride con. (mg/L)			Average final con. (mg/L)	NAMBC performance	
	C _{t1}	C _{t2}	C _{t3}		%F-removal	Q(mg/g)
0	10	10		10	0	0
2	0.27	0.27	0.26	0.27	97.3	0.4865
3	0.16	0.16	0.16	0.16	98.4	0.492
6	0.13	0.12	0.12	0.12	98.8	0.494
9	0.11	0.13	0.10	0.11	98.9	0.4945

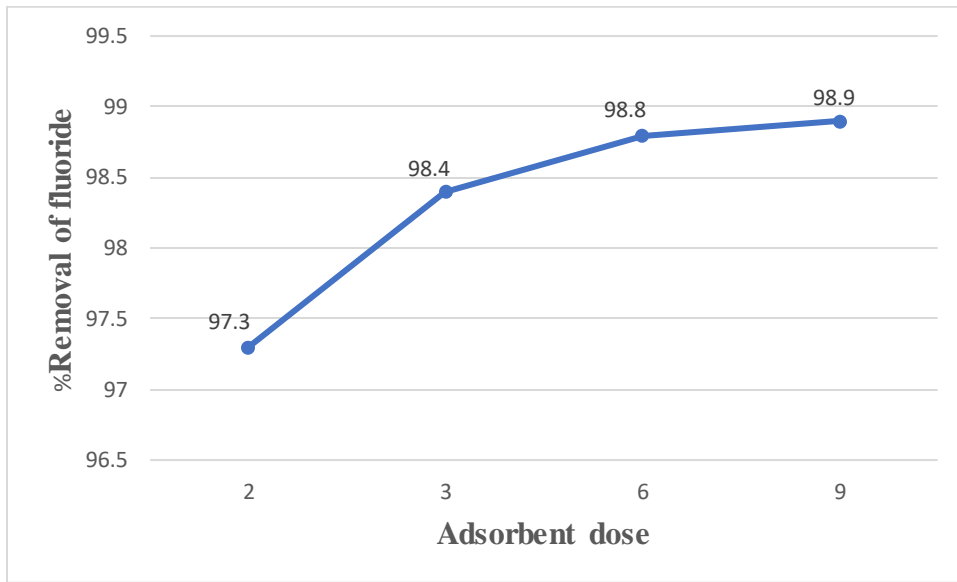


Figure 4. 16: The effect of adsorbent dose on the percentage removal of fluoride

The percentage of fluoride removal, shown on Figure 4.16, clearly suggested adsorption of fluoride ion directly proportional to amount of adsorbent dosage (Chatterjee, Mukherjee, et al., 2018).

4.6.4. Effect of initial fluoride concentration

Table 4.11 shown the general relation between the overall defluoridation efficiency and initial F⁻ concentration. Fluoride removal efficiency was gradually decreased from 98 to 81.05% as the latter increased from 5 to 20 mg/L. This is because, due to increased diffusion of fluoride to adsorption sites and utilization of less active sites of the adsorbent (Getachew et al., 2015).

Table4. 11 : The effect of initial fluoride concentration on fluoride removal efficiency

C _o (mg/l)	Residual fluoride con. (P _x)			Average final con. (mg/l)	NAMBC performance	
	C _{t1}	C _{t2}	C _{t3}		%F-removal	Q(mg/g)
5	0.1	0.1	0.1	0.1	98	0.245
10	0.29	0.28	0.26	0.27	97.3	0.4865
15	1.3	1.2	1.2	1.2	92	0.69
20	3.79	3.79	3.78	3.79	81.05	0.8105

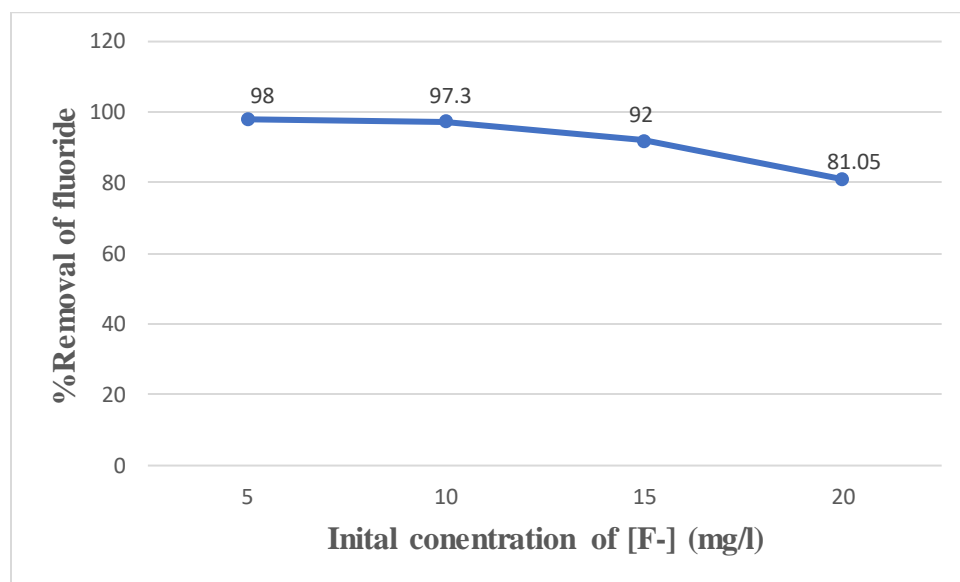


Figure 4. 17: The effect of initial fluoride ion concentration on the percentage removal of fluoride using 2 g NAMBC and 2hr contact time

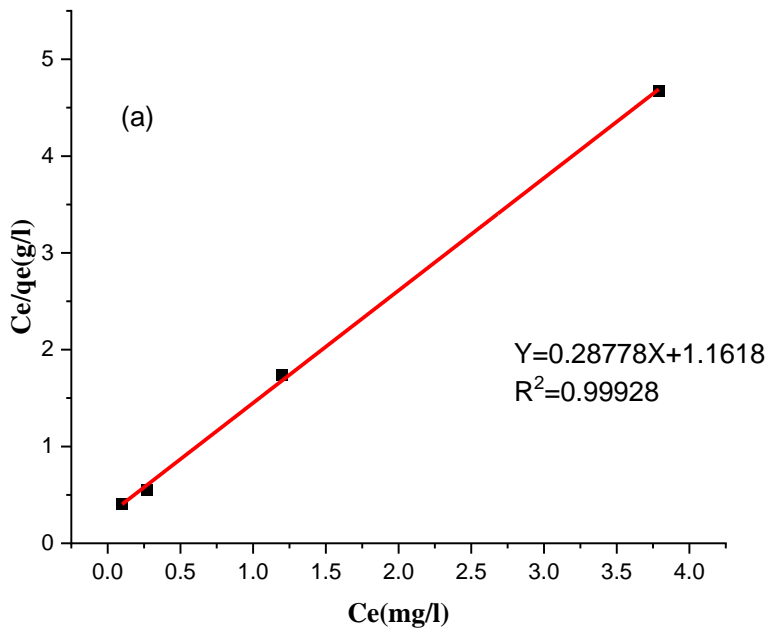
As seen in Figure 4.17, the percentage removal for modified bone char was almost constant up to 10 mg/L, there was a continuous decreased in the removal capacity to 81.05% then after. This may be due to fluoride interaction with the active sites at low initial fluoride concentrations leading to a higher percentage removal of fluoride. As the fluoride concentration increased, only a part of the fluoride interacts with the finite binding sites, resulting in a decreased in the percentage removal of fluoride(Shivaprasad et al., 2018).

4.7. Experimental Result on Adsorption Isotherm

Both Langmuir and Freundlich for fluoride ion adsorption on the composite adsorbent (NAMBC) were done at room temperature. Data for plotting isotherms were obtained by mixing a constant adsorbent dose of 2 g/100mL with a series of increased fluoride concentration (5, 10, 15 and 20mg/L). Based on the data generated (Table 4.12), adsorption isotherms were plotted in Fig 4.18.

Table4. 12: Langmuir's (C_e Vs C_e/q_e) and Freundlich's ($\log C_e$ Vs $\log q_e$) adsorption isotherm data

C_o (mg/l)	C_e (mg/l)	q_e (mg/g)	$\log C_e$	$\log q_e$	C_e/q_e (g/l)
5	0.1	0.245	-1	-0.61083	0.408163
10	0.27	0.4865	-0.56864	-0.31292	0.554985
15	1.2	0.69	0.079181	-0.16115	1.73913
20	3.79	0.8105	0.578639	-0.09125	4.676126



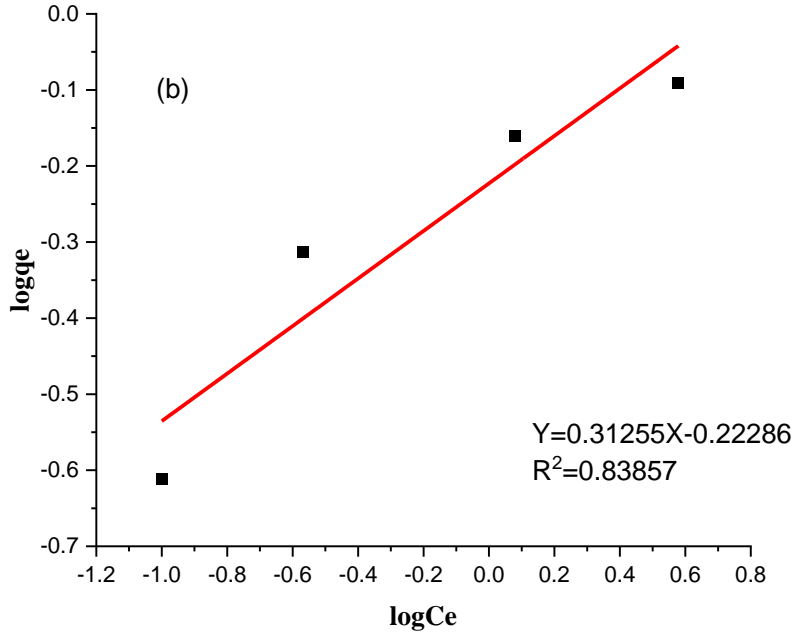


Figure 4. 18: Adsorption isotherms of NAMBC a) Langmuir Isotherm b) Freundlich Isotherm

The Langmuir adsorption isotherm model assumed monolayer adsorption on an adsorbent surface and limits adsorption once all surface sites were occupied. All the active surfaces have uniform energies of adsorption with no transmigration of the adsorbate in the surface plane, while the Freundlich model was used to represent multilayer adsorption on heterogeneous surfaces(Hart et al., 2023).

Table4. 13: Langmuir and Freundlich isotherm model parameters describing the NAMBC fluoride adsorption at a constant adsorbent dose of 2 g and contact time of 6 hr.

Langmuir isotherm parameters				Freundlich isotherm parameters		
q _{max}	K _L	R _L	R ²	K _F	1/n	R ²
3.474877	0.2477	0.287604	0.99928	0.598591	0.31255	0.83857
$Y = 0.28778X + 1.1618$				$Y = 0.31255X - 0.22286$		

The coefficients determined for isotherms were summarized in Table 4.13. In addition, Figure 4.18 was plotted using the experimental and predicted values obtained by linear regression methods for the two isotherm models. The correlation coefficient value for NAMBC was the highest for the Langmuir ($R^2 = 0.99928$) (Fig. 4.18) than Freundlich ($R^2 = 0.83857$) isotherms. The result was much better than (Nigri et al., 2017). As a result, the Langmuir isotherm was fitted well for adsorption of fluoride on NAMBC under the process conditions applied. These results predicted that the adsorption on NAMBC represent a monolayer adsorption with adsorbate/adsorbate interactions process. The maximum predicted adsorption capacity (q_m) for the NAMBC using Langmuir model was found to be 3.474877 mg/g.

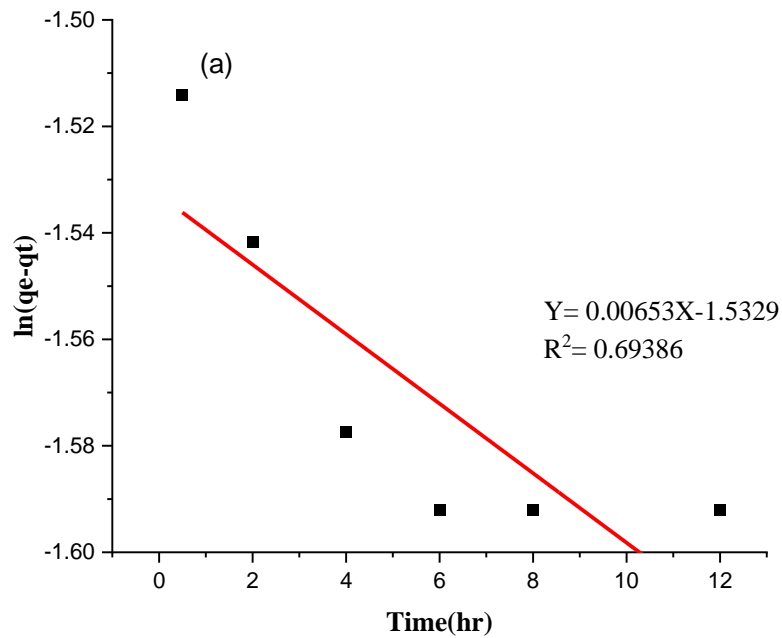
A further analysis of the Langmuir equation could be made based on a dimensionless equilibrium parameter, R_L also known as the separation factor, given by Eq (3.10). The effect of isotherm shape could be used to predict whether an adsorption system was favorable or unfavorable. The essential features of Langmuir isotherm could be expressed in terms of a dimensionless separation factor or equilibrium parameter, the isotherm was unfavorable when $R_L > 1$, linear when $R_L = 1$, favorable when $0 < R_L < 1$ and irreversible when $R_L = 0$. In this work the R_L value calculated was 0.2876 (Table 4.13), which suggested the favorable adsorption of fluoride onto NAMBC absorbent, under the conditions used for the experiment.

4.8. Adsorption kinetics model

The rate at which dissolved fluoride ions were removed from aqueous solution using the composite matter was a significant factor. The rapid adsorption processes were quite useful for practical use due to the need of short contact time in the actual process. In the present study, the kinetics of defluoridation was carried out to study the behavior NAMBC (Table 4.14). Figure 4.17 shown the pseudo first order and pseudo second order kinetics of fluoride ion sorption experiment at room temperature.

Table 4. 14: Kinetic data obtained by varying the contact time using a constant adsorbent dose of 2 g NAMBC, and 10 mg/L of fluoride concentration.

t(hr)	ce(mg/l)	qt(mg/g)	ln(qe-qt)	t/qt
0.5	0.6	0.47	-1.51413	1.06383
2	0.48	0.476	-1.54178	4.201681
4	0.33	0.4835	-1.57745	8.273009
6	0.27	0.4865	-1.59209	12.33299
8	0.27	0.4865	-1.59209	16.44399
12	0.27	0.4865	-1.59209	24.66598



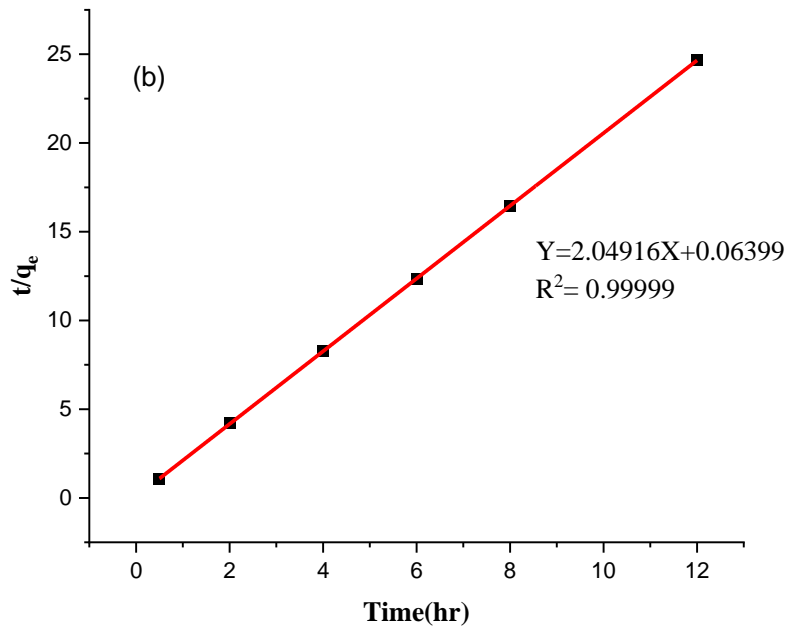


Figure 4. 19: Adsorption kinetic models for NAMBC a) Pseudo-first-order kinetics b) Pseudo-second-order kinetics

From the result of adsorption kinetic first-order and second-order data, it was possible to summarize the adsorption behavior of the adsorbents prepared (Table 4.14). The correlation coefficient (R^2) was found to be 0.69386 and 0.99999 for pseudo-first-order kinetics and pseudo-second-order kinetics, respectively. The value of R^2 for pseudo-second-order kinetics approached to one. The experimental equilibrium adsorption capacity and the calculated capacity are close to the R^2 value of 0.9999, which was better than (Nigri et al., 2017). This indicated that it was unity and the adequate linear fitting of the plots confirmed that the adsorption of fluoride ions using NAMBC followed pseudo-second-order kinetics. These results depicted that the rate-limiting process was the chemisorption process (Roba et al., 2023).

Table 4. 15: Adsorption kinetic parameters for pseudo-first-order kinetics and pseudo-second-order kinetics

Pseudo first order kinetics model				Pseudo second order kinetics model			
intercept	K ₁	q _e	R ²	intercept	K ₂	q _e	R ²
-1.5329	0.00653	0.215909	0.69386	0.06399	65.62047	0.488005	0.99999
$Y = 0.00653X - 1.5329$				$Y = 2.04916X + 0.06399$			

4.9. Comparison with other adsorbents

In order to investigate the kinetics process such as the mechanism of adsorption and potential rate controlling steps, basically the order of process has to be studied. Like most of the adsorbents studied previously such as activated silica gel and rice husk ash (Mondal et al., 2012), nano hydroxyapatite (Sani et al., 2016) and nanoparticles of gamma alumina (Dubey et al., 2017) the NAMBC studied in the present work also obeyed Langmuir adsorption isotherm with pseudo second order kinetics. Thus, fluoride adsorption followed chemisorption rather than physical adsorption with uniform monolayer coverage without transmigration of the adsorbate (F⁻) (Dubey et al., 2017). Direct comparison of the performance of these adsorbents with other adsorbent materials might be difficult, owing to the different experimental conditions under which they were applied. Nevertheless, the performance could at least be compared based on their maximum adsorption capacity (q_e). The q_e values depend on the initial concentration of the fluoride ions. There was a tendency of increment in q_e as initial concentration increased. The observed q_e for NAMBC, at initial concentration of 10 mg/L of fluoride was 3.47 mg/g. This is comparable to the q_e value of activated rice husk ash (0.426 mg/g) and activated silica gel (0.308 mg/g) at initial concentration of 15 mg/L of fluoride (Mondal et al., 2012).

Adsorption capacities of different products were shown in Table 4.16. Novel features of NAMBC compared to other adsorbents were observed from this table. First, modified bone char using nano gamma alumina have been attempted for the first time in this work. Second, the fluoride adsorption capacity was the highest in the case of NAMBC. All these materials have issue regarding

scalability, complexity in manufacturing, and most importantly cost. This makes the synthesized adsorbent, i.e., NAMBC, unique and highly beneficial in fluoride treatment of groundwater.

Table4. 16: Comparison of uptake capacity of NAMBC with other adsorbents

Adsorbent	Adsorption capacity(mg/g)	Ref.
Rice husk ash	0.426	(Mondal et al., 2012)
Silica gel	0.308	(Mondal et al., 2012)
Activated quartz	1.16	(Fan et al., 2003)
Aluminum iron treated corrosion	0.48	(García-Sánchez et al., 2013)
calcite	0.39	(Fan et al., 2003)
quartz	0.19	(Fan et al., 2003)
Bone char treated with trivalent-metal hydroxide	1.4365	(Roba et al., 2023)
Bone char	1.36	(Roba et al., 2023)

4.10. Regeneration of the NAMBC

For evaluating the application and lifespan of NAMBC, regeneration methods were necessary, which reduced the cost of the process and reduced the amount of unwanted waste. The regeneration of an adsorbent plays an important role in its evaluation. This aspect has only been reported in a few studies, which might limit industrial applications of BC. From an economic point of view, it was crucial to study the desorption and regeneration performance of adsorbents to evaluate their practical application potential. Batch experiments were carried out to verify the regeneration and reusability of NAMBC. The repeated experiments were performed as shown in Table 4.17 with a temperature of 25 °C, initial F- concentration of 10 mg/L, sample dosage of 10 g and 0.5M NaOH solution as the desorption reagent. The ion-exchange of hydroxyl groups with fluoride ions on BC

adsorbents was efficient in strong alkaline solution (Hu et al., 2017). Regeneration desorption mechanism:

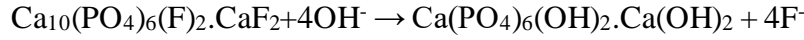


Table4. 17: number of cycle of regenerated NAMBC

No. of cycle	Residual fluoride Con. (mg/L)			Final con. (mg/l)	F ⁻ Removal (%)
	t-1	t-2	t-3		
1	0.17	0.14	0.16	0.15	98.5
2	0.33	0.3	0.32	0.33	96.7
3	0.48	0.48	0.47	0.48	95.2

As shown in Figure 4.20, a considerable reduction in adsorption efficiency occurred in the second and third cycle of adsorption after the regeneration (Niu et al., 2021). At the end of the third cycle, 95.2% regeneration efficiency was observed. Therefore, the current experiments prove that the modified adsorbent has relatively good stability and reusability.

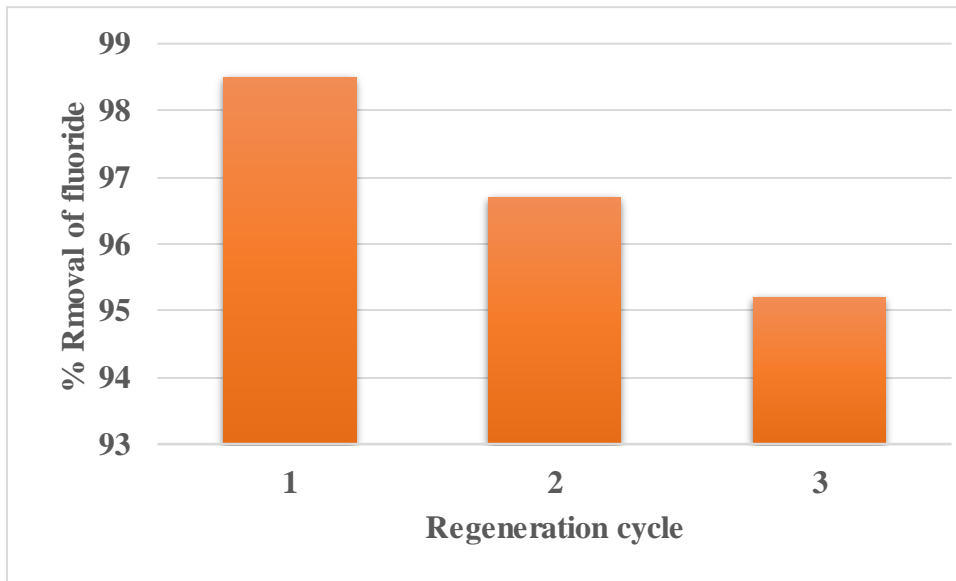


Figure 4. 20: NAMBC regeneration experiment

4.11. Application on real water sample

The chemical compositions of Beseka ground water were determined and presented in table 4.1

Table 4.1 characteristics of ground water

parameters	unit	value
PH	-	9
TDS	mg/L	3490
TH	mg/L	20
COD	mg/L	82
Turbidity	NTU	0.73
Color	PtCo	31
TSS	mg/L	-1
BOD	mg/L	32
Sulfate(SO ₄ ²⁻)	mg/L	200
Calcium(Ca ²⁺)	mg/L	12
Magnesium(Mg ²⁺)	mg/L	8
Fluoride(F ⁻)	mg/L	7.95

The fluoride concentration of the feed was 7.95 mg/L, which was reduced to 1.3 mg /L after 6 hr of time. The NAMBC performance was decreased when the solution was changed from synthetic to a real. This happens due to the presence of various dissolved ions such as calcium, magnesium and sulfate competing for the adsorption sites of NAMBC. Additionally, the water has a high pH of 9. As shown, Fig 4.14. bone char works best for fluoride removal in a pH range of <7. The high pH here may reduce the effectiveness of fluoride adsorption onto the bone char(Chatterjee, Jha, et al., 2018). The water has a high total dissolved solids (TDS) concentration, this could interfere with the adsorption sites on bone char, reducing its fluoride removal capacity (Maheshwari, 2006).The result shown, sulfate concentration was 200 mg/L. Sulfate ions could compete with fluoride for adsorption sites on bone char (Dubey et al., 2017; Shivaprasad et al., 2018). BOD, COD, color and TSS indicated the potential for organic/particulate fouling of the bone char filter. This might reduce fluoride removal efficiency.

CHAPTER FIVE

5. CONCLUSION AND RECOMMENDATION

5.1. Conclusion

Bone char which was found from cattle bone and modified using γ - Al_2O_3 nano particles. In order to analyze the formation of NAMBC composite and how it was modified FTIR analysis was performed. The analysis results revealed that the formation of NAMBC composite was confirmed by increasing OH characteristics peaks.

The synthesis of alumina nano particles was performed through sol-gel method and the formation and characteristics of the Al_2O_3 -NPs and was confirmed by using XRD, TGA, FTIR and the size of the nanomaterials confirmed by PSDA. The XRD results revealed that there was a phase transition due to increased temperature and the average crystalline size of gamma alumina and alpha alumina nano particles are 2.44 nm and 30.84 nm, respectively. The particle size distribution was poly disparity of two peaks, peak-1 having 79.82nm particle size with 57.4 % intensity, and peak-2 being recorded with a very smaller particle size of 15.23 nm with 42.6 % intensity.

Bone char shown good potential as an adsorbent for fluoride removal, with optimum pyrolysis temperature around 450°C, 3 hr. modifying the bone char by adding nano alumina improved the fluoride removal capacity compared to bone char alone. The best performance was with a 2:1 ratio of bone char to nano alumina. The maximum adsorption capacity of NAMBC achieved was around 4.47 mg/g. FTIR and XRD analysis confirmed fluoride adsorption occurred through ion exchange with the hydroxyapatite content in bone char. Nano alumina contributed additional hydroxyl groups and reactive sites. Solution pH, contact time, adsorbent dose and initial fluoride concentration all impacted the fluoride removal efficiency as expected. Optimal pH was near neutral since bone char has a point of zero charge around 7.6. Fluoride removal followed Langmuir adsorption isotherm and pseudo-second order kinetics. Regeneration of the spent adsorbent was shown to be feasible using NaOH, though performance declined with repeated cycles. As a result of the application of NAMBC adsorption property on the real water sample, fluoride concentration could be reduced to 1.3 mg/L (83.6% removal), which was lower than WHO standard (1.5 mg/L).

5.2. Recommendation

In this study, NAMBC composite which was synthesized from bone char and γ - Al_2O_3 NPs is perform good adsorption property to ward fluoride ion. The synthesis of Al_2O_3 -NPs was via sol-gel method and citric acid (which was used a metal complex agent) is less toxic due to its organic nature. Therefore, the NAMBC could be employed for the adsorption in real applications. Further research work should better to be done on the following areas.

The other potential future works could be on detail investigation to understand the mechanism of the modification to optimize the performance of alumina dispersion on bone char in defluoridation.

- Test performance in continuous column experiments should be studied.
- Investigate more cost-effective methods for nano alumina synthesis would also be a good task to do.
- Perform detailed adsorbent characterization with SEM and TEM to understand mechanism
- Evaluate other activating agents like acids, bases, or metal salts to improve bone char.
- Study regeneration in more depth to improve adsorbent reuse and process economics.
- Evaluate techno-economic feasibility compared to existing defluoridation technologies.
- Using NAMBC to remove other contaminants like arsenic along with fluoride will be a good research area.

Research Fund Acknowledgement

This research project is funded by Adama Science and Technology University under the grant number ASTU/SM-R/905/23 Adama, Ethiopia.

REFERENCE

- Abdellah, W., Abdelfattah, E., Diab, H., & Saad, E. (2018). Removal of Chromium from Liquid Waste by Gamma Aluminum Oxide (γ -Al₂O₃) Nanoparticles Synthesized Using Citrate Sol-gel Method. *Arab Journal of Nuclear Sciences and Applications*, 0(0), 1–9.
- Al-ghouti, M. A., & Da, D. A. (2020). Guidelines for the use and interpretation of adsorption isotherm models: A review. *Journal of Hazardous Materials*, 393, 122383.
- Albertus, J., Bregnhøj, H., & Kongpun, M. (2000). Bone char quality and defluoridation capacity in contact precipitation. 3rd International Workshop on Fluorosis Prevention and Defluoridation of Water, 61–72.
- Alhassan, S. I., Huang, L., He, Y., Yan, L., Wu, B., & Wang, H. (2021). Fluoride removal from water using alumina and aluminum-based composites: A comprehensive review of progress. *Critical Reviews in Environmental Science and Technology*, 51(18), 2051–2085.
- Alkurdi, S., Al-Juboori, R., Bundschuh, J., & Marchuk, A. (2022). Evaluating the Ability of Bone Char/nTiO₂ Composite and UV Radiation for Simultaneous Oxidation and Adsorption of Arsenite. *Sustainable Chemistry*, 3(1), 19–34.
- Alkurdi, S. S. A., Al-Juboori, R. A., Bundschuh, J., Bowtell, L., & McKnight, S. (2020). Effect of pyrolysis conditions on bone char characterization and its ability for arsenic and fluoride removal. *Environmental Pollution*, 262, 114221.
- Alkurdi, S. S. A., Al-Juboori, R. A., Bundschuh, J., & Hamawand, I. (2019). Bone char as a green sorbent for removing health threatening fluoride from drinking water. *Environment International*, 127, 704–719.
- Aoba, T. (1997). The effect of fluoride on apatite structure and growth. *Critical Reviews in Oral Biology and Medicine*, 8(2), 136–153.
- Asra, M. T., & Kebede, S. (2016). Optimization and Characterization of Synthesis Conditions of Adsorbent from Bone for Removal of Fluoride. *International Journal of Scientific Engineering and Technology*, 5(7), 394–399.
- Avinash Chunduri, L. A., Rattan, T. M., Molli, M., & Kamiseti, V. (2014). Single step preparation of nano size gamma alumina exhibiting enhanced fluoride adsorption. *Materials Express*, 4(3), 235–241.
- Banerjee, S., & Sujatha Devi, P. (2007). Effect of citrate to nitrate ratio on the decomposition characteristics and phase formation of alumina. *Journal of Thermal Analysis and Calorimetry*, 90(3), 699–706.
- Belekar, R. M., & Dhoble, S. J. (2018). Activated Alumina Granules with nanoscale porosity for water defluoridation. *Nano-Structures and Nano-Objects*, 16, 322–328.
- Ben Nasr, A., Walha, K., Charcosset, C., & Ben Amar, R. (2011). Removal of fluoride ions using cuttlefish bones. *Journal of Fluorine Chemistry*, 132(1), 57–62.
- Bianchini, G., Brombin, V., Marchina, C., Natali, C., Godebo, T. R., Rasini, A., & Salani, G. M. (2020). Origin of fluoride and arsenic in the main ethiopian rift waters. *Minerals*, 10(5).

- Brunson, L. R., & Sabatini, D. A. (2014). Practical considerations, column studies and natural organic material competition for fluoride removal with bone char and aluminum amended materials in the Main Ethiopian Rift Valley. *Science of the Total Environment*, 488–489(1), 580–587.
- Chandradass, J., & Kim, K. H. (2009). Effect of acidity on the citrate-nitrate combustion synthesis of alumina-zirconia composite powder. *Metals and Materials International*, 15(6), 1039–1043.
- Chatterjee, S., Jha, S., & De, S. (2018). Novel carbonized bone meal for defluoridation of groundwater: Batch and column study. *Journal of Environmental Science and Health - Part A Toxic/Hazardous Substances and Environmental Engineering*, 53(9), 832–846.
- Chatterjee, S., Mukherjee, M., & De, S. (2018). Defluoridation using novel chemically treated carbonized bone meal: batch and dynamic performance with scale-up studies. *Environmental Science and Pollution Research*, 25(18), 18161–18178.
- Chinnakoti, P., Chunduri, A. L. A., Vankayala, R. K., Patnaik, S., & Kamiseti, V. (2017). Enhanced fluoride adsorption by nano crystalline γ -alumina: adsorption kinetics, isotherm modeling and thermodynamic studies. *Applied Water Science*, 7(5), 2413–2423.
- Dahi, E. (2015). Optimisation of Bone Char Production Using the. *Research Report Fluoride*, 48(1), 29–36.
- de Melo, N. H., de Oliveira Ferreira, M. E., Silva Neto, E. M., Martins, P. R., & Ostroski, I. C. (2018). Evaluation of the adsorption process using activated bone char functionalized with magnetite nanoparticles. *Environmental Nanotechnology, Monitoring and Management*, 10, 427–434.
- Dehghani, M. H., Faraji, M., Mohammadi, A., & Kamani, H. (2017). Optimization of fluoride adsorption onto natural and modified pumice using response surface methodology: Isotherm, kinetic and thermodynamic studies. 34(2), 454–462.
- Delgadillo-Velasco, L., Hernández-Montoya, V., Cervantes, F. J., Montes-Morán, M. A., & Lira-Berlanga, D. (2017). Bone char with antibacterial properties for fluoride removal: Preparation, characterization and water treatment. *Journal of Environmental Management*, 201, 277–285.
- Dhillon, A., Prasad, S., & Kumar, D. (2017). Recent advances and spectroscopic perspectives in fluoride removal. *Applied Spectroscopy Reviews*, 52(3), 175–230.
- Dubey, S., Singh, A., Nim, B., & Singh, I. B. (2017). Optimization of molar concentration of AlCl₃ salt in the sol-gel synthesis of nanoparticles of gamma alumina and their application in the removal of fluoride of water. *Journal of Sol-Gel Science and Technology*, 82(2), 468–477.
- Fan, X., Parker, D. J., & Smith, M. D. (2003). Adsorption kinetics of fluoride on low cost materials. *Water Research*, 37(20), 4929–4937.
- Farahmandjou, M. (2015). Processing Research New pore structure of nano-alumina (Al₂O₃) prepared by sol gel method. *Journal of Ceramic Processing Research*, 16(2), 1-4.
- Farooq, M., & Ramli, A. (2015). Biodiesel production from low FFA waste cooking oil using

- heterogeneous catalyst derived from chicken bones. *Renewable Energy*, 76, 362–368.
- Fatemeh M, Hasmaliza M, L. C. (2011). Preparation of Nano-scale alfa Al_2O_3 Powder by the Sol-Gel Method. *Ceramics*, 55(4), 378–383.
- Fouda, H., Guo, L., & Elsharkawy, K. (2016). Preparation and Characterizations of Composite Material Based on Carbon Fiber and Two Thermoset Resins. *MATEC Web of Conferences*, 88.
- Gabelman, A. (2017). GABELMAN - adsorption basics part 2. August, 38–45.
- García-Sánchez, J. J., Martínez-Miranda, V., & Solache-Ríos, M. (2013). Aluminum and calcium effects on the adsorption of fluoride ions by corrosion products. *Journal of Fluorine Chemistry*, 145, 136–140.
- Getachew, T., Hussen, A., & Rao, V. M. (2015). Defluoridation of water by activated carbon prepared from banana (*Musa paradisiaca*) peel and coffee (*Coffea arabica*) husk. *International Journal of Environmental Science and Technology*, 12(6), 1857–1866.
- Gill, T., Tiwari, S., & Kumar, P. A. (2014). A Review on Feasibility of Conventional Fluoride Removal Techniques in Urban Areas. 4(2), 179–182.
- Giraldo, L. (2011). Study of the Textural Properties of Bovine Bones Char under Different Conditions. 2011(March), 176–181.
- Hart, A., Porbeni, D. W., & Omonmhenle, S. (2023). Waste bone char-derived adsorbents : characteristics , adsorption mechanism and model approach. *Environmental technology reviews*, 12(1), 175-204.
- He, J., Siah, T. S., & Paul Chen, J. (2014). Performance of an optimized Zr-based nanoparticle-embedded PSF blend hollow fiber membrane in treatment of fluoride contaminated water. *Water Research*, 56, 88–97.
- He, J., Yang, Y., Wu, Z., Xie, C., Zhang, K., Kong, L., & Liu, J. (2020). Review of fluoride removal from water environment by adsorption. In *Journal of Environmental Chemical Engineering* , 8(6), 104516.
- Ho, Y. S. (2004). Comment on ‘Cadmium removal from aqueous solutions by chitin : kinetic and equilibrium studies .’ 38, 2962–2964.
- Hu, J., Wu, D., Rao, R., Liu, R., & Lai, W. (2017). Adsorption kinetics of fluoride on bone char and its regeneration. *Environment Protection Engineering*, 43(3), 93–112.
- Kabir, H., Gupta, A. K., & Tripathy, S. (2020). Fluoride and human health: Systematic appraisal of sources, exposures, metabolism, and toxicity. *Critical Reviews in Environmental Science and Technology*, 50(11), 1116–1193.
- Kalaitzidou, K., Zouboulis, A., & Mitrakas, M. (2020). Cost evaluation for Se (IV) removal, by applying common drinking water treatment processes: Coagulation/precipitation or adsorption. *Journal of Environmental Chemical Engineering*, 8(5), 104209.
- Kanwal, F., Batool, A., Adnan, M., & Naseem, S. (2015). The effect of molecular structure, band gap energy and morphology on the dc electrical conductivity of polyaniline/aluminium oxide

- composites. *Materials Research Innovations*, 19(November), 354–358.
- Kaseva, M. E. (2006a). Optimization of regenerated bone char for fluoride removal in drinking water: a case study in Tanzania. 139–147.
- Kaseva, M. E. (2006b). Optimization of regenerated bone char for fluoride removal in drinking water: A case study in Tanzania. *Journal of Water and Health*, 4(1), 139–147.
- Kimambo, V., Bhattacharya, P., Mtalo, F., Mtamba, J., & Ahmad, A. (2019). Fluoride occurrence in groundwater systems at global scale and status of defluoridation—state of the art. *Groundwater for Sustainable Development*, 9, 100223.
- Kulkarni, S., & Kaware, J. (2014). Regeneration and Recovery in Adsorption- a Review. *International Journal of Innovative Science, Engineering & Technology(IJSET)*, 1(8), 61–64.
- Kumar, E., Bhatnagar, A., Kumar, U., & Sillanpää, M. (2011). Defluoridation from aqueous solutions by nano-alumina: Characterization and sorption studies. *Journal of Hazardous Materials*, 186(2–3), 1042–1049.
- Li, H., Yang, Y., Yang, S., Chen, A., & Yang, D. (2014). Infrared spectroscopic study on the modified mechanism of aluminum-impregnated bone charcoal. *Journal of Spectroscopy*, 2014.
- Li, J., Pan, Y., Xiang, C., Ge, Q., & Guo, J. (2006). Low temperature synthesis of ultrafine α -Al₂O₃ powder by a simple aqueous sol-gel process. *Ceramics International*, 32(5), 587–591.
- Li, J., Wu, Y., Pan, Y., & Guo, J. (2007). Alumina precursors produced by gel combustion. *Ceramics International*, 33(3), 361–363.
- Li, Y.-H., Wang, S., Cao, A., Zhao, D., Zhang, X., Xu, C., Luan, Z., Ruan, D., Liang, J., & Wu, D. (2001). Adsorption of fluoride from water by amorphous alumina supported on carbon nanotubes. *Chemical Physics Letters*, 350(5–6), 412–416.
- Liu, G., Liu, A., Zhu, H., Shin, B., Fortunato, E., Martins, R., Wang, Y., & Shan, F. (2015). Lowerature, nontoxic water-induced metal-oxide thin films and their application in thin-film transistors. *Advanced Functional Materials*, 25(17), 2564–2572.
- Liu, H., Gao, Y., Sun, L., Li, M., Li, B., & Sun, D. (2014). Assessment of relationship on excess fluoride intake from drinking water and carotid atherosclerosis development in adults in fluoride endemic areas, China. *International Journal of Hygiene and Environmental Health*, 217(2–3), 413–420.
- Ma, C., Chang, Y., Ye, W., Duan, L., & Wang, C. (2008). Hexagon γ -alumina nanosheets produced with the assistance of supercritical ethanol drying. *The Journal of Supercritical Fluids*, 45(1), 112–120.
- Maheshwari, R. C. (2006). Fluoride in drinking water and its removal. 137(March 2005), 456–463.
- Mall, I. D., Srivastava, V. C., Agarwal, N. K., & Mishra, I. M. (2005). Adsorptive removal of malachite green dye from aqueous solution by bagasse fly ash and activated carbon-kinetic

- study and equilibrium isotherm analyses. 264, 17–28.
- Medellin-Castillo, N. A., Leyva-Ramos, R., Ocampo-Perez, R., De La Cruz, R. F. G., Aragon-Piña, A., Martínez-Rosales, J. M., Guerrero-Coronado, R. M., & Fuentes-Rubio, L. (2007). Adsorption of fluoride from water solution on bone char. *Industrial and Engineering Chemistry Research*, 46(26), 9205–9212.
- Medellin-Castillo, N. A., Leyva-Ramos, R., Padilla-Ortega, E., Perez, R. O., Flores-Cano, J. V., & Berber-Mendoza, M. S. (2014). Adsorption capacity of bone char for removing fluoride from water solution. Role of hydroxyapatite content, adsorption mechanism and competing anions. *Journal of Industrial and Engineering Chemistry*, 20(6), 4014–4021.
- Medellin-Castillo, N. A., Padilla-Ortega, E., Tovar-García, L. D., Leyva-Ramos, R., Ocampo-Pérez, R., Carrasco-Marín, F., & Berber-Mendoza, M. S. (2016). Removal of fluoride from aqueous solution using acid and thermally treated bone char. *Adsorption*, 22(7), 951–961.
- Mirjalili, F., Hasmaliza, M., & Abdullah, L. C. (2010). Size-controlled synthesis of nano α -alumina particles through the sol-gel method. *Ceramics International*, 36(4), 1253–1257.
- Mittal, A., Kurup, L., & Mittal, J. (2007). Freundlich and Langmuir adsorption isotherms and kinetics for the removal of Tartrazine from aqueous solutions using hen feathers. *Journal of Hazardous Materials*, 146(1–2), 243–248.
- Mohamad, S. N. S., Mahmed, N., Che Halin, D. S., Abdul Razak, K., Norizan, M. N., & Mohamad, I. S. (2019). Synthesis of alumina nanoparticles by sol-gel method and their applications in the removal of copper ions (Cu^{2+}) from the solution. *IOP Conference Series: Materials Science and Engineering*, 701(1).
- Mondal, N. K., Bhaumik, R., Banerjee, A., Datta, J. K., & Baur, T. (2012). A comparative study on the batch performance of fluoride adsorption by activated silica gel and activated rice husk ash. *International Journal of Environmental Sciences*, 2(3), 1643–1661.
- Mondal, N. K., Bhaumik, R., & Datta, J. K. (2015). Removal of fluoride by aluminum impregnated coconut fiber from synthetic fluoride solution and natural water. *Alexandria Engineering Journal*, 54(4), 1273–1284.
- Moreno-Piraján, J. C., Gómez-Cruz, R., García-Cuello, V. S., & Giraldo, L. (2010). Binary system Cu (II)/Pb (II) adsorption on activated carbon obtained by pyrolysis of cow bone study. *Journal of Analytical and Applied Pyrolysis*, 89(1), 122–128.
- Musah, M., Azeh, Y., Mathew, J., Umar, M., Abdulhamid, Z., & Muhammad, A. (2022). Adsorption Kinetics and Isotherm Models: A Review. *Caliphate Journal of Science and Technology*, 4(1), 20–26.
- Mwakabona, H., Machunda, R., & Njau, K. (2014). The influence of stereochemistry of the active compounds on fluoride adsorption efficiency of the plant biomass.
- Nie, Y., Hu, C., & Kong, C. (2012). Enhanced fluoride adsorption using Al (III) modified calcium hydroxyapatite. *Journal of Hazardous Materials*, 233–234, 194–199.
- Nigri, E. M., Bhatnagar, A., & Rocha, S. D. F. (2017). Thermal regeneration process of bone char used in the fluoride removal from aqueous solution. *Journal of Cleaner Production*, 142,

3558–3570.

- Niu, C., Li, S., Zhou, G., Wang, Y., Dong, X., & Cao, X. (2021). Preparation and characterization of magnetic modified bone charcoal for removing Cu^{2+} ions from industrial and mining wastewater. *Journal of Environmental Management*, 297(June), 113221.
- Nyanguru, K. M., & Mosima Osano, A. (2020). Insights into the Quality and Quantity of Briquette Fuels from Bone Wastes. *International Journal of Innovative Studies in Sciences and Engineering Technology*, 4863.
- Of, C., Char, B., & Bone, C. O. W. (2012). Investigation of the effect of chemical activation and characterization of bone char: cow bone * Gumus , R.H., Wauton, I and Aliu A. M. 4(September), 34–45.
- Ofori, D. A., Anjarwalla, P., Mwaura, L., Jamnadass, R., Stevenson, P. C., Smith, P., Koch, W., Kukula-Koch, W., Marzec, Z., Kasperek, E., Wyszogrodzka-Koma, L., Szwerc, W., Asakawa, Y., Moradi, S., Barati, A., Khayyat, S. A., Roselin, L. S., Jaafar, F. M., Osman, C. P., ... Slaton, N. (2020).
- Ooi, C. Y., Hamdi, M., & Ramesh, S. (2007). Properties of hydroxyapatite produced by annealing of bovine bone. *Ceramics International*, 33(7), 1171–1177.
- Plush, S. E., & Hayball, J. D. (2017). *Activated Carbon, Carbon Nanotubes and Graphene: Materials and Composites for Advanced Water Purification*.
- Poinern, G. E. J., Ghosh, M. K., Ng, Y.-J., Issa, T. B., Anand, S., & Singh, P. (2011). Defluoridation behavior of nanostructured hydroxyapatite synthesized through an ultrasonic and microwave combined technique. *Journal of Hazardous Materials*, 185(1), 29–37.
- Potdar, H. S., Jun, K.-W., Bae, J. W., Kim, S.-M., & Lee, Y.-J. (2007). Synthesis of nano-sized porous γ -alumina powder via a precipitation/digestion route. *Applied Catalysis A: General*, 321(2), 109–116.
- Priyantha, N. (2011). Dragon Fruit Skin as a Potential Low- Cost Biosorbent for the Removal of Manganese (II) Ions. 10(8), 671–680.
- Pulkka, S., Martikainen, M., Bhatnagar, A., & Sillanpää, M. (2014). Electrochemical methods for the removal of anionic contaminants from water - A review. *Separation and Purification Technology*, 132, 252–271.
- Qiu, H., Lv, L., Pan, B., Zhang, Q., Zhang, W., & Zhang, Q. (2009). Critical review in adsorption kinetic models . 10(5), 716–724.
- Rajaeiyan, A., & Bagheri-Mohagheghi, M. M. (2013a). Comparison of sol-gel and co-precipitation methods on the structural properties and phase transformation of γ and α - Al_2O_3 nanoparticles. *Advances in Manufacturing*, 1(2), 176–182.
- Rajaeiyan, A., & Bagheri-Mohagheghi, M. M. (2013b). Comparison of urea and citric acid complexing agents and annealing temperature effect on the structural properties of γ - and α -alumina nanoparticles synthesized by sol-gel method. *Advances in Materials Science and Engineering*, 2013.

- Roba, B., Yilma, M., Abay, Y., Mekonnen, A., Periyasamy, S., Duraisamy, K., & Temesgen, T. (2023). A novel approach for the defluorination of groundwater using trivalent-metal hydroxide/bone-char composite adsorbent. *Urban Climate*, 47(April 2022), 101340.
- Rojas-Mayorga, C. K., Bonilla-Petriciolet, A., Aguayo-Villarreal, I. A., Hernández-Montoya, V., Moreno-Virgen, M. R., Tovar-Gómez, R., & Montes-Morán, M. A. (2013). Optimization of pyrolysis conditions and adsorption properties of bone char for fluoride removal from water. *Journal of Analytical and Applied Pyrolysis*, 104, 10–18.
- Rojas-Mayorga, C. K., Bonilla-Petriciolet, A., Silvestre-Albero, J., Aguayo-Villarreal, I. A., & Mendoza-Castillo, D. I. (2015). Physico-chemical characterization of metal-doped bone chars and their adsorption behavior for water defluoridation. *Applied Surface Science*, 355, 748–760.
- Sani, T., Gómez-Hortigüela, L., Pérez-Pariente, J., Chebude, Y., & Díaz, I. (2016). Defluoridation performance of nano-hydroxyapatite/stilbite composite compared with bone char. *Separation and Purification Technology*, 157, 241–248.
- Santos, P. S., Santos, H. S., & Toledo, S. P. de. (2000). Standard transition aluminas. Electron microscopy studies. *Materials Research*, 3, 104–114.
- Sawangjang, B., Induvesa, P., Wongrueng, A., Pumas, C., Wattanachira, S., Rakruam, P., Punyapalakul, P., Takizawa, S., & Khan, E. (2021). Evaluation of fluoride adsorption mechanism and capacity of different types of bone char. *International Journal of Environmental Research and Public Health*, 18(13).
- Shahid, M. K., Kim, J. Y., & Choi, Y. G. (2019). Synthesis of bone char from cattle bones and its application for fluoride removal from the contaminated water. *Groundwater for Sustainable Development*, 8, 324–331.
- Shahid, M. K., Kim, J. Y., Shin, G., & Choi, Y. (2020). Effect of pyrolysis conditions on characteristics and fluoride adsorptive performance of bone char derived from bone residue. *Journal of Water Process Engineering*, 37(April), 101499.
- Shivaprasad, P., Singh, P. K., Saharan, V. K., & George, S. (2018). Nano-Structures & Nano-Objects Synthesis of nano alumina for defluoridation of drinking water. *Nano-Structures & Nano-Objects*, 13, 109–120.
- Shukla, R., Ramkumar, J., & Tyagi, A. K. (2010). Nanocrystalline magnesia alumina mixed oxide: efficient defluoridation sorbent. *International Journal of Nanotechnology*, 7(9–12), 989–1002.
- Singh, I. B., Gupta, A., Dubey, S., Shafeeq, M., Banerjee, P., & Sinha, A. S. K. (2016). Sol-gel synthesis of nanoparticles of gamma alumina and their application in defluoridation of water. *Journal of Sol-Gel Science and Technology*, 77(2), 416–422.
- Smith, B. C. (2011). *Fundamentals of Fourier transform infrared spectroscopy*. CRC press.
- Smittakorn, S., Jirawongboonrod, N., Mongkolnchai-Arunya, S., & Durnford, D. (2010). Homemade bone charcoal adsorbent for defluoridation of groundwater in Thailand. *Journal of Water and Health*, 8(4), 826–836.

- Solanki, Y. S., Agarwal, M., Maheshwari, K., Gupta, S., Shukla, P., & Gupta, A. B. (2021). Removal of fluoride from water by using a coagulant (inorganic polymeric coagulant). *Environmental Science and Pollution Research*, 28(4), 3897–3905.
- Srivastav, A., & Srivastava, V. C. (2009). Adsorptive desulfurization by activated alumina. *Journal of Hazardous Materials*, 170(2–3), 1133–1140.
- Suhasinee Behera, P., Bhattacharyya, S., & Sarkar, R. (2017). Effect of citrate to nitrate ratio on the sol-gel synthesis of nanosized α -Al₂O₃ powder. *Ceramics International*, 43(17), 15221–15226.
- Tabesh, S., Davar, F., & Loghman-Estarki, M. R. (2017). The effects of chelating agent type on the morphology and phase evolutions of alumina nanostructures. *Ceramics International*, 43(13), 10247–10252.
- Tabesh, S., Davar, F., & Loghman-Estarki, M. R. (2018). Preparation of γ -Al₂O₃ nanoparticles using modified sol-gel method and its use for the adsorption of lead and cadmium ions. In *Journal of Alloys and Compounds (Vol. 730)*. Elsevier B.V.
- Tchomgui-Kamga, E., Alonzo, V., Nansu-Njiki, C. P., Audebrand, N., Ngamei, E., & Darchen, A. (2010). Preparation and characterization of charcoals that contain dispersed aluminum oxide as adsorbents for removal of fluoride from drinking water. *Carbon*, 48(2), 333–343.
- Tekle-Haimanot, R., Melaku, Z., Kloos, H., Reimann, C., Fantaye, W., Zerihun, L., & Bjorvatn, K. (2006). The geographic distribution of fluoride in surface and groundwater in Ethiopia with an emphasis on the Rift Valley. *Science of the Total Environment*, 367(1), 182–190.
- Thole, B. (2013). *Ground Water Contamination with Fluoride and Potential Fluoride Removal Technologies for East and Southern Africa. Perspectives in Water Pollution.*
- Wajima, T., Umata, Y., Narita, S., & Sugawara, K. (2009). Adsorption behavior of fluoride ions using a titanium hydroxide-derived adsorbent. *Desalination*, 249(1), 323–330.
- Wang, S., Ma, Y., Shi, Y., & Gong, W. (2009). Defluoridation performance and mechanism of nano-scale aluminum oxide hydroxide in aqueous solution. *Journal of Chemical Technology & Biotechnology: International Research in Process, Environmental & Clean Technology*, 84(7), 1043–1050.
- Workeneh, K., Zereffa, E. A., Segne, T. A., & Eswaramoorthy, R. (2019). Eggshell-derived nanohydroxyapatite adsorbent for defluoridation of drinking water from bofo of Ethiopia. *Journal of Nanomaterials*, 2019.
- Wu, F. C., Liu, B. L., Wu, K. T., & Tseng, R. L. (2010). A new linear form analysis of Redlich-Peterson isotherm equation for the adsorptions of dyes. *Chemical Engineering Journal*, 162(1), 21–27.
- Yadav, K. K., Gupta, N., Kumar, V., Khan, S. A., & Kumar, A. (2018). A review of emerging adsorbents and current demand for defluoridation of water: Bright future in water sustainability. *Environment International*, 111(November 2017), 80–108.
- Yu, C., Liu, L., Wang, X., Fu, J., Wu, Y., Feng, C., Wu, Y., & Shen, J. (2023). Fluoride removal performance of highly porous activated alumina. *Journal of Sol-Gel Science and Technology*,

106(2), 471–479.

Zhu, J., Zhao, H., & Ni, J. (2007). Fluoride distribution in electrocoagulation defluoridation process. *Separation and Purification Technology*, 56(2), 184–191.

Zúñiga-Muro, N. M., Bonilla-Petriciolet, A., Mendoza-Castillo, D. I., Reynel-Ávila, H. E., & Tapia-Picazo, J. C. (2017). Fluoride adsorption properties of cerium-containing bone char. *Journal of Fluorine Chemistry*, 197, 63–73.

Appendix

Appendix A: Colors of treated fluoride water.



Figure A1: treated fluoride containing water with bone char prepared at 450°C-800°C, each of the temperature set points; 1 and 2 h



Figure A2: treated fluoride containing water with different ratio of bone char to γ -Al₂O₃-NP

Appendix B: Proximate Analysis of bone char and alumina

	W1(weight of sample and crucible before drying)	W2(weight of sample and crucible after drying)	W3 (Mass of empty crucible)
Alumina	47.6591	47.6341	46.6591
BC	47.6591	47.6191	46.6591

i. Moisture content calculation

$$\%Moisture\ content(MC) = \frac{W_1 - W_2}{W_1 - W_3} * 100$$

Where, W1=weight of sample and crucible before drying

W2=weight of sample and crucible after drying

W3=Mass of empty crucible

$$BC\ \%MC = \frac{47.6591 - 47.6191}{47.6591 - 46.6591} * 100$$

$$alumina\ \%MC = \frac{47.6591 - 47.6341}{47.6591 - 46.6591} * 100$$

$$BC\ \%MC = 4\%$$

$$alumina\ \%MC = 2.5\%$$

	W1(weight of sample and crucible before drying)	W2(weight of sample and crucible after drying)	W3 (Mass of empty crucible)
Alumina	47.6591	47.6541	46.6591
BC	47.6591	47.4337	46.6591

ii. Volatile matter (VM)

$$\%Volatile\ Matter(VM) = \frac{W_1 - W_2}{W_1 - W_3} * 100$$

Where, W1=weight of sample and crucible before drying

W2=weight of sample and crucible after drying

W3=Mass of empty crucible

$$BC\ \%VM = \frac{47.6591 - 47.4337}{47.6591 - 46.6591} * 100$$

$$alumina\ \%VM = \frac{47.6591 - 47.6541}{47.6591 - 46.6591} * 100$$

	W1(weight of sample and crucible before drying)	W2(weight of sample and crucible after drying)	W3 (Mass of empty crucible)
Alumina	47.6591	47.6291	46.6591
BC	47.6591	47.1791	46.6591

BC % VM = 22.54%

alumina % VM = 0.5%

iii. Ash content (AC)

$$\%Ash\ Content(AC) = \frac{W_2 - W_3}{W_1 - W_3} * 100$$

Where, W1=weight of sample and crucible before drying

W2=weight of sample and crucible after drying

W3=Mass of empty crucible

$$BC\ \% AC = \frac{47.1791 - 46.6591}{47.6591 - 46.6591} * 100$$

$$alumina\ \% AC = \frac{47.6291 - 47.6591}{47.6591 - 46.6591} * 100$$

BC %AC = 52%

alumina %AC = 97%

iv. Fixed carbon content calculation

$$\%Fixed\ carbon\ content(FCC) = 100 - (MC\% + VM\% + AC\%)$$

$$BC\ \%FCC = 100 - (4\% + 22.54\% + 52\%) = 21.46\%$$

$$alumina\ \%FCC = 100 - (2.5\% + 0.5\% + 97\%) = 0\%$$

Appendix C: Particle size analysis (PSA), particle size distribution of Al₂O₃-NPs

Size Distribution Report by Intensity

v2.2



Sample Details

Sample Name: AN 3
 SOP Name: mansettings.nano
 General Notes:

File Name: CNC.dts Dispersant Name: Ethanol
 Record Number: 1351 Dispersant RI: 1.361
 Material RI: 1.59 Viscosity (cP): 0.9830
 Material Absorption: 0.010 Measurement Date and Time: Monday, July 10, 2023 10:03:...

System

Temperature (°C): 20.0 Duration Used (s): 50
 Count Rate (kopc): 98.1 Measurement Position (mm): 0.65
 Cell Description: Disposable sizing cuvette Attenuator: 11

Results

	Size (d.nm):	% Intensity:	St Dev (d.n...)
Z-Average (d.nm): 1508	Peak 1: 923.7	100.0	55.95
PdI: 0.440	Peak 2: 0.000	0.0	0.000
Intercept: 0.699	Peak 3: 0.000	0.0	0.000

Result quality : Refer to quality report

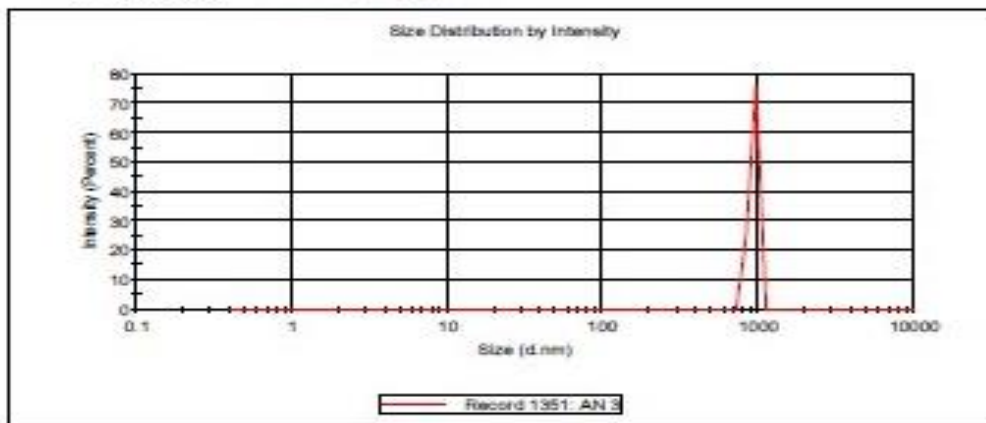


Figure D1: Analysis result of Zeta potential for Al₂O₃ nanoparticle (ethanol used as dispersant)

Size Distribution Report by Intensity

v2.2



Sample Details

Sample Name: AN 2
SOP Name: mansettings.nano
General Notes:

File Name: CNC.cts Dispersant Name: SODIUM HYDROXIDE
Record Number: 1345 Dispersant RI: 1.358
Material RI: 1.59 Viscosity (cP): 78.0000
Material Absorption: 0.010 Measurement Date and Time: Friday, July 7, 2023 3:00:51 ...

System

Temperature (°C): 25.0 Duration Used (s): 50
Count Rate (kcps): 103.2 Measurement Position (mm): 0.65
Cell Description: Disposable sizing cuvette Attenuator: 11

Results

	Size (d.nm):	% Intensity:	St Dev (d.nm):
Z-Average (d.nm): 29.16	Peak 1: 79.82	57.4	13.24
PdI: 0.385	Peak 2: 15.23	42.6	1.707
Intercept: 0.797	Peak 3: 0.000	0.0	0.000

Result quality : Refer to quality report

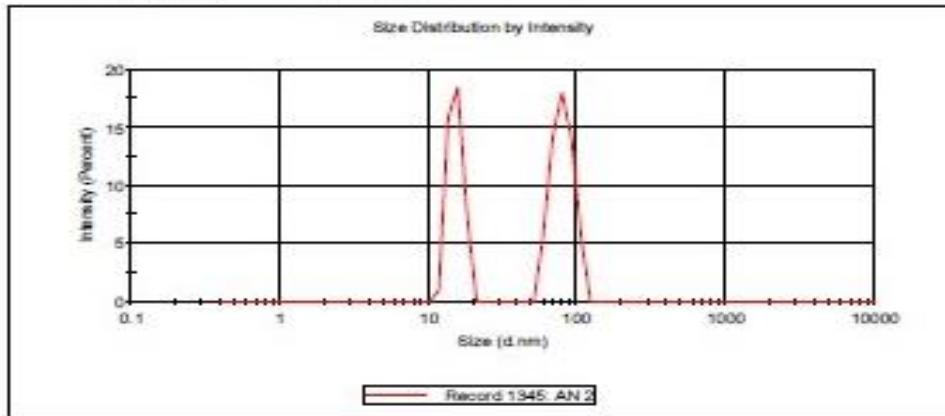


Figure D2: Analysis result of Zeta potential for Al₂O₃ nanoparticle (NaOH used as dispersant)

Appendix D: characterization of real water



Figure D1: COD test



Figure D4: Color test



Figure D2: TSS test



Figure D5: Turbidity test

Appendix E: Thermal analysis of alumina and bone

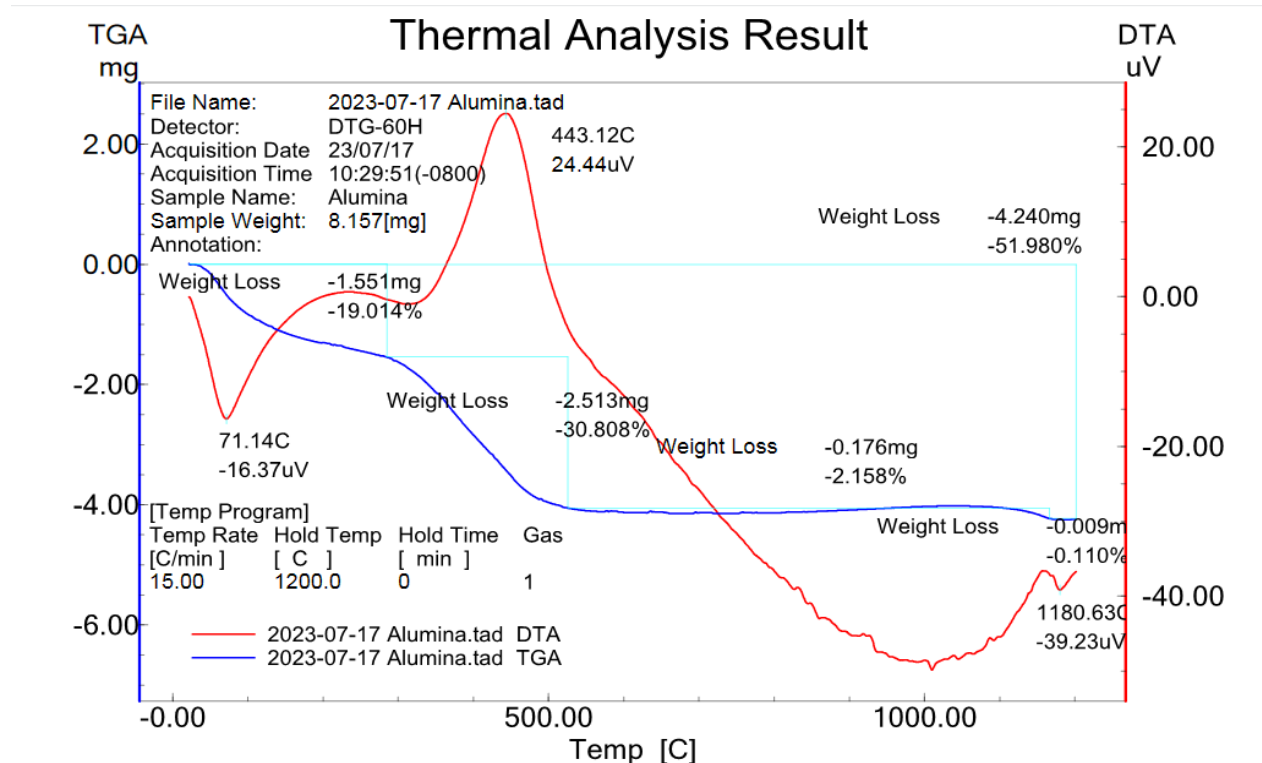


Figure E1: TGA/DTA curve for Al_2O_3

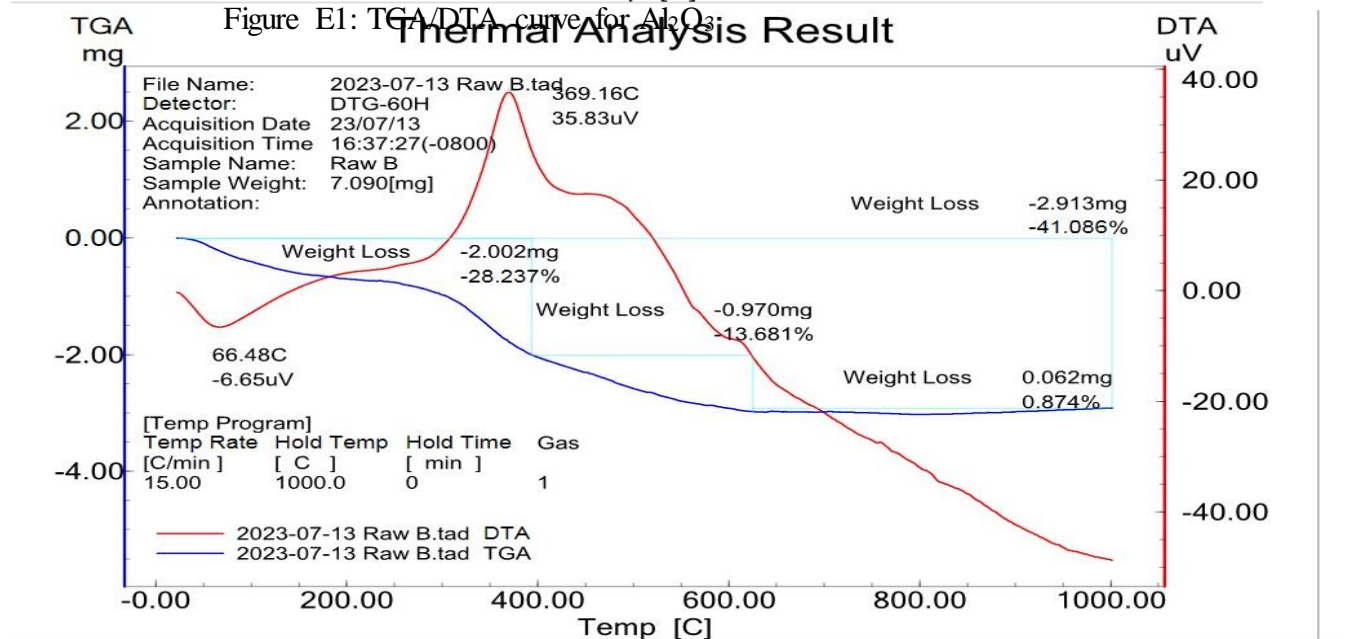


Figure E2: TGA/DTA curve for bone

Appendix F: BET analysis of BC and NAMBC

Quantachrome NovaWin - Data Acquisition and Reduction
for NOVA instruments
©1994-2010, Quantachrome Instruments
version 11.0

Analysis Report
Operator:alex Date:2007/01/01 Operator:alex Date:7/20/2023
Sample ID: BC 1 Filename: C:\QCdata\Physisorb\BC 1.qps
Sample Desc: sample Comment: TEST
Sample weight: 0.08 g Sample Volume: 0.02051 cc Sample Density:3.9 g/cc
Outgas Time: 8.0 hrs OutgasTemp: 300.0 C
Analysis gas: Nitrogen Bath Temp: 77.3 K
Press. Tolerance:0.100/0.100 (ads/des) Equil time: 60/60 sec (ads/des) Equil timeout: 240/240 sec (ads/des)
Analysis Time: 69.4 min End of run: 2023/04/28 15:47:02 Instrument: Nova Station B
Cell ID: 2 F/W version: 0.00
Adsorbate Nitrogen Temperature 77.350K
Molec. Wt.: 28.013 g Cross Section: 16.200 Å² Liquid Density: 0.808 g/cc

Relative Pressure P/Po	Volume @ STP cc/g	1 / [W((Po/P) - 1)]
4.73030e-02	23.6020	1.6832e+00
1.33264e-01	52.8375	2.3283e+00
1.98783e-01	74.3676	2.6693e+00
2.83548e-01	102.1092	3.1012e+00
3.49486e-01	123.7937	3.4724e+00

BET summary
Slope = 5.777
Intercept = 1.481e+00
Correlation coefficient, r = 0.996418
C constant = 4.901
Surface Area = 479.796 m²/g

Figure F1: BET analysis for BC

Analysis		Report	
Operator:alex	Date:2007/01/01	Operator:alex	Date:7/20/2023
Sample ID: bc an 2	Filename: C:\QCdata\Physisorb\bc an 1.qps		
Sample Desc: sample	Comment: TEST		
Sample weight: 0.08 g	Sample Volume: 0.02051 cc	Sample Density:3.9 g/cc	
Outgas Time: 8.0 hrs	OutgasTemp: 300.0 C		
Analysis gas: Nitrogen	Bath Temp: 77.3 K		
Press. Tolerance:0.100/0.100 (ads/des)	Equil time: 60/60 sec (ads/des)	Equil timeout: 240/240 sec (ads/des)	
Analysis Time: 69.4 min	End of run: 2007/01/01 7:21:36	Instrument: Nova Station B	
Cell ID: 2		F/W version: 0.00	
Adsorbate Nitrogen	Temperature 77.350K		
Molec. Wt.: 28.013 g	Cross Section: 16.200 Å ²	Liquid Density: 0.808 g/cc	

Relative Pressure P/Po	Volume @ STP cc/g	1 / [W((Po/P) - 1)]
6.18260e-02	57.2944	9.2029e-01
1.28453e-01	79.2830	1.4874e+00
2.03663e-01	101.8484	2.0091e+00
2.77491e-01	123.9118	2.4800e+00
3.54163e-01	147.3754	2.9772e+00

BET summary

Slope =	6.950
Intercept =	5.491e-01
Correlation coefficient, r =	0.998351
C constant=	13.657
Surface Area =	464.365 m ² /g

Figure F2: BET analysis for NAMBC